INTEGRAL METHODS FOR THREE-DIMENSIONAL BOUNDARY LAYERS

by

BILAL HAFEEZ MUGHAL

B.S., University of Virginia (1990)
S.M., Massachusetts Institute of Technology (1992)

SUBMITTED TO THE
DEPARTMENT OF AERONAUTICS AND ASTRONAUTICS
IN PARTIAL FULFILLMENT OF THE REQUIREMENTS
FOR THE DEGREE OF

DOCTOR OF PHILOSOPHY

at the

MASSACHUSETTS INSTITUTE OF TECHNOLOGY

February 1998

Author_____
Department of Aeronautics and Astronautics
December 3, 1997

Certified by_____
Mark Drela
Thesis Supervisor, Associate Professor of Aeronautics and Astronautics

Certified by_____
Jaime Peraire
Associate Professor of Aeronautics and Astronautics

Certified by_____
Marten Landahl
Professor of Aeronautics and Astronautics

Accepted by_____
Jaime Peraire
Associate Professor
Chairman, Department Graduate Committee

Integral Methods for Three-Dimensional Boundary Layers

by

Bilal Hafeez Mughal

Submitted to the Department of Aeronautics and Astronautics
on December 3, 1997, in partial fulfillment of the
requirements for the degree of
Doctor of Philosophy

Abstract

Several distinct issues important in integral approximations of the three-dimensional boundary-layer equations are addressed. One of these is the requirement, justified on the basis of the nature of the full differential equations, for hyperbolicity of integral equation systems. It is generally not feasible to analytically determine the mathematical character of these systems, except in very simple cases, because of the empiricism necessary for closure. Furthermore, the use of general systems is inhibited because there is no guarantee that they are hyperbolic. A novel method accommodating the role of both equations and closure, so that systems are always hyperbolic with physically-consistent characteristic directions, is proposed. Another issue considered is the calculation of bidirectional crossflows for which a well-conditioned system, for use in Newton solvers, is devised. The validity of this system is demonstrated by comparing results with a numerical solution of the full differential boundary-layer equations for the case of an infinite-swept wing. Finally, a fully-simultaneous scheme coupling inviscid flow, calculated using a simple Panel method, to general integral systems is devised with the facility to use empirical closure parameters as system parameters. The coupling scheme is demonstrated by computing the separated flow downstream of a smooth obstacle. For calculations, the equations are posed in conservation form in local Cartesian coordinates and discretized using the finite-element method. Unlike dissipation schemes used in previous methods, a Petrov-Galerkin streamline upwinding weight function, adapted heuristically for the coupled equation system, is used to control spurious oscillations.

Thesis Supervisor: Mark Drela
Associate Professor of Aeronautics and Astronautics

Acknowledgments

I am indebted to Professor Mark Drela for taking me on as an apprentice. I have greatly benefited from his extraordinary physical insight, his intrinsic emphasis on substance over superfluous quantity and from an unparalleled access made possible by a now legendary work ethic. I am also indebted to my thesis committee, Professors Jaime Peraire and Marten Landahl, for their valuable suggestions. Professors Justin Kerwin and Jerome Milgram of Ocean Engineering graciously agreed to be official readers for which I am grateful.

Since joining the CFDL and its subsequent incarnations, the CASL and the FDRL, I have learnt much from many colleagues. In particular, I would like to mention Dr. Brian Nishida, Dr. Thomas Sorensen, Professor David Darmofal, Dr. Jon Anh, Ali Merchant and Jonathan Elliot. Thanks to Bob Haimes for getting me out of more than one hardware glitch, not to mention his early-morning sanguinity.

Of the many friends on whom I have leaned heavily, I would particularly like to mention Amr Mohammed, Mohamed Mekias, Sabbir Rahman, Jinevra Howard, Farhan Rana, and especially Lucy McCauley, Issam Lakkis and Kate Hopkins.

And finally, I would like to thank my family whose constant support, patience and affection carried me through the difficult times.

Support was given by the Boeing Company, with Dr. Wen-Huei Jou and Dr. Forrester Johnson as the Technical Monitors.

Contents

List of Figures **9**

List of Tables **13**

Nomenclature **14**

1 Introduction **17**

1.1 Context and general objectives 17

1.2 General features of a three-dimensional boundary layer 18

1.3 Brief literature survey 20

1.3.1 Conventional integral methods 21

1.3.2 Related methods 23

1.4 Overview of thesis 24

2 Derivation of Integral Equations **26**

2.1 Differential equations 27

2.1.1 Boundary conditions 28

2.2 Derivation of steady integral equations 29

2.2.1 Preliminaries 29

2.2.2 Entrainment equation 31

2.2.3 Momentum equations 31

2.2.4 Kinetic-energy equation components 33

2.2.5 Total kinetic-energy equation 36
2.2.6 Mixed-component kinetic-energy equation 37
2.2.7 Summary of individual equations 39
2.3 Derivation of an unsteady parent integral equation 40
2.4 Information content of the equations 43
2.5 Constructing practical equation systems 45

3 Assumptions in Closure of Integral Equations 46

3.1 Wall-normal boundary-layer behavior at edges 48
3.2 Streamwise velocity profiles 49
3.2.1 Laminar flow 49
3.2.2 Turbulent flow 51
3.3 Cross-stream velocity profiles 54
3.3.1 Laminar flow 55
3.3.2 Turbulent flow 55
3.4 Models for the complete profile 58
3.5 Skin friction 59

4 Nature of the Unsteady Differential Equation System 60

4.1 Characteristic analysis 60
4.2 Subcharacteristic analysis 63
4.3 Influence and dependence zones 66
4.4 Appendix: Determination of characteristic surfaces 70

5 Nature of Integral Equation Systems 72

5.1 Justification of integral-system hyperbolicity 72
5.2 The eigenvalues of integral systems 73
5.2.1 The problem and its possible solution 77
5.2.2 Literature review 78

5.3 Analysis of some integral systems 80
5.3.1 A second-order system 80
5.3.2 A third-order system with Johnston's crossflow model 81
5.4 Summary 84

6 Synthesis of Hyperbolic Integral Systems **85**
6.1 Symmetric Jacobian-matrices? 86
6.2 System/closure construction by induction 86
6.3 Eigenvalue-based hyperbolic systems 88
6.3.1 Steady equations 89
6.3.2 Some practical issues 92
6.3.3 A note on steady non-linear application 94
6.3.4 Unsteady equations 95
6.4 Boundary Conditions 97
6.5 Solution strategies 98
6.5.1 Steady flow solution by space marching 99
6.5.2 Unsteady flow solution by time stepping 100
6.5.3 Steady flow solution using Newton's method 101
6.6 Appendix: Formulae for flux derivatives 102

7 Spatial Numerical Method **104**
7.1 Curvilinear and Cartesian coordinate systems 104
7.2 Global and local coordinate systems 105
7.3 Finite-element discretization 106
7.4 Method of weighted residuals 108
7.5 Choice of weight functions 108
7.5.1 Upwinding the scalar wave equation 110
7.5.2 Complete upwinding for a coupled system 113

7.5.3 Simplified upwinding for a coupled system 114
7.6 Appendix I: Relevant variables in general orientations 117
7.7 Appendix II: Streamline upwinding applied to a model problem 119

8 Application I: Bidirectional Crossflow **121**

8.1 Choice of additional equation 122
8.1.1 Ill-conditioning property of equation system 123
8.1.2 Possible remedies 124
8.2 Calculation with periodic outer-edge velocity 126
8.3 Validation of equation system 129

9 Application II: Separated Flows **135**

9.1 Separation and singularities in the equations 136
9.1.1 Two-dimensional flow 136
9.1.2 Three-dimensional flow 137
9.1.3 Ill-conditioning of residual Jacobian matrix 142
9.2 A fully-simultaneous coupling scheme 143
9.2.1 Inviscid flow 144
9.2.2 Incorporation of displacement effects 146
9.2.3 Equivalent boundary-layer parameters 147
9.2.4 Direct and interactive algorithms/data structures 149
9.2.5 A word on the mathematical nature of the coupled system 152
9.3 Calculation of a separated flow 152

10 Concluding Remarks **159**

10.1 Hyperbolic integral-equation systems 159
10.2 Application of streamline upwinding 160
10.3 Well-conditioned system for bidirectional flows 160
10.4 Fully-simultaneous Panel coupling for general systems 160

10.5 Other contributions . . . 161
10.6 Recommendations for future work . . . 161

Bibliography **163**

List of Figures

1-1 Streamwise and cross-stream velocity components in a typical three-dimensional boundary layer. 19

1-2 Unidirectional and bidirectional crossflows in a three-dimensional boundary layer. . . 20

1-3 The distinction between (a) streamline-aligned Cartesian coordinates and (b) streamline curvilinear coordinates. 25

2-1 Variation of the weight function with increasing values of k_u ($k_w = 0$) for a Blasius boundary layer. 44

4-1 A characteristic surface defined by the family of subcharacteristics through a wall-normal line. In steady flow, the subcharacteristics are streamlines; in unsteady flow, they are pathlines. 64

4-2 Characteristic nature of the steady differential equations, (a) a streamline (subcharacteristic) on the wall-normal, (b) the characteristic surface tangent to the streamline, (c) influence and dependence zones defined by normal surfaces containing the outermost streamlines on the wall normal. 66

4-3 The surface swept by the $(\mathbf{x}_0, t_0)$ streakline in the time interval $4\Delta t$. 67

4-4 Characteristic nature of the unsteady differential equations, (a) a pathline (subcharacteristic) and streakline $(t-t_0)$ on the wall-normal, (b) characteristic surface tangent to the pathline, (c) influence and dependence volumes V_0 defined by normal surfaces containing the outer-most streaklines and pathlines. Here, the length of the pathline is given by $l(t) = \int_{t_0}^{t} q_e(x(t'), z(t'), t')dt'$. These volumes are an estimate of the range of influence and domain of dependence for $(t - t_0)/T_{ref} \ll 1$. 68

5-1 (a) Characteristic directions for a steady third order integral system for unidirectional and bidirectional crossflows. (b) Characteristic lines in $(\mathbf{x}, t)$ emanating from a point (x_0, z_0, t_0) and the characteristic velocity implied by their slope. 74

5-2 The kinetic-energy shape factor (H^*) variation and resulting normalized characteristic directions for Johnston's crossflow model. 83

6-1 Characteristic equations of the original and augmented coefficient matrices for N=2, (a) real eigenvalues with sufficient conditions $u_j v_j > 0 \ \ \forall j$, as shown, or $u_j v_j < 0 \ \ \forall j$, indicated by the intersection of the thick lines with the constant σ line, (b) complex eigenvalue pair if the hyperbolicity conditions are not met. 88

6-2 Inward-pointed characteristic line indicating the necessity to impose a Dirichlet-type boundary condition. 97

6-3 A space-marching solution algorithm for the eigenvalue-based method applied to the steady equations under the paradigm where the eigenvalue is replaced only if complex in the *laissez-faire* system. 98

7-1 The normal vector and coordinate system for an element. 106

7-2 Weight functions for the Galerkin, Crank-Nicolson and characteristic upwinding ($\alpha = 0.5$) schemes for a characteristic oriented, as shown, at an angle of 30^0 with respect to the s-axis. 109

7-3 Element size in characteristic direction. 112

7-4 The effects of different weight functions: contours of δ_2^* (20 steps from -0.0002 to 0.00001, 30 $\times$ 30 elements) with boundary conditions $\delta = 0.1$, $c = 0.0$ on the left ($x = 0$), $\delta = 0.01$, $c = 0.5$ at the bottom ($z = 0$), and $H = 2.6$ on both edges. The external velocity components are $u_e = 1.0$ and $w_e = 0.5$. (a) Galerkin weighting, (b) Crank-Nicolson weighting in the x direction, (c) upwind weighting with $\alpha = 1$ and $\hat{\mathbf{e}}_k = 0^0$, (d) upwind weighting with $\alpha = 1$ and $\hat{\mathbf{e}}_k = 20^0$. 116

7-5 Upwinding weight function (solid line) compared to the Galerkin weight function (dashed line) in one dimension. Here the flow is from left to right. 119

8-1 Imposed velocity and calculated streamwise displacement thickness 127

8-2 Calculated shape factor and the two empirical crossflow parameters 128

8-3 Calculated crossflow displacement thickness and skin friction 128

8-4 (a) Outer-edge streamlines and comparison stations. (b) Imposed chordwise outer-edge velocity distribution. 129

8-5 Comparison of calculated shape factor and momentum Reynolds-number distributions. The solid line is for the integral system solution. 131

8-6 Comparison of calculated displacement-thickness components. 131

8-7 Comparison of calculated skin-friction components. 132

8-8 Comparison of velocity profiles computed by the finite-difference method (thin lines) with those computed from the integral solution (bold lines). The streamwise profiles are too close to be differentiable here. 134

9-1 The physical separation line (envelope of coalescing limiting wall streamlines shown as thick lines) contrasted with the direct-mode mathematical singularity line (envelope of coalescing outer-most characteristic lines shown as thin lines) in the diverging flow in front of a blunt obstacle. Also marked are two features of special interest. 139

9-2 The determinant of the residual Jacobian matrix near separation. 143

9-3 The variation of the wall-normal component of mass flux in real viscous flow (RVF) and equivalent inviscid flow (EIF). 147

9-4 Nodal neighbors of i. 149

9-5 Main features of the direct-mode algorithm. 150

9-6 Main features of the interactive-mode algorithm. 151

9-7 (a) Surface-relief contours and computational grid. (b) Profile (not-to-scale) of surface along diagonal. 154

9-8 (a) Selected outer-edge velocity streamlines, and boundaries where the input conditions are applied. (b) Outer-edge velocity magnitude along streamwise diagonal. . . 155

9-9 (a) Selected limiting wall streamlines. (b) Close-up detail of separated region. 155

9-10 (a) Momentum Reynolds-number contours. (b) Variation along streamwise diagonal. 156

9-11 (a) Boundary layer thickness parameter contours. (b) Variation along streamwise diagonal. 156

9-12 (a) Crossflow magnitude parameter contours. (b) Variation along cross-stream diagonal.157

9-13 (a) Shape-factor contours. (b) Variation along streamwise diagonal. 157

9-14 Velocity profiles at stations A,B and C. 158

List of Tables

2.1 The value of exponents in the parent integral equation corresponding to individual equations. 43

8.1 Calculated boundary-layer parameters from the integral system calculation which are used to generate the velocity profiles for comparison with the finite-difference solution. 132

Nomenclature

Roman symbols

D	dissipation integral
F	entrainment coefficient
H	shape factor
H^*	kinetic-energy shape factor
M	Mach number
N	finite-element interpolation function
Re	Reynolds number
W	finite-element weight function
c	crossflow magnitude measure
c_f	skin friction
k	weight function exponent
	streamline upwinding coefficient
m	mass flux
n	Cartesian coordinate normal to streamline
	exponent
p	pressure
q	velocity magnitude
r	recovery factor
	radius of curvature
s	Cartesian coordinate aligned with streamline
t	time
u	velocity component along x or s
v	wall-normal velocity component
w	velocity component along z or n
x, y, z	Cartesian coordinates

Greek symbols

Δ	element length scale
Δ_{map}	mapping function
Λ	Pohlhausen parameter
Ω	characteristic surface
Φ	total potential

α	auxiliary parameter
β	characteristic angle
γ	ratio of specific heats
δ	boundary-layer thickness
ζ	profile parameter
	density profile mode
σ	panel source strength
η	curvilinear coordinate normal to streamline
	scaled wall-normal coordinate
η_0	laminar profile-family parameter
λ	eigenvalue
μ	kinematic viscosity
ν	dynamic viscosity
ξ	curvilinear coordinate along streamline
ρ	density
τ	shear stress
ψ	u velocity profile mode
ϕ	integration weight function
	w velocity profile mode
	perturbation potential

Integral quantities

$\vec{\delta}^*$	displacement thickness vector
$\vec{\delta}^**$	density thickness vector
$\vec{\theta}_x$	x-direction momentum thickness vector
$\vec{\theta}_z$	z-direction momentum thickness vector
$\vec{\theta}^*$	total kinetic-energy thickness vector
$\vec{\vartheta}$	kinematic displacement thickness vector
$\vec{E}_m$	mixed-component kinetic-energy thickness vector
$\vec{E}_x$	x-direction kinetic-energy thickness vector
$\vec{E}_z$	z-direction kinetic-energy thickness vector

Matrices and vectors

$\mathbf{\Lambda}$	diagonal matrix of eigenvalues
$\mathbf{D}, \mathbf{P}$	influence matrices
$\mathbf{I}$	identity matrix
$\mathbf{J}$	*laissez-faire* Jacobian
$\mathbf{K}$	hyperbolic-method Jacobian
	diagonal matrix of upwinding coefficients
$\mathbf{X}$	eigenvectors
$\mathbf{b}$	auxiliary parameter sensitivities
$\mathbf{f}, \mathbf{g}$	fluxes
$\mathbf{e}$	characteristic tangent vector
$\mathbf{h}$	source terms

$\mathbf{p}$	empirical profile parameters
$\mathbf{q}$	velocities
$\mathbf{r}$	residuals
$\mathbf{u}$	conserved quantities
$\mathbf{v}$	characteristic variables
ι, n, k	coordinate vectors

Subscripts, superscripts and accents

$()_\infty$	freestream
$()_I$	non-perturbed inviscid velocity
$()_1$, $()_s$	streamline aligned
$()_2$, $()_n$	cross-stream aligned
$()_b$	boundary
$()_c$	cosine
$()_e$	value at boundary-layer outer edge
$()_{ep}$	equivalent parameter
$()_k$	element number
	characteristic aligned
$()_l$	local node number
$()_i, ()_j, ()_m$	global node numbers
$()_s$	sine
$()_t$	time coordinate
$()_v$	characteristic
$()_w$	value at wall
$()^+$	wall-scaled variable
$\overline{()}$	meanflow component, incompressible variable, etc.
	wall-parallel quantity
	quantity evaluated at $\delta, c = 1$
$\tilde{()}$	mass-weighted variable
	RBLP vector
$\hat{()}$	unit-length vector
	local residual
$()'$	fluctuating component
	differentiation
	elemental coordinate

Acronyms

EBLP	equivalent boundary-layer parameters
EIF	equivalent inviscid flow
RBLP	real boundary-layer parameters
RVF	real viscous flow
SUPG	Petrov-Galerkin streamline upwinding

Chapter 1

Introduction

1.1 Context and general objectives

The ability to predict viscous flows in three dimensions quickly is essential for the modern designer. To this end, against a background of progressively increasing computational resources, a hierarchy of general approaches of varying sophistication have been proposed in the literature. Near the apex are optimization codes that solve the complete Navier-Stokes equations. More economical, however, are codes of less generality based on viscous-inviscid interaction techniques that use the boundary-layer equations to solve the viscous flow physics. Such approaches can be very effectively applied to design efforts [44, 55].

Boundary-layer solution methods are based on either the full differential equations or some integral approximation of these equations. The economy of using the differential boundary-layer equations compared to the Navier-Stokes equations is eroding with time. However, there are two major factors that work in their favor that will keep them in the designer's tool box for the foreseeable future. The first is the remarkable success of the boundary-layer concept itself which has been convincingly demonstrated by a large corpus of research in the literature. The second, which applies to turbulent flows, is the necessity for an empirical turbulence model which masks the formal accuracy of retaining the higher-order terms in the Navier-Stokes equations. Consequently, within a design framework, there is an enduring justification not to resort to solving the full Navier-Stokes equations regardless

of the diminishing relative economies of cost.

Much of the improved economy of the boundary-layer approximation results from the change in the mathematical character of the equations which allows attached, and with special techniques even separated, flows to be solved by marching algorithms. Furthermore, a large body of research has led to substantial insight into the physical behavior of viscous flows as a function of distance in the wall-normal direction. This naturally has driven the development of integral solution methods for the boundary-layer equations resulting in significant computational savings. Very roughly, solving the integral equations amounts to an N^2 effort compared to an N^3 one for the differential boundary-layer equations. Moreover, many comparative studies have shown that integral methods are, on average, just as accurate as differential ones [63].

In going from the Navier-Stokes equations to the differential boundary-layer equations, the mathematical character changes from one that is elliptic (boundary value problem) to one that is hyperbolic (initial value problem). This metamorphosis is understood well and, furthermore, related problems associated with separation have been mastered to an adequate degree with the development of viscous-inviscid interaction schemes. On the other hand, the applicability of this change in character to the integral equations has received scant mention in the literature. In view of the variety of systems possible and of the pivotal importance of the character in devising numerical schemes, this paucity represents an enormous gap in the theory and implementation of integral equation systems. Much of the focus of this thesis is an attempt to fill this gap for direct-mode boundary-layer equation systems.

There are two other objectives of this thesis. One is to develop and validate a general integral system for predicting bidirectional crossflows suitable for Newton/implicit solution methods. The second is to develop a method to simultaneously couple integral boundary-layer systems to an inviscid flow without restricting the ability to use different assumed closure models within it.

1.2 General features of a three-dimensional boundary layer

A three-dimensional boundary layer is characterized by the existence of a cross-stream component of velocity. It is customary to refer to the velocity component in the streamwise direction, namely the component projected in the plane of the outer-edge streamline tangent, as streamwise flow and the component in the cross-stream direction as crossflow. These two components are used as convenient

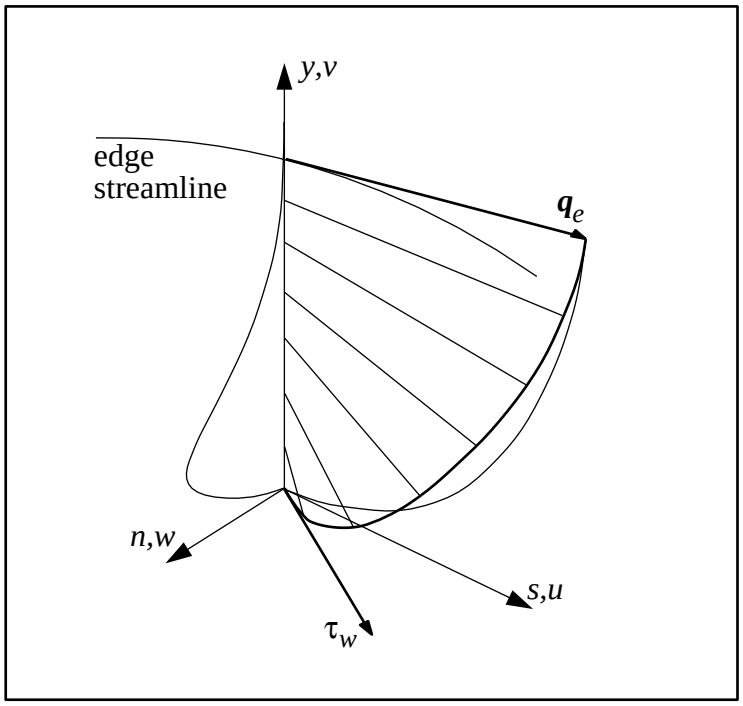

Figure 1-1: Streamwise and cross-stream velocity components in a typical three-dimensional boundary layer.

graphical representations for the wall-normal boundary-layer velocity-vector distribution as shown in Figure 1.1.

The predominant physical mechanism for the generation of crossflow in an aeronautical context is a cross-stream (or transverse) pressure gradient indicated in Figure 1.1 by the curvature of the outer-edge streamline. The lower-momentum fluid near the wall responds more rapidly to the pressure gradient than higher-momentum fluid nearer the edge thereby skewing the velocity vector across the boundary layer.

The same mechanism can cause the velocity vector to skew is such a way so as to produce crossover profiles. Figure 1.2 shows the skewing in the crossflow resulting from a change in the direction of the cross-stream pressure gradient. In Figure 1.2, limiting streamlines are also indicated. These correspond to surface oil-flow trace lines in visualization experiments and are tangent to the shear-stress gradient vector at the wall shown in Figure 1.1. Crossflows can also be generated by shear gradients.

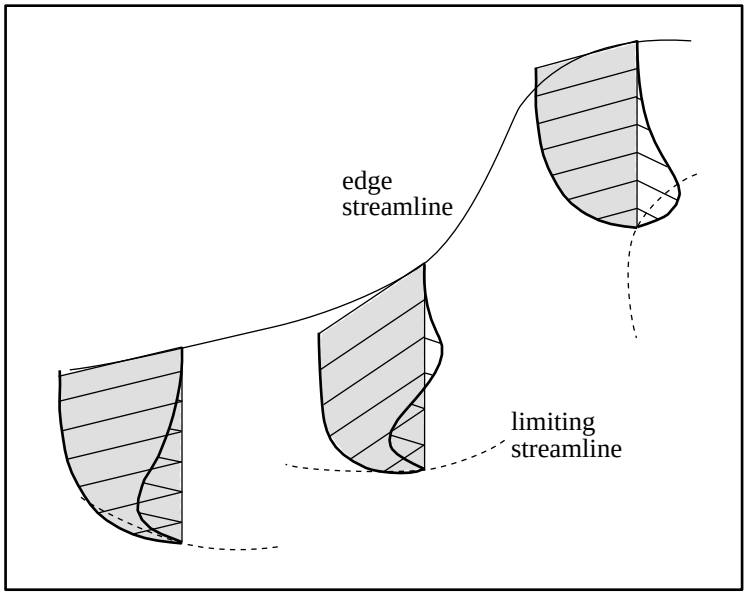

Figure 1-2: Unidirectional and bidirectional crossflows in a three-dimensional boundary layer.

1.3 Brief literature survey

A variety of integral solution methods for three-dimensional boundary layers have been devised dating as far back as one by Prandtl. In the 1960's, their number proliferated rapidly, most based on a frequently-used three-equation system. More sophistication in both physical modeling and in the use of additional equations for greater flexibility has since resulted.

Before presenting a representative survey of methods described in the literature, it will be important to highlight the use of different coordinate systems. The equations solved in this thesis are all posed in conservation form in simple Cartesian coordinate systems and solved using the finite-element (or finite-volume) method. This approach was devised in the author's Masters thesis [40, 41], and was refined by Nishida [44]. It is significantly different from the approach invariably used in the literature. This traditional approach is driven by finite-difference numerical schemes and involves the use of equations posed in orthogonal or non-orthogonal curvilinear coordinates. The resulting equations are analytically cumbersome and require the explicit numerical approximation of coordinate metrics and curvatures and often also the careful prior consideration of streamline orientation (which can place awkward limits on the computational scheme). Under the new approach, the *analytical* approximation of grid stretching and curving is obviated, the need fulfilled conveniently and simply at the *numerical* level through the finite-element method.

In the surveys that follow, references are made to equations and models of physical behavior that are described in greater detail in the body of this thesis. The list is not meant to be exhaustive, merely representative of methods presented in the literature. Salient features of some 'conventional' integral methods are summarized first followed by those of a few closely related ones.

1.3.1 Conventional integral methods

Hall (1959), Cooke (1961)

In one of the earliest methods devised for computing three-dimensional boundary layers, Hall [27] used the two momentum equations in curvilinear streamline coordinates with a closure scheme that was an extension of Thwaites' method in two dimensions for laminar flow. A very similar method was also described by Cooke [6].

Smith (1966, 1972), Cumpsty and Head (1967), Myring (1970)

Smith developed methods based on the two momentum equations and the entrainment equation on curvilinear orthogonal [53], and later on non-orthogonal [54], curvilinear coordinates for turbulent flow. Simple one-parameter streamwise profiles (power law) and cross-stream profiles (Mager, Johnston) were used. Cumpsty and Head [12, 13] used the same system and closure scheme to compute turbulent flows on a wing. Myring's [42] method served as the prototype for Smith's non-orthogonal one. Myring's paper is also notable in that it contains the first detailed study of the nature of the resulting integral system, which was performed for both Mager's and Johnston's crossflow models.

Stock (1977)

Stock [56] augmented Myring's method for turbulent flow with two additional equations, the first for the streamwise variation of skin friction based on a two-parameter assumed velocity profile, and the second for the source term in the entrainment equation. The second equation was a lag-type equation to account for upstream history effects in the streamwise direction. For laminar flow, in order to allow for bidirectional cross-stream velocities, crossflow profiles were constructed in a somewhat ad-hoc manner to ensure symmetry and correct cross-over directions. The equation system used for the laminar calculations were the two momentum equations (called the "x-pulse" and "y-pulse" equations) and the two kinetic-energy component equations (called the "moment of momentum" equations).

Cousteix and Houdeville (1981), Cousteix (1986)

In a series of papers [7, 8, 9, 10], the authors use Myring's system, with their own closure relation-

ships, to investigate the nature of singularities in the equations for turbulent flow. Furthermore, with approximate one-parameter closure (neglecting Reynolds number dependence) for the streamwise flow and Johnston's crossflow model, the system was demonstrated to be hyperbolic [10]. In reality, the closure relationships in this characteristic analysis differ very slightly from those in Myring's original investigation. However, the authors further demonstrate an analogy between steady three-dimensional flow and mildly unsteady two-dimensional flow to illustrate the difference between separation lines and singularity lines.

Yoshihara and Wai (1984)

Yoshihara and Wai [72] solve for separated flow over a wing using a four-equation system comprising the entrainment equation, the two momentum equations and Green's lag entrainment equation [26]. A characteristic analysis reveals regimes of non-hyperbolic behavior and is used to restrict the operating range to the hyperbolic regime. The solution is marched in direct mode using the method of characteristics to ensure compliance with domain of dependence constraints. The difficulty posed by the separation line, near which only a unique external pressure gradient is admitted by the equations, is dealt with by explicitly modifying the source terms in the characteristic-basis ordinary differential equations to comply with compatibility conditions. Downstream of the separation line, a sign of the characteristic marching coordinate is reversed to satisfy flow of information constraints.

Swafford and Whitfield (1985)

Swafford and Whitfield [59] use time-dependent versions of the two momentum equations and the total kinetic-energy equation in their system formulated for non-orthogonal curvilinear coordinates. Steady-state solutions are computed by explicit time stepping using a Runge-Kutta scheme. Time-dependent pressure gradient terms are neglected in the transient solution. Side boundary conditions are not applied; the solution is simply extrapolated from the interior. Johnston's model for the crossflow is used, which, as demonstrated in this thesis with similar streamwise closure, yields a hyperbolic system. Consequently, the authors are able to use backward (upstream) space differencing in their discretization scheme obviating the need for explicit artificial smoothing. However, the CFL condition for the size of time steps with this scheme is twice as restrictive compared to that for central differencing.

Karimipanah and Olsson (1992)

Karimipanah and Olsson [31] use Myring's system in curvilinear streamline coordinates to investigate the effects of rotation and compressibility on rotor-blade boundary layers. Empirical closure is based on formulae devised by Michel et. al. [24].

Mention should also be made of several methods based on small-crossflow assumptions (where the streamwise flow is computed first and then used to compute the crossflow) that have been used in the literature [2, 50].

1.3.2 Related methods

It may be worthwhile to briefly mention three techniques described in the literature that are related to conventional integral methods.

Caille and Schetz (1992)

Caille and Schetz [4] extend the two-dimensional strip integral method of Moses to turbulent boundary layers in three dimensions. The usual integral-momentum equations, which extend from the wall to the boundary layer edge, are supplemented by two additional integral equations for momentum extending from the wall to an arbitrary point in the boundary layer. The latter two equations are not used in conventional integral methods. The solution is space marched using a Runge-Kutta scheme.

Degani and Walker (1992)

Degani and Walker [14, 15] replace the wall region in a conventional three-dimensional turbulent solution method by analytical functions based on an asymptotic analysis of the region in the limit of infinite Reynolds number [16, 17]. The outer region is calculated as in conventional differential calculations and the wall boundary condition is replaced by a criterion for smooth transition from the outer solution to the embedded analytical function. Corrections to leading order (in terms of the pressure-gradient parameters) are made to account for non-collateral conditions near the wall. The method appears to be accurate and is about twice as economical as conventional differential solvers.

Holt (1984)

Holt [29] applies Dorodnytsin's Method of Integral Relations to the three-dimensional boundary-layer equations. The *gradients* of velocity in the wall-normal direction are expanded in a power series of the velocity components (the whole series suitably scaled by the asymptotic behavior of velocity in y) are used to evaluate the integrals in a number of moment-of-momentum equations. The result is an equal number of lower-order differential equations for the velocity gradients at equally-spaced locations across the boundary layer. The number of equations used is based on the number of terms in the series expansion. Holt also makes a clever modification to the original moment-of-

momentum method by replacing the usual set of weighting functions with its orthonormal version. This effectively removes the need to invert a matrix because it decouples the unknowns, which are the velocity-gradient values, from one another.

1.4 Overview of thesis

In Chapter 2, compact and systematic derivations of common integral equations are presented. These are supplemented by the derivation of an unsteady 'parent' integral equation from which all the individual equations used here fall out. Chapter 3 is devoted to the discussion of empirical models used to close equation systems. In Chapter 4, the nature of the unsteady *differential* equations is presented and used to motivate the requirements on the nature of integral systems which are discussed in Chapter 5. The practical realization of these requirements for direct-mode integral boundary-layer systems, which constitute the major contribution of this thesis, are discussed in Chapter 6. A description of the finite-element method applied to the equations, in particular the implementation of streamline upwinding, is presented in Chapter 7. The computation of bidirectional crossflows is the subject of Chapter 8. In Chapter 9, separation-related singularities are briefly discussed followed by the description of a viscous-inviscid interaction method to compute simple separated flows. Finally, the original contributions of this work are summarized in Chapter 10 with some recommendations for future work.

The thesis essentially has three main parts. The first, Chapters 2 and 3, deal with traditional issues. The second, Chapters 4 to 6, are used to justify and construct a useful closure model for hyperbolicity. However, this model is not actually implemented in the third part, Chapters 7 to 9, because in the bidirectional flow examples it is not applicable, while in the separated flow example, the usual closure model is used on the *assumption* that the system is hyperbolic (numerically verified). This work does not rest on the development of one single method, rather it is concerned with several different issues that share a common theme.

There may be instances of ambiguity in the meaning of some terms used in the text of the thesis. It may be useful, at this juncture, to clearly draw attention to them:

1. The terms wall and surface are used interchangeably. Of course, the latter is not to be confused with the mathematical notion of a characteristic surface.
2. The term order is used to refer both to the number of equations in a system as well as to the

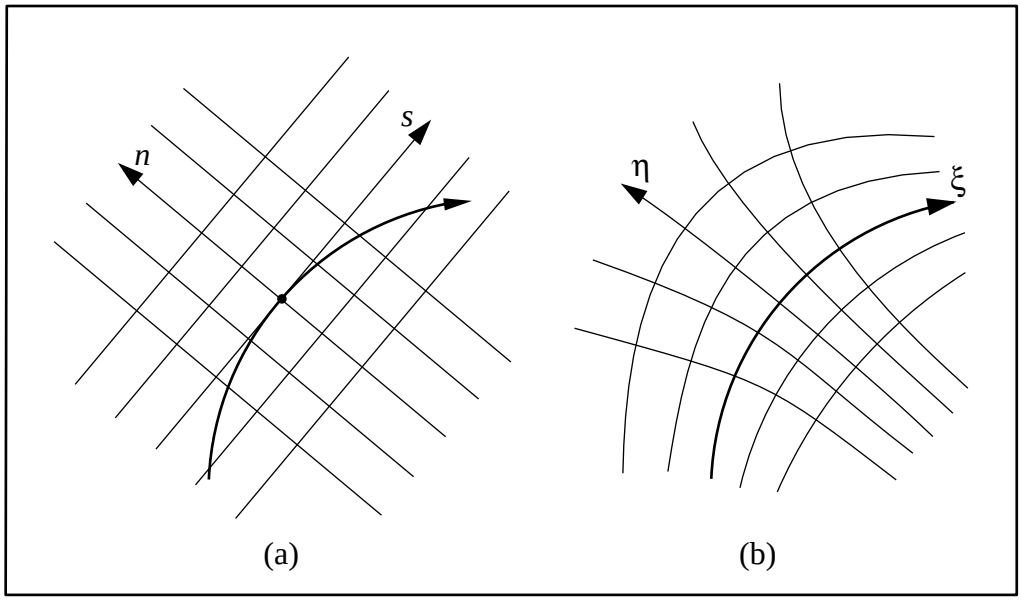

Figure 1-3: The distinction between (a) streamline-aligned Cartesian coordinates and (b) streamline curvilinear coordinates.

degree of the highest derivative in an equation.

3. The "differential" equations refer only to the starting boundary-layer equations from which integral equations are derived. The integral equations are, of course, also differential equations but are generally not referred to as such.

4. There is a distinction between derivative-term Jacobian matrices and the residual-vector Jacobian matrix (which includes source-term dependence).

5. In this thesis, streamline coordinates will always mean Cartesian coordinates aligned with the outer-edge streamline at some point ($w_e \equiv 0, \frac{\partial w_e}{\partial s} \neq 0$). In the literature, streamline coordinates usually mean curvilinear orthogonal coordinates embedded in the external streamline field ($w_e \equiv 0, \frac{\partial w_e}{\partial s} \equiv 0$). The difference is illustrated in Figure 1.4.

Chapter 2

Derivation of Integral Equations

This chapter contains compact derivations of integral equations used in this thesis and also commonly used in the literature. The starting equations are the differential boundary-layer equations. The algebra involved, which can become quite tedious, is facilitated by the use of special notation used only in this chapter.

Steady forms of each of the individual equations are derived first. The process is then generalized so that all of the individual equations can be written in a single common form called the parent integral equation. This equation is also extended to include unsteady forms of the equations and clearly shows the sequential nature of the individual equations as part of an infinite series of moment-of-momentum equations. It can also be used to illustrate the differences in the quality of information contained in the individual equations. The chapter ends with a discussion on the construction of practical systems of integral equations.

It has already been mentioned that, in this thesis, advantage is taken of the finite-element method to allow the use of simple Cartesian coordinates for the equations. Hence, only Cartesian coordinates are considered here. For the interested reader, a brief derivation of the unsteady forms of the momentum and total kinetic energy-equations, in non-orthogonal curvilinear coordinates, is provided by Swafford and Whitfield [59].

2.1 Differential equations

The first-order ($\delta/r_{min} \ll 1$) differential boundary-layer equations for compressible flow expressed in Cartesian coordinates are

$$\frac{\partial \rho}{\partial t} + \nabla \cdot (\rho \mathbf{q}) = 0$$

$$\rho \frac{\partial u}{\partial t} + \rho \mathbf{q} \cdot \nabla u + \frac{\partial p}{\partial x} = \frac{\partial \tau_x}{\partial y}, \quad \tau_x = \mu \frac{\partial u}{\partial y} - \rho \overline{u'v'}$$

$$\rho \frac{\partial w}{\partial t} + \rho \mathbf{q} \cdot \nabla w + \frac{\partial p}{\partial z} = \frac{\partial \tau_z}{\partial y}, \quad \tau_z = \mu \frac{\partial w}{\partial y} - \rho \overline{w'v'}$$

For turbulent flow, the equations are ensemble averaged after the addition of a small fluctuating component to meanflow quantities. The shear-stress terms contain the usual wall-parallel Reynolds stresses. In the continuity equation, the assumptions $\overline{\rho' u'} \ll \bar{\rho}\bar{u}$ and $\overline{\rho' w'} \ll \bar{\rho}\bar{w}$ have been made, consistent with boundary-layer theory. The third fluctuating component $\overline{\rho' v'} = \mathcal{O}(\bar{\rho}\bar{v})$ cannot be neglected, however. The problem is conveniently skirted by the introduction in both the continuity equation and the momentum equations of a mass-weighted velocity in the wall-normal direction [1]

$$\tilde{v} = \left(\bar{\rho}\bar{v} + \overline{\rho' v'}\right) / \bar{\rho}\,.$$

Therefore, for turbulent flow in the equations above, the velocity vector $\mathbf{q} = u\hat{\imath} + \tilde{v}\hat{\jmath} + w\hat{k}$, where the overbar notation for meanflow quantities has been dropped (and will be dropped henceforth) for brevity. The wall-normal pressure gradient is only first order in δ/r_{min} and is normally neglected in first-order boundary-layer theory. In turbulent flow, this pressure gradient can also result from the wall-normal gradient of a component of the Reynold's stress tensor $\rho\overline{v'v'}$. This mechanism is ignored here but may not be negligible in supersonic flows with adverse pressure gradients [68].

In this thesis, the objective is the solution of steady-state flows. The unsteady terms are included to aid discussion of the eigenvalue problem in later chapters. Furthermore, only adiabatic conditions are of interest. Therefore, the enthalpy equation can be replaced by the algebraic Crocco-Busemann relation (for temperature in terms of velocity), which when combined with the equation of state relates density directly to the velocity and outer-edge Mach number. The velocity used here is the total magnitude but it may be approximated by the streamwise component

$$\frac{\rho}{\rho_e} = \left(1 + r\frac{\gamma - 1}{2} M_e^2 (1 - \frac{q^2}{q_e^2})\right)^{-1}.$$

The recovery factor r has different values in laminar and turbulent flows. The Crocco-Busemann relation is an excellent approximation to the enthalpy equation for adiabatic, near-unity Prandtl number laminar and turbulent flows, even with pressure gradients [49, 68].

2.1.1 Boundary conditions

The wall and outer-edge boundary conditions for the differential equations are

$$\mathbf{q} = \mathbf{0},\ \rho = \rho_w \ \text{ if } y = 0,$$

$$u = u_e(x,z),\ w = w_e(x,z),\ \rho = \rho_e(x,z),\ \tau_x = 0,\ \tau_z = 0 \ \text{ if } y = \delta.$$

for a direct-mode calculation. The subscripts w and e are adopted to denote wall and outer-edge conditions. Note that at the edge, prescription of the two wall-parallel velocities and the density automatically fixes v_e through the equations. Furthermore, the fluctuating component $[\overline{\rho' v'}]_e \approx 0 \Rightarrow \tilde{v}_e = v_e$ [42].

Of more relevance to the derivations that follow is the following consequence of first-order boundary-layer theory at the outer edge:

$$\frac{\partial u_e}{\partial y} = 0\,, \quad \frac{\partial w_e}{\partial y} = 0$$

Furthermore, since the Reynolds stresses also vanish at the edge in turbulent flow

$$\frac{\partial \tau_{e_x}}{\partial y} = 0\,, \tag{2.1}$$

$$\frac{\partial \tau_{e_z}}{\partial y} = 0\,. \tag{2.2}$$

2.2 Derivation of steady integral equations

2.2.1 Preliminaries

Integral equations are derived by integrating special combinations of the differential equations along the y-axis, from the wall to the boundary-layer outer edge. The process of integration aims to reduce the equations from three space dimensions to two. The integration algebra is facilitated by defining some notation and mathematical rules.

Notation

Define the total and wall-parallel gradient operators respectively as

$$\nabla = \frac{\partial}{\partial x}\hat{\imath} + \frac{\partial}{\partial y}\hat{n} + \frac{\partial}{\partial z}\hat{k}, \quad \bar{\nabla} = \frac{\partial}{\partial x}\hat{\imath} + \frac{\partial}{\partial z}\hat{k}$$

and the corresponding total velocity and wall-parallel velocities as

$$\mathbf{q} = u\hat{\imath} + \tilde{v}\hat{n} + w\hat{k}, \quad \bar{\mathbf{q}} = u\hat{\imath} + w\hat{k}\,.$$

The overbar notation in used only in this chapter; in other chapters, it is dropped for clarity. It should also not be confused with the usual notation for meanflow quantities in turbulent flow (which are implied here). In other chapters, both the gradient operator and velocity vector are assumed meant in the wall-parallel sense. Define also the wall-parallel edge velocity magnitude $\bar{q}_e = |\bar{\mathbf{q}}_e|$. Note that the normal velocity component is mass-weighted.

Algebraic identities

The following three identities will be helpful in facilitating the integration algebra. In the derivations that follow, their use will be indicated by Roman numerals at the end of the step.

For a vector function $\phi(x, y, z)\mathbf{q}$ where

$$\phi = 0 \text{ if } y = \delta\,,$$

the following identity holds

$$I: \quad \int_0^\delta \bar{\nabla} \cdot \phi \bar{\mathbf{q}} \, dy \equiv \int_0^\delta \nabla \cdot \phi \mathbf{q} \, dy \, .$$

Furthermore, if ϕ also vanishes for $y > \delta$, Leibnitz's rule states that (by allowing the integration to tend to ∞)

$$II: \quad \bar{\nabla} \cdot \int_0^\delta \phi \bar{\mathbf{q}} \, dy \equiv \int_0^\delta \bar{\nabla} \cdot \phi \bar{\mathbf{q}} \, dy \, .$$

The final identity is a consequence of first-order boundary-layer theory because at the outer edge, the wall-normal gradient of $\bar{\mathbf{q}}_e$ is neglected. Therefore

$$III: \quad \bar{\nabla} u_e \equiv \nabla u_e \, , \quad \bar{\nabla} w_e \equiv \nabla w_e \, .$$

Pressure-gradient terms

The pressure-gradient terms can be expressed in terms of inviscid velocities and density by evaluating the momentum equations at the outer edge

$$\frac{\partial p}{\partial x} = -\rho_e \mathbf{q}_e \cdot \nabla u_e = -\rho_e \bar{\mathbf{q}}_e \cdot \bar{\nabla} u_e \quad (III)$$

$$\frac{\partial p}{\partial z} = -\rho_e \mathbf{q}_e \cdot \nabla w_e = -\rho_e \bar{\mathbf{q}}_e \cdot \bar{\nabla} w_e \quad (III)$$

For irrotational external flows $\nabla \times \mathbf{q} = \mathbf{0}$. This simplifies for first-order boundary layers to

$$\left| \bar{\nabla} \times \bar{\mathbf{q}}_e \right| = 0 \quad \Rightarrow \frac{\partial w_e}{\partial x} = \frac{\partial u_e}{\partial z} \quad \Rightarrow \bar{\nabla} u_e = \frac{\partial \bar{\mathbf{q}}_e}{\partial x}, \; \bar{\nabla} w_e = \frac{\partial \bar{\mathbf{q}}_e}{\partial z} \tag{2.3}$$

$$\frac{\partial v_e}{\partial x} = 0 \tag{2.4}$$

$$\frac{\partial v_e}{\partial z} = 0 \tag{2.5}$$

of which the first can be used to simplify the external velocity-gradient terms in some of the derived integral equations.

2.2.2 Entrainment equation

A form of the integral entrainment equation can be derived by integrating the continuity equation in defect form:

$$\int_0^\delta \nabla \cdot (\rho_e \mathbf{q}_e - \rho \mathbf{q})\, dy = 0$$

$$\int_0^\delta \bar{\nabla} \cdot (\rho_e \bar{\mathbf{q}}_e - \rho \bar{\mathbf{q}})\, dy = -\int_0^\delta \frac{\partial \rho_e v_e}{\partial y}\, dy + \int_0^\delta \frac{\partial \rho v}{\partial y}\, dy$$

$$\bar{\nabla} \cdot \int_0^\delta (\rho_e \bar{\mathbf{q}}_e - \rho \bar{\mathbf{q}})\, dy = \int_0^\delta \left(\frac{\partial \rho_e u_e}{\partial x} + \frac{\partial \rho_e w_e}{\partial z} \right) dy + \rho_e v_e \quad (II)$$

$$\bar{\nabla} \cdot \int_0^\delta (\rho_e \bar{\mathbf{q}}_e - \rho \bar{\mathbf{q}})\, dy = \delta \left(\frac{\partial \rho_e u_e}{\partial x} + \frac{\partial \rho_e w_e}{\partial z} \right) + \rho_e v_e$$

where

$$\rho_e \bar{q}_e \vec{\delta^*} = \int_0^\delta (\rho_e \bar{\mathbf{q}}_e - \rho \bar{\mathbf{q}})\, dy \quad \text{(displacement-thickness vector)}$$

Rewriting

$$\bar{\nabla} \cdot (\rho_e \bar{q}_e \vec{\delta^*}) = \delta\, \bar{\nabla} \cdot \rho_e \bar{\mathbf{q}}_e + \rho_e v_e$$

In the literature, this equation is more frequently written as

$$\bar{\nabla} \cdot \rho_e (\bar{\mathbf{q}}_e \delta - \bar{q}_e \vec{\delta^*}) = \rho_e \bar{\mathbf{q}}_e \cdot \bar{\nabla} \delta - \rho_e v_e = F$$

where F is the dimensional rate of change of mass flow in the boundary layer (entrainment coefficient). Note that the fluctuating normal component at the outer edge $[\overline{\rho' v'}]_e \approx 0$ as indicated before is neglected.

2.2.3 Momentum equations

There are two momentum equation components governing the flux of momentum-deficit in the two coordinate directions x and z.

x-momentum

An equation of the Kármán type governing the flux of momentum deficit in the x direction is derived from:

$$\int_0^\delta (u-u_e)[\nabla\cdot(\rho\mathbf{q})] + [\rho\mathbf{q}\cdot\nabla u + \frac{\partial p}{\partial x} - \frac{\partial \tau_x}{\partial y}]\,dy = 0$$

$$\int_0^\delta \nabla\cdot(\rho\mathbf{q}(u-u_e)) - \rho\mathbf{q}\cdot\nabla(u-u_e) + [\rho\mathbf{q}\cdot\nabla u + \frac{\partial p}{\partial x} - \frac{\partial \tau_x}{\partial y}]\,dy = 0$$

$$\int_0^\delta \bar{\nabla}\cdot(\rho\bar{\mathbf{q}}(u-u_e)) - \rho\mathbf{q}\cdot\nabla u + \rho\mathbf{q}\cdot\nabla u_e + [\rho\mathbf{q}\cdot\nabla u + \frac{\partial p}{\partial x} - \frac{\partial \tau_x}{\partial y}]\,dy = 0 \quad (I)$$

$$\int_0^\delta \bar{\nabla}\cdot(\rho\mathbf{q}(u-u_e)) + (\rho\bar{\mathbf{q}} - \rho_e\bar{\mathbf{q}}_e)\cdot\bar{\nabla}u_e - \frac{\partial \tau_x}{\partial y}\,dy = 0 \quad (III)$$

$$\bar{\nabla}\cdot\int_0^\delta \rho\bar{\mathbf{q}}(u_e-u)\,dy + \bar{\nabla}u_e\cdot\int_0^\delta(\rho_e\bar{\mathbf{q}}_e - \rho\bar{\mathbf{q}})\,dy - \tau_{x_w} = 0 \quad (II)$$

where

$$\rho_e\bar{q}_e^2\vec{\theta_x} = \int_0^\delta \rho\bar{\mathbf{q}}(u_e-u)\,dy \quad \text{(x-direction momentum-thickness vector)}$$

τ_{x_w} (x-direction wall shear stress)

Rewriting

$$\bar{\nabla}\cdot(\rho_e\bar{q}_e^2\vec{\theta_x}) + \bar{\nabla}u_e\cdot(\rho_e\bar{q}_e\vec{\delta^*}) = \tau_{x_w}$$

z-momentum

Similarly for the z direction, consider:

$$\int_0^\delta (w-w_e)[\nabla\cdot(\rho\mathbf{q})] + [\rho\mathbf{q}\cdot\nabla w + \frac{\partial p}{\partial x} - \frac{\partial \tau_z}{\partial y}]\,dy = 0$$

$$\int_0^\delta \nabla\cdot(\rho\mathbf{q}(w-w_e)) - \rho\mathbf{q}\cdot\nabla(w-w_e) + [\rho\mathbf{q}\cdot\nabla w + \frac{\partial p}{\partial z} - \frac{\partial \tau_z}{\partial y}]\,dy = 0$$

$$\int_0^\delta \bar{\nabla}\cdot(\rho\bar{\mathbf{q}}(w-w_e)) - \rho\mathbf{q}\cdot\nabla w + \rho\mathbf{q}\cdot\nabla w_e + [\rho\mathbf{q}\cdot\nabla w + \frac{\partial p}{\partial z} - \frac{\partial \tau_z}{\partial y}]\,dy = 0 \quad (I)$$

$$\int_0^\delta \bar{\nabla}\cdot(\rho\bar{\mathbf{q}}(w-w_e)) + (\rho\bar{\mathbf{q}} - \rho_e\bar{\mathbf{q}}_e)\cdot\bar{\nabla}w_e - \frac{\partial\tau_z}{\partial y}\,dy = 0 \quad (III)$$

$$\bar{\nabla}\cdot\int_0^\delta \rho\bar{\mathbf{q}}(w_e-w)\,dy + \bar{\nabla}w_e\cdot\int_0^\delta(\rho_e\bar{\mathbf{q}}_e - \rho\bar{\mathbf{q}})\,dy - \tau_{z_w} = 0 \quad (II)$$

where

$$\rho_e\bar{q}_e^2\vec{\theta}_z = \int_0^\delta \rho\bar{\mathbf{q}}(w_e-w)\,dy \quad \text{(z-direction momentum-thickness vector)}$$

$$\tau_{z_w} \quad \text{(z-direction wall shear stress)}$$

Rewriting

$$\bar{\nabla}\cdot(\rho_e\bar{q}_e^2\vec{\theta}_z) + \bar{\nabla}w_e\cdot(\rho_e\bar{q}_e\vec{\delta^*}) = \tau_{z_w}$$

In streamline-aligned coordinates, the momentum thickness components satisfy the identity

$$\theta_{12} \equiv \theta_{21} - \delta_2^* \,.$$

Note that no assumption of external-flow irrotationality has been made here.

2.2.4 Kinetic-energy equation components

Two equations for kinetic-energy deficit, each associated with the flux of an energy 'component', are derived individually. When considered separately, the value of each equation as a statement of a fundamental physical law is questionable since some mechanics of kinetic-energy exchange between the two are lost. Individually, therefore, each is considered merely a mathematical condition.

The component equations are derived individually first and summed next to provide the complete kinetic-energy/dissipation balance.

x-kinetic energy

Integrating the following provides the relation for the component in the x-direction:

$$\int_0^\delta (u_e^2 - u^2)[\nabla \cdot (\rho \mathbf{q})] - 2u[\rho \mathbf{q} \cdot \nabla u + \frac{\partial p}{\partial x} - \frac{\partial \tau_x}{\partial y}]\, dy = 0$$

$$\int_0^\delta \nabla \cdot (\rho \mathbf{q}(u_e^2 - u^2)) - \rho \mathbf{q} \cdot \nabla (u_e^2 - u^2) - 2u[\rho \mathbf{q} \cdot \nabla u + \frac{\partial p}{\partial x} - \frac{\partial \tau_x}{\partial y}]\, dy = 0$$

$$\int_0^\delta \bar{\nabla} \cdot (\rho \bar{\mathbf{q}}(u_e^2 - u^2)) - \rho \mathbf{q} \cdot \nabla u_e^2 + 2u\rho \mathbf{q} \cdot \nabla u - 2u[\rho \mathbf{q} \cdot \nabla u - \rho_e \mathbf{q}_e \cdot \nabla u_e - \frac{\partial \tau_x}{\partial y}]\, dy = 0 \quad (I)$$

$$\int_0^\delta \bar{\nabla} \cdot (\rho \bar{\mathbf{q}}(u_e^2 - u^2)) - \rho \bar{\mathbf{q}} \cdot \bar{\nabla} u_e^2 + 2u\rho_e \bar{\mathbf{q}}_e \cdot \bar{\nabla} u_e + 2u \frac{\partial \tau_x}{\partial y}\, dy = 0 \quad (III)$$

$$\int_0^\delta \bar{\nabla} \cdot (\rho \bar{\mathbf{q}}(u_e^2 - u^2)) - (\rho_e \bar{\mathbf{q}}_e - \rho \bar{\mathbf{q}}) \cdot \bar{\nabla} u_e^2 + \rho_e \bar{\mathbf{q}}_e (u_e - u) \cdot \bar{\nabla} u_e + 2u \frac{\partial \tau_x}{\partial y}\, dy = 0$$

$$\bar{\nabla} \cdot \int_0^\delta \rho \bar{\mathbf{q}}(u_e^2 - u^2)\, dy + \bar{\nabla} u_e^2 \cdot \int_0^\delta (\rho_e \bar{\mathbf{q}}_e - \rho \bar{\mathbf{q}})\, dy - 2\bar{\mathbf{q}}_e \cdot \bar{\nabla} u_e \rho_e \int_0^\delta (u_e - u)\, dy$$

$$= \int_0^\delta 2\tau_x \frac{\partial u}{\partial y}\, dy \quad (II)$$

where the last integral has been integrated by parts. Here

$$\rho_e \bar{q}_e^3 \vec{E}_x = \int_0^\delta \rho \bar{\mathbf{q}}(u_e^2 - u^2)\, dy \quad \text{(x-direction kinetic-energy thickness vector)}$$

$$\bar{q}_e \vartheta_x = \int_0^\delta (u_e - u)\, dy \quad \text{(x-direction kinematic-displacement thickness)}$$

$$D_x = \int_0^\delta \tau_x \frac{\partial u}{\partial y}\, dy \quad \text{(x-component of the dissipation integral)}$$

Rewriting

$$\bar{\nabla} \cdot (\rho_e \bar{q}_e^3 \vec{E}_x) + \bar{\nabla} u_e^2 \cdot (\rho_e \bar{q}_e \vec{\delta}^*) - (2\bar{\mathbf{q}}_e \cdot \bar{\nabla} u_e)(\rho_e \bar{q}_e \vartheta_x) = 2D_x$$

For an irrotational external velocity field, $2\mathbf{q}_e \cdot \bar{\nabla} u_e$ can be replaced by $\partial \bar{q}_e^2 / \partial x$.

The equation is simplified when considered in streamline-aligned coordinates (without the irrotational assumption)

$$\bar{\nabla}_s \cdot (\rho_e \bar{q}_e^3 \vec{E}_1) + \bar{\nabla}_s u_e^2 \cdot (\rho_e \bar{q}_e \vec{\delta^*}) - 2u_e \frac{\partial u_e}{\partial s}(\rho_e \bar{q}_e \vartheta_1) = 2D_1 \, .$$

z-kinetic energy

Similarly for the z direction:

$$\int_0^\delta (w_e^2 - w^2)[\nabla \cdot (\rho \mathbf{q})] - 2w[\rho \mathbf{q} \cdot \nabla w + \frac{\partial p}{\partial z} - \frac{\partial \tau_z}{\partial y}] \, dy = 0$$

$$\int_0^\delta \nabla \cdot (\rho \mathbf{q}(w_e^2 - w^2)) - \rho \mathbf{q} \cdot \nabla (w_e^2 - w^2) - 2w[\rho \mathbf{q} \cdot \nabla w + \frac{\partial p}{\partial z} - \frac{\partial \tau_z}{\partial y}] \, dy = 0$$

$$\int_0^\delta \bar{\nabla} \cdot (\rho \bar{\mathbf{q}}(w_e^2 - w^2)) - \rho \mathbf{q} \cdot \nabla w_e^2 + 2w\rho \mathbf{q} \cdot \nabla w - 2w[\rho \mathbf{q} \cdot \nabla w - \rho_e \mathbf{q}_e \cdot \nabla w_e - \frac{\partial \tau_z}{\partial y}] \, dy = 0 \quad (I)$$

$$\int_0^\delta \bar{\nabla} \cdot (\rho \bar{\mathbf{q}}(w_e^2 - w^2)) - \rho \bar{\mathbf{q}} \cdot \bar{\nabla} w_e^2 + 2w\rho_e \bar{\mathbf{q}}_e \cdot \bar{\nabla} w_e + 2w \frac{\partial \tau_z}{\partial y} \, dy = 0 \quad (III)$$

$$\int_0^\delta \bar{\nabla} \cdot (\rho \bar{\mathbf{q}}(w_e^2 - w^2)) - (\rho_e \bar{\mathbf{q}}_e - \rho \bar{\mathbf{q}}) \cdot \bar{\nabla} w_e^2 + \rho_e \bar{\mathbf{q}}_e (w_e - w) \cdot \bar{\nabla} w_e + 2w \frac{\partial \tau_z}{\partial y} \, dy = 0$$

$$\bar{\nabla} \cdot \int_0^\delta \rho \bar{\mathbf{q}}(w_e^2 - w^2) \, dy + \bar{\nabla} w_e^2 \cdot \int_0^\delta (\rho_e \bar{\mathbf{q}}_e - \rho \bar{\mathbf{q}}) \, dy - 2\bar{\mathbf{q}}_e \cdot \bar{\nabla} w_e \rho_e \int_0^\delta (w_e - w) \, dy$$

$$= \int_0^\delta 2\tau_z \frac{\partial w}{\partial y} \, dy \quad (II)$$

where the last integral also has been integrated by parts. Here

$$\rho_e \bar{q}_e^3 \vec{E}_z = \int_0^\delta \rho \bar{\mathbf{q}}(w_e^2 - w^2) \, dy \quad \text{(z-direction kinetic-energy thickness vector)}$$

$$\bar{q}_e \vartheta_z = \int_0^\delta (w_e - w) \, dy \quad \text{(z-direction kinematic-displacement thickness)}$$

$$D_z = \int_0^\delta \tau_z \frac{\partial w}{\partial y}\, dy \quad \text{(z-component of the dissipation integral)}$$

Rewriting

$$\bar{\nabla} \cdot (\rho_e \bar{q}_e^3 \vec{E}_z) + \bar{\nabla} w_e^2 \cdot (\rho_e \bar{q}_e \vec{\delta^*}) - (2\bar{\mathbf{q}}_e \cdot \bar{\nabla} w_e)(\rho_e \bar{q}_e \vartheta_z) = 2D_z$$

For an irrotational external velocity field, $2\mathbf{q}_e \cdot \bar{\nabla} w_e$ can be replaced by $\partial \bar{q}_e^2 / \partial z$. The equation is substantially simplified when considered in streamline-aligned coordinates

$$\bar{\nabla}_s \cdot (\rho_e \bar{q}_e^3 \vec{E}_2) - 2u_e \frac{\partial w_e}{\partial s}(\rho_e \bar{q}_e \vartheta_2) = 2D_2 \,.$$

Of course $\frac{\partial w_e}{\partial s}$, which in fact is a measure of the curvature of the streamline, may be replaced by $\frac{\partial u_e}{\partial n}$ for an irrotational external velocity field.

2.2.5 Total kinetic-energy equation

The total kinetic-energy deficit equation is obtained by summing the x-direction and z-direction kinetic-energy equations. Defining the vector of thicknesses

$$\vec{\theta^*} = \vec{E}_x + \vec{E}_z \,,$$

and a total dissipation integral

$$D = D_x + D_z \,,$$

the total kinetic energy equation can written as

$$\bar{\nabla} \cdot (\rho_e \bar{q}_e^3 \vec{\theta^*}) + \int_0^\delta (2\rho_e \bar{\mathbf{q}}_e \cdot (u\bar{\nabla} u_e + w\bar{\nabla} w_e) - \rho \bar{\mathbf{q}} \cdot \bar{\nabla} \bar{q}_e^2)\, dy - 2D = 0 \,.$$

The assumption of an irrotational external velocity field greatly simplifies the pressure-gradient terms

$$2\rho_e \bar{\mathbf{q}}_e \cdot (u\bar{\nabla} u_e + w\bar{\nabla} w_e) = \rho_e \bar{\mathbf{q}} \cdot \bar{\nabla} \bar{q}_e^2 \,.$$

Then, the total kinetic-energy equation simplifies to

$$\bar{\nabla}\cdot(\rho_e\bar{q}_e^3\vec{\theta}^*)+\bar{\nabla}\bar{q}_e^2\cdot(\rho_e\bar{q}_e\vec{\delta}^{**})-2D=0\,,$$

where the density thicknesses are defined by the vector

$$\rho_e\bar{q}_e\vec{\delta}^{**}=\int_0^\delta\bar{\mathbf{q}}(\rho_e-\rho)\,dy\equiv\rho_e\bar{q}_e\vec{\delta}^{*}-\rho_e\bar{q}_e\vec{\vartheta}\,.\quad\text{(density-thickness vector)}$$

The pressure-gradient terms are seen to vanish completely for incompressible flows. Note that each of the three terms in the equation is rotationally invariant.

2.2.6 Mixed-component kinetic-energy equation

An equation governing the flux of the mixed-component kinetic-energy deficit is derived by considering:

$$\begin{aligned}\int_0^\delta(u_ew_e-uw)[\nabla\cdot(\rho\mathbf{q})] \quad &- \quad w[\rho\mathbf{q}\cdot\nabla u+\frac{\partial p}{\partial x}-\frac{\partial\tau_x}{\partial y}]\\ &- \quad u[\rho\mathbf{q}\cdot\nabla w+\frac{\partial p}{\partial z}-\frac{\partial\tau_z}{\partial y}]\;dy=0\end{aligned}$$

$$\begin{aligned}\int_0^\delta\nabla\cdot(\rho\mathbf{q}(u_ew_e-uw))-\rho\mathbf{q}\cdot\nabla(u_ew_e-uw) \quad &- \quad w[\rho\mathbf{q}\cdot\nabla u+\frac{\partial p}{\partial x}-\frac{\partial\tau_x}{\partial y}]\\ &- \quad u[\rho\mathbf{q}\cdot\nabla w+\frac{\partial p}{\partial z}-\frac{\partial\tau_z}{\partial y}]\;dy=0\end{aligned}$$

$$\begin{aligned}\int_0^\delta\bar{\nabla}\cdot(\rho\bar{\mathbf{q}}(u_ew_e-uw)) \quad &- \quad \rho\mathbf{q}\cdot\nabla(u_ew_e)+\rho\mathbf{q}\cdot\nabla(uw)\\ &- \quad w[\rho\mathbf{q}\cdot\nabla u-\rho_e\mathbf{q}_e\cdot\nabla u_e-\frac{\partial\tau_x}{\partial y}]\\ &- \quad u[\rho\mathbf{q}\cdot\nabla w-\rho_e\mathbf{q}_e\cdot\nabla w_e-\frac{\partial\tau_z}{\partial y}]\;dy=0\quad(I)\end{aligned}$$

$$\begin{aligned}\int_0^\delta\bar{\nabla}\cdot(\rho\bar{\mathbf{q}}(u_ew_e-uw))-\rho\bar{\mathbf{q}}\cdot\bar{\nabla}(u_ew_e) \quad &+ \quad \rho_e\bar{\mathbf{q}}_e\cdot(w\bar{\nabla}u_e+u\bar{\nabla}w_e)\\ &+ \quad\left(w\frac{\partial\tau_x}{\partial y}+u\frac{\partial\tau_z}{\partial y}\right)\;dy=0\quad(III)\end{aligned}$$

For an irrotational external flow, the pressure-gradient terms may be written in terms of the density thicknesses

$$\begin{aligned}\int_0^\delta \rho_e \bar{\mathbf{q}}_e \cdot (w\bar{\nabla}u_e + u\bar{\nabla}w_e)\,dy \quad &- \quad \rho\bar{\mathbf{q}}\cdot\bar{\nabla}(u_e w_e) \\ &= \quad \frac{1}{2}\left(\frac{\partial \bar{q}_e^2}{\partial z}\int_0^\delta (\rho_e-\rho)u\,dy + \frac{\partial \bar{q}_e^2}{\partial x}\int_0^\delta (\rho_e-\rho)w\,dy\right) \\ &+ \quad \left(\frac{\partial w_e}{\partial z} - \frac{\partial u_e}{\partial x}\right)\left|\bar{\mathbf{q}}_e \times (\rho_e \bar{q}_e \vec{\delta}^*)\right| .\end{aligned}$$

Integrating the dissipation terms by parts, the equation becomes

$$\begin{aligned}\bar{\nabla}\cdot\int_0^\delta \rho\bar{\mathbf{q}}(u_e w_e - uw)\,dy \quad &+ \quad \frac{1}{2}\left(\frac{\partial \bar{q}_e^2}{\partial z}\rho_e\bar{q}_e\delta_x^{**} + \frac{\partial \bar{q}_e^2}{\partial x}\rho_e\bar{q}_e\delta_z^{**}\right) \\ &+ \quad \left(\frac{\partial w_e}{\partial z} - \frac{\partial u_e}{\partial x}\right)\left|\bar{\mathbf{q}}_e \times (\rho_e \bar{q}_e \vec{\delta}^*)\right| = \int_0^\delta \tau_x\frac{\partial w}{\partial y} + \tau_z\frac{\partial u}{\partial y}\,dy \quad (II)\end{aligned}$$

where

$$\rho_e \bar{q}_e^3 \vec{E}_m = \int_0^\delta \rho\bar{\mathbf{q}}(u_e w_e - uw)\,dy \quad \text{(mixed-component kinetic-energy thickness)}$$

$$D_m = \int_0^\delta \tau_x\frac{\partial w}{\partial y} + \tau_z\frac{\partial u}{\partial y}\,dy \quad \text{(mixed-component dissipation integral)}$$

Rewriting

$$\bar{\nabla}\cdot\rho_e\bar{q}_e^3\vec{E}_m + \frac{1}{2}\left(\frac{\partial \bar{q}_e^2}{\partial z}\rho_e\bar{q}_e\delta_x^{**} + \frac{\partial \bar{q}_e^2}{\partial x}\rho_e\bar{q}_e\delta_z^{**}\right) + \left(\frac{\partial w_e}{\partial z} - \frac{\partial u_e}{\partial x}\right)\left|\bar{\mathbf{q}}_e \times (\rho_e \bar{q}_e \vec{\delta}^*)\right| = D_m$$

Care should be taken in using this equation because it is directionally dependent. Also, in streamline-aligned coordinates

$$E_{31} \equiv E_{12} + \delta_2^* ,$$

and

$$E_{32} \equiv E_{21} .$$

2.2.7 Summary of individual equations

Entrainment

$$\bar{\nabla} \cdot (\rho_e \bar{q}_e \vec{\delta^*}) = \delta \, \bar{\nabla} \cdot \rho_e \bar{\mathbf{q}}_e + \rho_e v_e \tag{2.6}$$

Momentum components

$$\bar{\nabla} \cdot (\rho_e \bar{q}_e^2 \vec{\theta}_x) + \bar{\nabla} u_e \cdot (\rho_e \bar{q}_e \vec{\delta^*}) = \tau_{x_w} \tag{2.7}$$

$$\bar{\nabla} \cdot (\rho_e \bar{q}_e^2 \vec{\theta}_z) + \bar{\nabla} w_e \cdot (\rho_e \bar{q}_e \vec{\delta^*}) = \tau_{z_w} \tag{2.8}$$

Kinetic energy components

$$\bar{\nabla} \cdot (\rho_e \bar{q}_e^3 \vec{E}_x) + \bar{\nabla} u_e^2 \cdot (\rho_e \bar{q}_e \vec{\delta^*}) - (2\bar{\mathbf{q}}_e \cdot \bar{\nabla} u_e)(\rho_e \bar{q}_e \vartheta_x) = 2D_x \tag{2.9}$$

$$\bar{\nabla} \cdot (\rho_e \bar{q}_e^3 \vec{E}_z) + \bar{\nabla} w_e^2 \cdot (\rho_e \bar{q}_e \vec{\delta^*}) - (2\bar{\mathbf{q}}_e \cdot \bar{\nabla} w_e)(\rho_e \bar{q}_e \vartheta_z) = 2D_z \tag{2.10}$$

Total kinetic energy

(Irrotational external flow)

$$\bar{\nabla} \cdot (\rho_e \bar{q}_e^3 \vec{\theta^*}) + \bar{\nabla} \bar{q}_e^2 \cdot (\rho_e \bar{q}_e \vec{\delta^{**}}) = 2D \tag{2.11}$$

Mixed-component kinetic energy

(Irrotational external flow)

$$\bar{\nabla} \cdot \rho_e \bar{q}_e^3 \vec{E}_m + \frac{1}{2} \left(\frac{\partial \bar{q}_e^2}{\partial z} \rho_e \bar{q}_e \delta_x^{**} + \frac{\partial \bar{q}_e^2}{\partial x} \rho_e \bar{q}_e \delta_z^{**} \right) + \left(\frac{\partial w_e}{\partial z} - \frac{\partial u_e}{\partial x} \right) \left| \bar{\mathbf{q}}_e \times (\rho_e \bar{q}_e \vec{\delta^*}) \right| = D_m \tag{2.12}$$

2.3 Derivation of an unsteady parent integral equation

The derivation of integral equations considered here can be viewed as integrating velocity moments of the differential boundary-layer equations. The process can be generalized such that velocity moment is considered a hierarchical weight function ϕ defined as

$$\phi(k_u, k_w; u, w) = u^{k_u} w^{k_w}, \quad k_u, k_w \geq 0\,,$$

where the exponents are considered to be positive integers. Particular ϕ's will later yield easily recognizable equations. Further define the lower-order (in velocity) weight functions

$$\phi^{(u)} = \frac{\partial \phi}{\partial u} = k_u \phi(k_u - 1, k_w)\,,$$

$$\phi^{(w)} = \frac{\partial \phi}{\partial w} = k_w \phi(k_u, k_w - 1)\,,$$

and note that

$$\phi^{(u)} = 0 \text{ if } k_u = 0 \quad \text{and}$$

$$\phi^{(w)} = 0 \text{ if } k_w = 0\,.$$

Leibnitz's rule also applies to the time-derivative term in the same manner as it applies to the space-gradient terms as in Identity II. The pressure-gradient terms are now time dependent

$$\frac{\partial p}{\partial x} = -\rho_e \frac{\partial u_e}{\partial t} - \rho_e \bar{\mathbf{q}}_e \cdot \bar{\nabla} u_e\,,$$

$$\frac{\partial p}{\partial z} = -\rho_e \frac{\partial w_e}{\partial t} - \rho_e \bar{\mathbf{q}}_e \cdot \bar{\nabla} w_e\,.$$

The continuity equation is multiplied by the weight function in defect form, the momentum equations are multiplied by the lower-order weight functions and the sum integrated. This particular combination will yield thicknesses directly in deficit form

$$\begin{aligned}\int_0^\delta (\phi_e - \phi)[\frac{\partial \rho}{\partial t} + \nabla \cdot (\rho \mathbf{q})] \quad &- \quad \phi^{(u)}[\rho \frac{\partial u}{\partial t} + \rho \mathbf{q} \cdot \nabla u + \frac{\partial p}{\partial x} - \frac{\partial \tau_x}{\partial y}] \\ &- \quad \phi^{(w)}[\rho \frac{\partial w}{\partial t} + \rho \mathbf{q} \cdot \nabla w + \frac{\partial p}{\partial z} - \frac{\partial \tau_z}{\partial y}]\, dy = 0\,.\end{aligned}$$

The steady continuity equation contribution can be written as

$$\int_0^\delta (\phi_e - \phi)[\nabla \cdot (\rho \mathbf{q})]\, dy = \int_0^\delta \bar{\nabla} \cdot (\rho \bar{\mathbf{q}}(\phi_e - \phi)) - \rho \mathbf{q} \cdot \nabla \phi_e + \rho \mathbf{q} \cdot \nabla \phi \, dy \quad (I).$$

The last term above may be further expanded

$$\rho \mathbf{q} \cdot \nabla \phi = \phi^{(u)} \rho \mathbf{q} \cdot \nabla u + \phi^{(w)} \rho \mathbf{q} \cdot \nabla w$$

and is recognized to exactly cancel the momentum convective terms. The second to last term is combined with the steady, pressure-gradient terms

$$\begin{aligned} & -\rho \mathbf{q} \cdot \nabla \phi_e - \phi^{(u)} \left.\frac{\partial p}{\partial x}\right|_{st} - \phi^{(w)} \left.\frac{\partial p}{\partial z}\right|_{st} \\ = \;& -\phi_e^{(u)} \rho \bar{\mathbf{q}} \cdot \bar{\nabla} u_e - k_w \frac{\phi_e}{w_e} \rho \bar{\mathbf{q}} \cdot \bar{\nabla} w_e + \phi^{(u)} \rho_e \bar{\mathbf{q}}_e \cdot \bar{\nabla} u_e + \phi^{(w)} \rho_e \bar{\mathbf{q}}_e \cdot \bar{\nabla} w_e \quad (III) \\ = \;& \left(\phi_e^{(u)} \bar{\nabla} u_e + \phi_e^{(w)} \bar{\nabla} w_e\right) \cdot (\rho_e \bar{\mathbf{q}}_e - \rho \bar{\mathbf{q}}) - \left((\phi_e^{(u)} - \phi^{(u)}) \bar{\nabla} u_e + (\phi_e^{(w)} - \phi^{(w)}) \bar{\nabla} w_e\right) \cdot \rho_e \bar{\mathbf{q}}_e \,. \end{aligned}$$

The unsteady continuity equation contribution can be written as

$$\int_0^\delta (\phi_e - \phi)[\frac{\partial \rho}{\partial t}]\, dy = \int_0^\delta \frac{\partial}{\partial t}(\rho(\phi_e - \phi)) - \rho \frac{\partial \phi_e}{\partial t} + \rho \frac{\partial \phi}{\partial t} \,.$$

The last term exactly cancels the unsteady convective terms in the momentum equations

$$\rho \frac{\partial \phi}{\partial t} - \phi^{(u)} \rho \frac{\partial u}{\partial t} - \phi^{(w)} \rho \frac{\partial w}{\partial t} \equiv 0 \,.$$

The second to last term is combined with the unsteady pressure-gradient contribution

$$\begin{aligned} & -\rho \frac{\partial \phi_e}{\partial t} + \phi^{(u)} \rho_e \frac{\partial u_e}{\partial t} + \phi^{(w)} \rho_e \frac{\partial w_e}{\partial t} \\ = \;& \left[(\rho_e - \rho)\phi_e^{(u)} - (\phi_e^{(u)} - \phi^{(u)})\rho_e\right] \frac{\partial u_e}{\partial t} + \left[(\rho_e - \rho)\phi_e^{(w)} - (\phi_e^{(w)} - \phi^{(w)})\rho_e\right] \frac{\partial w_e}{\partial t} \,. \end{aligned}$$

Finally, the shear-stress gradient terms are integrated by parts

$$\int_0^\delta \phi^{(u)} \frac{\partial \tau_x}{\partial y} + \phi^{(w)} \frac{\partial \tau_z}{\partial y}\, dy = -\left.(\phi^{(u)} \tau_x + \phi^{(w)} \tau_z)\right|_{y=0} - \int_0^\delta \tau_x \frac{\partial \phi^{(u)}}{\partial y} + \tau_z \frac{\partial \phi^{(w)}}{\partial y}\, dy \,,$$

where the outer-edge boundary conditions on the shear terms 2.1 and 2.2 have been used.

For clarity, define the differentiated weight-function vector

$$\vec{\phi}' = \phi^{(u)}\hat{\imath} + \phi^{(w)}\hat{k}$$

and the shear-stress vector

$$\vec{\tau} = \tau_x\hat{\imath} + \tau_z\hat{k}\,.$$

Collecting terms, and defining $k = k_u + k_w$, the equation becomes:

$$\begin{aligned}
&\frac{\partial}{\partial t}\int_0^\delta (\rho(\phi_e - \phi))\,dy + \vec{\phi}'_e \cdot \frac{\partial \bar{\mathbf{q}}_e}{\partial t}\int_0^\delta (\rho_e - \rho)\,dy - \rho_e \frac{\partial \bar{\mathbf{q}}_e}{\partial t}\cdot\int_0^\delta (\vec{\phi}'_e - \vec{\phi}')\,dy \\
&\quad + \bar{\nabla}\cdot\int_0^\delta (\rho\bar{\mathbf{q}}(\phi_e - \phi))\,dy + \left(\phi_e^{(u)}\bar{\nabla}u_e + \phi_e^{(w)}\bar{\nabla}w_e\right)\cdot\int_0^\delta (\rho_e\bar{\mathbf{q}}_e - \rho\bar{\mathbf{q}})\,dy \\
&\quad - \rho_e\bar{\mathbf{q}}_e\cdot\bar{\nabla}u_e\int_0^\delta (\phi_e^{(u)} - \phi^{(u)})\,dy - \rho_e\bar{\mathbf{q}}_e\cdot\bar{\nabla}w_e\int_0^\delta (\phi_e^{(w)} - \phi^{(w)})\,dy \\
&\quad = \vec{\phi}'\cdot\vec{\tau}\Big|_{y=0} + \int_0^\delta \vec{\tau}\cdot\frac{\partial\vec{\phi}'}{\partial y}\,dy \quad (II)
\end{aligned}$$

where

$$\rho_e\bar{q}_e^k\zeta = \int_0^\delta (\rho(\phi_e - \phi))\,dy$$

$$\rho_e\theta_\rho = \int_0^\delta (\rho_e - \rho)\,dy$$

$$\bar{q}_e^{k-1}\vec{\Phi} = \int_0^\delta (\vec{\phi}'_e - \vec{\phi}')\,dy$$

$$\rho_e\bar{q}_e^{k+1}\vec{\theta} = \int_0^\delta (\rho\bar{\mathbf{q}}(\phi_e - \phi))\,dy$$

$$D_p = \int_0^\delta \vec{\tau}\cdot\frac{\partial\vec{\phi}'}{\partial y}\,dy$$

Rewriting

$$\begin{aligned}
&\frac{\partial}{\partial t}\rho_e\bar{q}_e^k\zeta + \bar{\nabla}\cdot(\rho_e\bar{q}_e^{k+1}\vec{\theta}) + \vec{\phi}'_e\cdot\frac{\partial\bar{\mathbf{q}}_e}{\partial t}\rho_e\theta_\rho - \frac{\partial\bar{\mathbf{q}}_e}{\partial t}\cdot(\rho_e\bar{q}_e^{k-1}\vec{\Phi}) \\
&+ \left(\phi_e^{(u)}\bar{\nabla}u_e + \phi_e^{(w)}\bar{\nabla}w_e\right)\cdot(\rho_e\bar{q}_e\vec{\delta}^*) - \bar{\mathbf{q}}_e\cdot\bar{\nabla}u_e(\rho_e\bar{q}_e^{k-1}\Phi_x) - \bar{\mathbf{q}}_e\cdot\bar{\nabla}w_e(\rho_e\bar{q}_e^{k-1}\Phi_z)
\end{aligned}$$

Equation	k_u	k_w
x-momentum	1	0
z-momentum	0	1
x-kinetic energy	2	0
z-kinetic energy	0	2
mixed-kinetic energy	1	1
entrainment	∞	∞

Table 2.1: The value of exponents in the parent integral equation corresponding to individual equations.

$$= \vec{\phi}' \cdot \vec{\tau}\Big|_{y=0} + D_p \tag{2.13}$$

The first two terms are flux derivatives, the remaining terms on the left-hand-side are related to the external flow pressure gradient and the terms on the right-hand-side are the wall-shear or dissipation-integral-like sources. Also, note that no assumption of irrotationality of the external flow has been made. This is a convenient general equation from which specific useful equations fall out for different integer values of the exponents k_u and k_w as shown in Table 2.3.

In order to easily connect the notation used in this chapter and that used in subsequent ones, note that any set of individual equations obtained from Equation 2.13 ($i = 1, \ldots, N$) can be written with the flux-derivative terms balancing the remaining terms

$$\frac{\partial}{\partial t}\rho_e \bar{q}_e^{k_i}\zeta_i + \bar{\nabla}\cdot(\rho_e \bar{q}_e^{k_i+1}\vec{\theta}_i) = \frac{\partial \mathbf{u}}{\partial t} + \frac{\partial \mathbf{f}}{\partial x} + \frac{\partial \mathbf{g}}{\partial z} = \mathbf{h}\,,$$

where $\mathbf{u}$ is a flux vector of length N and is not to be confused with the u component of velocity.

2.4 Information content of the equations

From a purely *mathematical* point of view, the exponents k_u and k_w in Equation 2.13 may assume any arbitrary numerical value. It has also already been indicated that setting either exponent equal to one yields the momentum equations. Higher values yield other equations; in the limit, $k_u, k_w \to \infty$, the parent equation simply degenerates into the entrainment equation, which contains no direct information about the viscous details of the boundary layer. This suggests that higher values of the

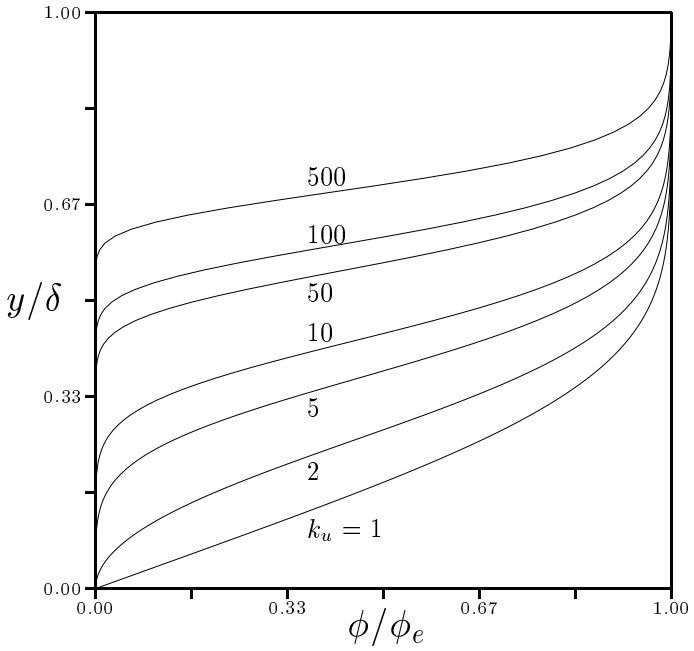

Figure 2-1: Variation of the weight function with increasing values of k_u ($k_w = 0$) for a Blasius boundary layer.

exponents yields equations with less information content than lower values. Walz [66] made similar comments for a steady two-dimensional version of Equation 2.13 derived by Geropp [25].

A more rigorous argument can be made by examining the dependence of the weight function ϕ on the value of the exponents k_u and k_w . With no loss of generality, consider ϕ for the two-dimensional Blasius velocity profile which is plotted in Figure 2.4 as a function of k_u. As k_u increases, the resulting derived equation contains progressively less information about the boundary layer near the wall. Significantly, ϕ has a non-zero gradient at the wall only for $k_u = 1$ (which manifests itself in wall-shear stress terms in the momentum equations). At the other extreme, for $k_u \to \infty$, the parent equation devolves into simply the displacement effect of the boundary layer on the outer inviscid flow.

The fact that lowest integer values of the exponents yield the momentum and kinetic-energy equations is independent of the intrinsic physical value of these equations. These equations are set apart from others because it is possible to derive them directly by considering force/momentum and kinetic energy/dissipation balances on a suitable control volume in the boundary layer. In any integral solution scheme, it is highly desirable to satisfy them on their physical merit alone and to consider

the other equations as satisfying auxiliary mathematical conditions.

Again from a mathematical point of view, it is also possible to consider positive non-integer values for the exponents. Then, it may be argued that for $0 < k_u, k_w < 1$, Equation 2.13 has even more information about the boundary layer near the wall than the momentum equations. It also motivates the question of what, if any, system of equations obtained from Equation 2.13 (that is to say what series of velocity-moments) converges to the exact solution as the size of the system tends to infinity. These questions, though very interesting, are beyond the scope of this work.

2.5 Constructing practical equation systems

An endless number of systems can be constructed from the variety of equations available. As indicated in the literature survey in § 1.3, a natural paradigm has emerged: the two momentum equations augmented with one additional equation, either the entrainment or total kinetic-energy, as a 'compatibility' equation. Accumulated practical experience validates the utility of this basic system (which is not to say that other possible systems are not useful). The streamwise momentum equation augmented by the compatibility equation successfully emulates Goldstein's singularity (direct-mode calculations), while the crossflow is essentially governed by a cross-stream momentum balance. The major shortcoming of this third-order system is its inability to calculate general cross-over profiles. Additional equations need to be added to the system to calculate such flows.

For turbulent flows, other equations with independent physical meaning can be derived. These solve for the transport of turbulent kinetic energy is some form. As indicated in § 1.3, a few researchers have used such an equation for the entrainment coefficient in the streamwise direction to capture the large lag effects found in turbulent boundary layers through . Others have used some form of Reynold's stress evolution equations, again in a streamwise (or a chordwise on wings) direction; for example, Drela [19] and Nishida [44] use an equation governing the maximum Reynold's stress value.

The equations have been derived for general orientations in the (x, z) plane for use in a finite-element solver. It is important to recognize that this rotational invariance must be maintained in any credible solution scheme. This precludes, for example, the use of one of the momentum equations in isolation. A necessary exception exists, however, for equations that are intrinsically directional such as the mixed kinetic-energy equation. Systems containing this equation can only be used if identified with a unique or special direction (streamline-aligned, for example).

Chapter 3

Assumptions in Closure of Integral Equations

The fundamental idea behind integral methods for boundary-layer equations is to reduce the problem from one that is three-dimensional to one that is two-dimensional. This is predicated on the good assumption that the physical behavior of the flow is well understood in the direction of integration (normal to the wall). The three-dimensional differential problem is closed and no additional information is necessary to solve it aside from a turbulence model. In integral methods, the number of unknowns introduced into the problem exceeds the number of equations available; the problem is closed by assuming parametric functional forms (profile families) for the two wall-parallel velocity components and density in the wall-normal direction

$$u = u(\mathbf{p};\eta), \quad w = w(\mathbf{p};\eta), \quad \rho = \rho(\mathbf{p};\eta)\,,$$

where u and w in this chapter are assumed normalized by q_e, $\mathbf{p}$ is a vector of N profile parameters and $\eta = y/\delta$. For turbulent flow, the Reynolds stresses will need to be modeled in a similar manner through a turbulence model. Only velocity profiles are considered here, the density follows from the Crocco-Busemann relation $\rho = \rho(M_e;q)$.

Of the elements of $\mathbf{p}$, $N-2$ are shape parameters. It should be emphasized that these shape parameters do not have to have the same meaning for different profile-family definitions (such as

the usual shape factor $H = \delta_1^*/\theta_{11}$). This facility is useful because it allows the general postulation of profile families in terms of intrinsic, empirical parameters. Of the remaining two parameters, one is automatically the boundary layer thickness δ. Another is assumed to be the crossflow magnitude c (or c and c_1, the magnitude for each mode where the crossflow has two independent modes). These two parameters are applicable to all profile families equally and, in the separated flow method described later in this thesis, provide a convenient means to relate (linearly in this case) the mass-defect variables to boundary-layer shape parameters.

In some integral methods, the profile families are substituted into unknown integrals *a priori* and their parametric variation modeled through devised empirical curve fits (see, for example, [19, 59]). In this thesis, the unknown integrals are computed by numerical quadrature on the fly. This is a more flexible approach which allows the substitution of different profile families easily into a computational scheme.

Virtually all models of closure used in the past assume that the streamwise velocity profile u in a three-dimensional flow behaves like the profile in a two-dimensional boundary layer. This is generally a good assumption but is obviously most valid when the crossflow is small [43]. One fortunate consequence is that the accumulated body of research on two-dimensional boundary layers carries over to three-dimensional boundary layers. The crossflow velocity profile w is invariably defined in terms of the streamwise one. There are some notable exceptions to the streamwise-oriented modeling approach for the case of turbulent flow which are also briefly mentioned.

The modeling of Reynolds stresses is an important issue. Briefly, this includes upstream history effects for non-equilibrium boundary layers captured in some studies by using integral versions of the turbulent kinetic energy equation (see, for example Drela [19] for a two-dimensional method). Furthermore, in three-dimensional boundary layers, the Reynolds-stress vector is also known to lag behind the velocity-gradient vector [3]. Cousteix [9] has modeled this by modifying the usual mixing-length turbulence model.

Before proceeding to a discussion of profile families, it will be of use to briefly review some exact boundary-layer velocity behavior at the wall-normal edges.

3.1 Wall-normal boundary-layer behavior at edges

Boundary conditions used in the solution of the differential equations were listed in Chapter 2. Using these conditions, information about the behavior of the velocity components near the wall and the outer-edge can be gleaned from the equations themselves.

For both turbulent and laminar boundary layers, evaluating the differential momentum equations at the wall leads to expressions for the velocity component curvatures in terms of the pressure gradients

$$\left.\frac{\partial^2 u}{\partial y^2}\right|_{y=0} = \frac{1}{\nu}\frac{\partial p}{\partial s}\,, \tag{3.1}$$

$$\left.\frac{\partial^2 u}{\partial y^2}\right|_{y=0} = \frac{1}{\nu}\frac{\partial p}{\partial n}\,. \tag{3.2}$$

From the definitions of the shear stress components, evaluated at the wall, and using L'Hopital's rule, the tangent of the angle subtended by the wall limiting streamline to the outer-edge streamline is

$$\tan\beta_w = \left.\frac{w}{u}\right|_{\lim y\to 0} = \left.\frac{\partial w}{\partial u}\right|_{y=0} = \left.\frac{\partial w/\partial y}{\partial u/\partial y}\right|_{y=0} = \frac{\tau_{w_2}}{\tau_{w_1}}\,.$$

Combining this with Equations 3.1 and 3.2, the wall curvature of the hodograph curve is obtained

$$\left.\frac{\partial^2 w}{\partial u^2}\right|_{y=0} = \left[\frac{1}{\partial u/\partial y}\frac{\partial}{\partial y}\left(\frac{\partial w/\partial y}{\partial u/\partial y}\right)\right]_{y=0} = \frac{\mu}{\tau_{w_1}^2}\left(\frac{\partial p}{\partial n} - \frac{\tau_{w_2}}{\tau_{w_1}}\frac{\partial p}{\partial s}\right)\,, \tag{3.3}$$

which shows that the flow is collateral ($\left.\frac{\partial^2 w}{\partial u^2}\right|_{y=0} = 0 \quad \Rightarrow w \sim u$) near the wall only if the pressure gradient is parallel to the limiting streamline, which, of course, is not true in the general case.

For incompressible *two-dimensional* boundary layers, a series of gradient conditions at the wall can be derived by differentiating the momentum equation (see for example, Rosenhead [47])

$$\left.\frac{\partial^3 u}{\partial y^3}\right|_{y=0} = 0, \quad \left.\frac{\partial^4 u}{\partial y^4}\right|_{y=0} = \frac{1}{\nu}\left.\frac{\partial u}{\partial y}\right|_{y=0}\left.\frac{\partial^2 u}{\partial s \partial y}\right|_{y=0}, \quad \cdots \tag{3.4}$$

These conditions are useful in so far as two-dimensional behavior is assumed for the streamwise direction because they are not strictly valid for three-dimensional boundary layers.

At the boundary-layer edge δ, in constructing velocity profile families, as many of the following derivative conditions, which strictly apply only at $y = \infty$, as are warranted by the particular functional form chosen, should be used

$$\left.\frac{\partial^n u}{\partial y^n}\right|_{y=\delta} = 0, \quad \left.\frac{\partial^n w}{\partial y^n}\right|_{y=\delta} = 0, \quad n \to \infty \,. \tag{3.5}$$

This is a consequence of first-order boundary-layer theory. Taking the y-derivative of the continuity equation further dictates that

$$\left.\frac{\partial^2 v}{\partial y^2}\right|_{y=\delta} = 0 \,.$$

These set of conditions can serve as guidelines in the postulation of velocity profiles. For integral methods, strict compliance is clearly not necessary because the resultant error is unlikely to be larger than from other sources.

3.2 Streamwise velocity profiles

3.2.1 Laminar flow

Beginning with the venerable Pohlhausen method (1921), many profile families have been proposed in the literature. A comprehensive account of early attempts can be found in Rosenhead [47].

The Falkner-Skan profile family for a class of similar flows has been shown to be a very good one-parameter approximation to attached, non-similar flows [19]. A general empirical curve fit to the solution of the Falkner-Skan equation is

$$u(\zeta;\eta) = 1 - (1-\eta)^{\zeta}(1 + a_1\eta + a_2\eta^2) \,. \tag{3.6}$$

Satisfying boundary conditions (Equation 3.4) at the wall

$$\left.\frac{\partial^2 u}{\partial \eta^2}\right|_{\eta=0} = -\Lambda \,, \quad \left.\frac{\partial^3 u}{\partial \eta^3}\right|_{\eta=0} = 0 \,,$$

where $\Lambda = \frac{\delta^2}{\mu q_e}\frac{\partial p}{\partial s}$ is the Pohlhausen parameter, relates the coefficients to the parameters

$$a_1(\zeta,\Lambda) = \frac{2}{3}(\zeta-1) + \frac{\Lambda}{\zeta+1}, \quad a_2(\zeta,\Lambda) = \frac{\zeta(\zeta-1)}{6}(\zeta-1) + \frac{\Lambda}{2}.$$

The largest integer less than the exponent ζ is also the number of zero outer-edge gradient conditions that are satisfied (Equation 3.5). Fair agreement with the Falkner-Skan profiles is given by

$$\zeta(\Lambda) = -\frac{7}{40}\Lambda + 5.$$

so that Λ now becomes the free parameter. A more sophisticated, and more accurate, two-parameter approximation obtained by including another polynomial term in the second factor of Equation 3.6 was proposed by Wieghart and can be obtained from Rosenhead.

While the Falkner-Skan family is a good approximation for attached profiles, it tends to overpredict the negative velocities in separated regions [21]. An early approach for attached boundary layers developed by Kármán and Millikan [32] and Stratford [57], based on various pseudo-physical assumptions, was to join inner and outer profiles in the neighborhood of the inflexion point. The outer profiles were displaced outwards in decelerating flows, implicitly defining a profile family. This idea is extended here to the complete profile family which is obtained by sliding the origin (corresponding to the wall) along a suitable fixed function (that resembles the wake function in turbulent flow) and scaling the result. Here, the profiles are derived from the fixed function (with η_0 as the free parameter)

$$u(\eta_0;\eta) = 1 - e^{f_0 - f(\eta)}, \tag{3.7}$$

$$f(\eta) = (\eta(\eta_e-\eta_0)+\eta_0)^3 + \eta_1 \tanh(k\eta(\eta_e-\eta_0)+C), \quad f_0 = \begin{cases} f(0) & \text{if} \quad \eta_0 \geq 0 \\ \eta_1 \tanh C & \text{if} \quad \eta_0 < 0 \end{cases}$$

and the empirical constants are set to:

$$\begin{aligned} \eta_1 &= -0.03 \text{ (approximate maximum reversed velocity)} \\ \eta_e &= 2.5 \\ k &= 4.0 \\ C &= 0.0 \end{aligned}$$

This profile exhibits the experimentally observed lift-off in separated regions and is a good approximation to Falkner-Skan profiles in attached regions. It does not work as well as the Falkner-Skan profiles for very strong accelerating flows but is used nevertheless as the better overall profile family.

One-parameter profile families are sufficiently accurate for most purposes. In principle, however, at least one other free parameter c is available as an additional degree of freedom. This parameter can be used, if desired, to model the effect of crossflow magnitude on the streamwise profile shape.

3.2.2 Turbulent flow

A crude approximation for the turbulent streamwise profile used in several early methods was a one-parameter profile family,

$$u(\zeta;\eta) = \eta^{\frac{1}{\zeta}},$$

with $\zeta \approx 7$ in flat-plate boundary layers. It still finds use in more recent methods (see, for example, Tai (1987) [61, 60]).

The two-dimensional turbulent velocity profile is actually two-layered and may be written as the sum of universal inner and outer profiles [5]:

$$\begin{aligned} u(U_\tau, U_\beta;\eta) &= u_{\text{I}}(U_\tau;\eta) + u_{\text{O}}(U_\beta;\eta) \\ u_{\text{I}}(U_\tau;\eta) &= U_\tau u^+(y^+) \\ u_{\text{O}}(U_\beta;\eta) &= U_\beta f^*(\eta) \end{aligned}$$

Both profiles are well substantiated by experiment in two-dimensional flow [43, 68]. The inner profile is multiplied by the normalized friction velocity

$$U_\tau = s\sqrt{\frac{|\tau_{w_1}|}{\rho_e u_e^2}}\,, \quad s = \mathrm{sign}(\tau_{w_1})\,, \tag{3.8}$$

while the outer profile is multiplied by the normalized defect velocity U_β, which can be conveniently taken to be a free parameter. The choice of the other free parameter, in fact, will depend on how the inner profile is defined and doesn't necessarily have to be U_τ. The use of s allows applicability to separated flow profiles.

Outer profile

The outer profile is the wake function. It does not contribute to the velocity gradients at either the wall or the outer edge. Coles approximated it by the expression

$$f^*(\eta) = \frac{1-\cos(\pi\eta)}{2}\,,$$

which has found wide use. A variety of other empirical formulae have been proposed, some in an attempt to approximate non-equilibrium conditions (see for example [11, 36, 39]).

Le Balleur [35] has proposed an expression for the outer profile that is a better approximation for separated flows than Coles' wake function. Here, the wake layer is assumed to lift-off ("disassociate" from the wall) by a distance approximately linearly proportional to δ_1^*/δ in the separated range ($\delta_1^*/\delta > \approx 0.45$). The region closer to the wall is assumed to be of constant (in η) velocity, with the maximum reverse velocity ($\approx 0.2 q_e$) occurring at around $\delta_1^*/\delta = 0.60$.

Inner profile

The inner profile is expressed in terms of the inner coordinate

$$y^+ = \frac{y U_\tau u_e}{\nu} = \eta U_\tau Re_\delta\,,$$

which at the boundary layer edge has the value

$$y_e^+ = U_\tau Re_\delta \Rightarrow u_e^+\,. \tag{3.9}$$

The following identity then ensures that the $u(1) = 1$:

$$U_\tau u_e^+ + U_\beta \equiv 1 \tag{3.10}$$

If in the law of the wall, the small regions adjacent to the wall, the sublayer and the transition zone, are ignored, the inner profile can be expressed explicitly as

$$u^+ = \frac{1}{\kappa} \ln(y^+) + B \,, \tag{3.11}$$

where κ and B are numerical constants with values 0.4 and 5.5, respectively [43]. Following Coles, many methods have used this expression to generate closure relationships. Theoretically, the near-wall regions can be ignored in the evaluation of most integral thicknesses (with the notable exception of the dissipation integrals). This expression is explicit but not well suited to numerical quadrature in practice, however, because of the singular behavior of the log term at the wall (note that here the natural choice for the other free parameter would be y_e^+).

A more robust approach is to use the Spalding expression for the inner profile. The velocity is defined implicitly

$$y^+ = u^+ + e^{-\kappa B} \left(e^{\kappa u^+} - 1 - \kappa u^+ - \frac{(\kappa u^+)^2}{2} - \frac{(\kappa u^+)^3}{6} \right) . \tag{3.12}$$

Here, it is more natural to use u_e^+ as the inner profile parameter which, in turn, fixes Re_δ through Equations 3.12 and 3.9. The implicit definition of velocity is actually advantageous from the point of view of the accuracy of numerical quadrature of integral thicknesses. The y-coordinate grid spacing is automatically stretched so that points are clustered near the wall where the velocity gradients are largest. This same stretching would also be used for the outer profile.

In both Equations 3.11 and 3.12, it should be noted that for small values of Re_δ (near laminar flow), undesirably large velocity gradients are possible at the outer edge. Pfeil and Amberg [45] propose a modified form for the inner law, that includes the viscous sublayer and transition zone, with a corrective term to ensure that the edge gradient is zero.

A complete profile

Swafford [58] proposed a complete explicit analytical expression for attached and mildly separated flows where the profile family is expressed in terms of transcendental functions

$$u = \frac{s}{0.09u_e^+}\tan^{-1}(0.09y^+) + \left(1 - \frac{s\pi}{0.18u_e^+}\right)\sqrt{\tanh\left(a\eta^b\right)}\,. \tag{3.13}$$

Here, the free parameters are a, b and the skin friction (through u_e^+). Note that the actual meaning of the first two parameters is different from those in Swafford's paper because there the y coordinate is scaled by the momentum thickness and not δ. The third parameter can be related to the other two by assuming an empirical function for skin friction. Using such a function, Swafford describes a procedure to compute the profile with the inputs being the shape factor H and momentum Reynolds number Re_θ instead of a and b based on matching the output of Equation 3.13 for two points in the boundary layer to empirical curve fits. This, of course, is not necessary here.

3.3 Cross-stream velocity profiles

For turbulent flows, the crossflow velocity is expressed in terms of the streamwise velocity (or, equivalently, in terms of a hodograph curve) [30]. The prototypical one-parameter form was suggested by Prandtl (1946) [43]

$$\frac{w}{u}(\tan\beta_w;\eta) = g^*(\eta)\tan\beta_w\,, \quad g^*(0) = 1, \quad g^*(1) = 0\,, \tag{3.14}$$

where g^* was postulated to be a universal function.

Some representative and popular empirical models for laminar and turbulent boundary layers in the literature are presented below. For simplicity, only additional parameters arising out of the crossflow model are indicated and those parameters due to the crossflow velocity-profile dependence on the streamwise velocity are implied.

3.3.1 Laminar flow

An early profile family set for infinite swept flow due to Wild (1949) is given by Schetz [48]. It is based on different wall-normal scaling for the chordwise and spanwise directions

$$u_c(\Lambda;\eta) = F(\eta) + \Lambda G(\eta), \quad w_c(\alpha;\eta) = F(\alpha\eta)$$

where

$$F(\eta) = \eta(2 - 2\eta^2 + \eta^3), \quad G(\eta) = \frac{1}{6}\eta(1-\eta)^3$$

In the chordwise direction, the profile is identical to Pohlhausen's. The spanwise profile is independent of the shape of the chordwise one (appropriate assumption for infinite-span conditions). The cross-stream free parameter is the scale-multiplier α.

For more general calculations, the cross-stream profile, as in turbulent flow is assumed to have a streamwise flow dependence. A simple two-parameter model is

$$w(c, c_1; \eta) = c(1-u)(\eta + \tilde{c}_1\eta^2)) = (1-u)(c\eta + c_1\eta^2)) \,.$$

This expression admits bidirectional profiles. For unidirectional crossflow calculations, c_1 is set to zero.

3.3.2 Turbulent flow

Some of the more commonly-used models in the literature are briefly described below.

Johnston

Based on experimental observations, Johnston [30] proposed a two-layer, two-parameter triangular profile

$$w(c, \beta_w; \eta) = \begin{cases} \tan\beta_w u & \text{if } \eta \le \eta^* \\ c(1-u) & \text{if } \eta > \eta^* \end{cases} \tag{3.15}$$

where the apex of the triangle is experimentally found to lie very close to the wall [43, 54]. Therefore, the model for inner-layer which assumes collateral flow in violation of Equation 3.3, is tolerated. In practice, in the boundary-layer thickness' integrations (except the dissipation integrals), the wall region contribution is negligible. For dissipation integrals, both wall and wake regions have to considered, where the kink in the profile represents a problem.

The two parameters are interdependent because the velocity at the edges of the two layers must match at the triangle apex. Experimentally, this has been proposed to lie at $q(\eta^*)/U_\tau \approx 10\sqrt{2}$. Then, the two parameters can be related [54], in compressible flow (density at the wall given by the Crocco-Busemann relation), through

$$c(\beta_w) = \tan\beta_w \frac{\sqrt{c_{f_1}\cos\beta_w(1 + r\frac{\gamma-1}{2}M_e^2)}}{0.10 - \sqrt{c_{f_1}\cos\beta_w(1 + r\frac{\gamma-1}{2}M_e^2)}}\,.$$

The obvious choice for the free parameter is β_w.

Mager

Mager [37] suggested that a simple parabolic polynomial be Prandtl's universal crossflow function so that

$$w(c;\eta) = c(1-\eta)^2 u\,.$$

This model, like Johnston's, has been widely used in the literature.

Eichelbrenner and Peube

The authors [23] have proposed a crossflow model, amongst others, which is a fifth-order polynomial of the hodograph function $w = w(u)$. The polynomial coefficients are reduced from five to two by assuming

$$\left.\frac{\partial w^2}{\partial u^2}\right|_w = 0\,, \tag{3.16}$$

$$\left.\frac{\partial w^2}{\partial u^2}\right|_e = 0\,, \tag{3.17}$$

and applying the boundary condition

$$w(u_e) = 0\,.$$

Note that the wall boundary condition is automatically satisfied. The resulting crossflow model is

$$w(c, \beta_w; \eta) = \tan\beta_w(u - 6u^3 + 8u^4 - 3u^5) - c(4u^3 - 7u^4 + 3u^5)\,.$$

where the remaining coefficients have the same meaning as in Johnston's crossflow model

$$\begin{aligned} \tan\beta_w &= \left.\frac{w}{u}\right|_{\lim\eta\to 0}\,, \\ c &= \left.\frac{w}{1-u}\right|_{\lim\eta\to 1}\,. \end{aligned}$$

This two-parameter model admits bidirectional crossflows. It also removes the sharp kink in Johnston's model. The authors propose an equation for c in terms of the curvature of the outer-edge streamlines, based on inviscid arguments for unidirectional flow, as suggested by Johnston (see, for example, Schetz [48]). This, of course, reduces the model to just one free parameter (which is how it was used in a computational method of Smith [53]). For bidirectional crossflows, the two-parameter version can be retained.

Assumption 3.16 assumes that the near wall flow is collateral contradicting Equation 3.3 under general conditions. If this assumption is removed, a three-parameter model results

$$\begin{aligned} w(c, \beta_w, \tan'\beta_w; \eta) = \tan\beta_w(u - 6u^3 + 8u^4 - 3u^5) - c(4u^3 - 7u^4 + 3u^5) \\ + \frac{\tan'\beta_w}{2}(u^2 - 3u^3 + 3u^4 - u^5)\,, \end{aligned}$$

where the wall curvature parameter can be directly related to the external flow pressure gradients [43]

$$\tan'\beta_w = \left.\frac{\partial^2 w}{\partial u^2}\right|_w = -\frac{\mu}{\tau_{w_1}^2}(1 + \tan^2\beta_w)\left(\tan\beta_w\frac{\partial p}{\partial s} + \frac{\partial p}{\partial n}\right)\,.$$

Shanebrook and Sumner

Shanebrook and Sumner [51] propose a crossflow profile family of arbitrary generality based on Taylor series expansions of the hodograph profile about $u = 0$ and $u = 1$ and then requiring one

or more consecutive derivative terms of the expansions at each edge to be zero. They find good agreement with compressible-flow experimental data with this approach including crossover profiles.

3.4 Models for the complete profile

The models presented so far have been based on separate definitions for the streamwise and cross-stream velocity profiles. Attempts have also been made to model the complete profile in an integrated manner for turbulent flow. Two are briefly mentioned here.

Tai [60, 61] proposed that instead of using the two-dimensional velocity profile in the streamwise direction, the streamwise and cross-stream velocity profiles be defined such that two-dimensional velocity profile is the magnitude of the total velocity vector in three dimensions. The crossflow velocity profiles may be modeled as before. In large crossflows, this approach avoids the physically unrealistic swelling of the total velocity magnitude near the wall.

Coles [5] suggested that the inner and outer layers be added vectorially, instead of as scalars only in the streamwise direction:

$$\begin{aligned} \mathbf{q}(U_\tau, U_\beta; \eta) &= \mathbf{q}_{\mathrm{I}}(U_\tau; \eta) + \mathbf{q}_{\mathrm{O}}(\vec{U}_\beta; \eta) \\ \mathbf{q}_{\mathrm{I}}(U_\tau; \eta) &= U_\tau \vec{u}^{\,+}(y^+) \\ \mathbf{q}_{\mathrm{O}}(\vec{U}_\beta; \eta) &= \vec{U}_\beta f^*(\eta) \end{aligned}$$

Here, $\vec{u}^{\,+}(y^+)$ is in the direction of the wall shear-stress vector and U_τ is proportional to the square root of the magnitude of this vector. The normalized defect-velocity components are related to each other by the identity

$$\mathbf{q} \equiv U_\tau \vec{u}_e^{\,+} + \vec{U}_\beta \, .$$

The inner and outer profiles in this formulation do not necessarily have be those used for two-dimensional boundary layers. Note that with the two-dimensional profiles, the model is limited to just three free parameters. Furthermore, note that the inner profile assumes that the law of the wall applies in the wall shear-stress direction which, as shown by Degani and Walker [17], is only true in the limit of infinite Re_δ.

3.5 Skin friction

The skin friction and hence shear-stress components can be derived directly from the profile definitions. Alternatively, empirical formulae based on experimental data can be used. Examples of such formulae for the streamwise component in the literature are Ludwig-Tilmann [43], Swafford et. al. [58] and Drela [19, 21, 44].

Chapter 4

Nature of the Unsteady Differential Equation System

An analysis of the nature of the steady incompressible boundary layer equations was first performed by Raetz [46]. A subsequent study was performed by Wang [67] who analyzed the nature of the steady incompressible Navier-Stokes equations and studied changes that occur in the boundary-layer approximation. An analysis which also included the energy equation (with temperature as variable) by Krause [33] found that the mechanics of information flow were identical to those for the incompressible case. The analysis presented here is an extension of Wang's analysis to the unsteady compressible case, but with the Crocco-Busemann relation replacing the energy equation.

4.1 Characteristic analysis

The pressure gradients are considered known because they are a function only of the prescribed external flow. The unknowns are the velocity components. Based on the Crocco-Busemann relation, density is assumed to have the functional form

$$\rho = \rho(u, w)\,,$$

where it is important to note the lack of dependence on the wall-normal component of velocity (consistent with the first-order boundary-layer approximation $v \ll \sqrt{u^2 + w^2}$).

The equations, for the purposes here, are best written as:

$$\frac{\partial \rho}{\partial u}\frac{\partial u}{\partial t} + (\rho + u\frac{\partial \rho}{\partial u})\frac{\partial u}{\partial x} + v\frac{\partial \rho}{\partial u}\frac{\partial u}{\partial y} + w\frac{\partial \rho}{\partial u}\frac{\partial u}{\partial z}$$

$$+\rho\frac{\partial v}{\partial y} + \frac{\partial \rho}{\partial w}\frac{\partial w}{\partial t} + u\frac{\partial \rho}{\partial w}\frac{\partial w}{\partial x} + v\frac{\partial \rho}{\partial w}\frac{\partial w}{\partial y} + (\rho + w\frac{\partial \rho}{\partial w})\frac{\partial w}{\partial z} = 0$$

$$\rho\frac{\partial u}{\partial t} + \rho u\frac{\partial u}{\partial x} + \rho v\frac{\partial u}{\partial y} + \rho w\frac{\partial u}{\partial z} = -\frac{\partial p}{\partial x} + \frac{\partial}{\partial y}\left(\mu\frac{\partial u}{\partial y} - \rho\overline{u'v'}\right)$$

$$\rho\frac{\partial w}{\partial t} + \rho u\frac{\partial w}{\partial x} + \rho v\frac{\partial w}{\partial y} + \rho w\frac{\partial w}{\partial z} = -\frac{\partial p}{\partial z} + \frac{\partial}{\partial y}\left(\mu\frac{\partial w}{\partial y} - \rho\overline{w'v'}\right)$$

Under the adiabatic-wall assumption, the viscosity μ is considered a function only of outer-edge conditions and, therefore, taken to be prescribed. For a turbulent flow, in theory the effects of the Reynolds stresses can be related to the mean-flow velocity components through some turbulence model. Then these stresses would have a bearing on the nature of the equations to some degree determined by the particular turbulence model used. However, in the *integral* equations in this thesis, the Reynolds stresses appear only in the shear-stress gradient integrals which are source terms and, consequently, do not play a role in the determination of the characteristic nature. On these grounds, they will be neglected in the following analysis.

To determine the characteristics, the highest-order terms in each of the differential equations are considered. These terms can be written in operator form for the unknown variables u,v and w as:

$$\begin{bmatrix} \frac{\partial \rho}{\partial u}\frac{\partial}{\partial t} + \mathbf{a}_u \cdot \nabla & \rho\frac{\partial}{\partial y} & \frac{\partial \rho}{\partial w}\frac{\partial}{\partial t} + \mathbf{a}_w \cdot \nabla \\ \mu\frac{\partial^2}{\partial y^2} & 0 & 0 \\ 0 & 0 & \mu\frac{\partial^2}{\partial y^2} \end{bmatrix}$$

Here, for brevity, the space Jacobian terms for u and w in the continuity equation have been lumped together in $\mathbf{a}_u$ and $\mathbf{a}_w$, respectively.

Determination of the characteristic structure requires the characteristic determinant corresponding to the operator matrix to be set to zero, as described in the appendix to this chapter. Here, it is

$$
\begin{aligned}
Q_c &= \begin{vmatrix} \frac{\partial \rho}{\partial u}\frac{\partial \Omega}{\partial t} + \mathbf{a}_u \cdot \nabla\Omega & \rho\frac{\partial \Omega}{\partial y} & \frac{\partial \rho}{\partial w}\frac{\partial \Omega}{\partial t} + \mathbf{a}_w \cdot \nabla\Omega \\ \mu\left(\frac{\partial \Omega}{\partial y}\right)^2 & 0 & 0 \\ 0 & 0 & \mu\left(\frac{\partial \Omega}{\partial y}\right)^2 \end{vmatrix} = 0\,, \\
&\Rightarrow \quad -\left(\rho\frac{\partial \Omega}{\partial y}\right)\left(\mu\left(\frac{\partial \Omega}{\partial y}\right)^2\right)^2 = 0\,.
\end{aligned}
$$

The determinant is the product of two factors, the first being a contribution from the continuity equation, and the second resulting from the diffusion terms in the momentum equations. There are five real and equal roots: the equations are parabolic. These roots indicate that all surfaces $\Omega(x, z, t) = 0$ normal to the wall are characteristic surfaces. There is no other direct information available from the determinant. In particular, nothing is revealed about the characteristic behavior in the wall-parallel planes.

This result is identical to the one for incompressible equations found by Wang because here the density is not considered a function of v. This outcome is fortuitous because only then do the equations capture the basic nature of the complete compressible system, which includes the full energy equation [1]. It is interesting to note the potentially drastic change in the character that could result from admitting even a minor dependence of ρ on v. This is exactly analogous to the complete change in going from the Navier-Stokes equations to the boundary-layer equations. Van Dyke [65] makes a related observation about dramatic changes in character in going from a governing partial differential equation to a perturbation form.

There are two physical inferences that can be made here. First, one of the factors in the characteristic determinant is due to the continuity equation. The resulting parabolic property, as Wang points out, is not due to any real or apparent incompressibility despite the fact the pressure is constant in the wall-normal direction. This is because compressibility is defined as the ratio of changes in pressure and density; here the pressure terms do not appear in the characteristic determinant. Second, and more importantly, the other factor in the determinant is due to the diffusion terms. This alone and

[1] The enthalpy and momentum convection-derivative operators are identical. Furthermore, for unity Prandtl numbers, the diffusion operators are identical as well. In this case, the mathematical character is preserved for both the characteristic and subcharacteristic analyses.

not the continuity equation, based on well-known properties of well-posedness of elliptic/parabolic problems, provides the physical mechanism for the infinite speed of information propagation in the wall-normal direction.

Finally, note that the time derivatives in the continuity equation play no role in the characteristic structure. Note particularly, that this is because the density is not a function of v. The results of the characteristic analysis are therefore identical for both the unsteady and the steady equations.

4.2 Subcharacteristic analysis

Wang first applied the concept of "subcharacteristics" to the boundary layer equations. These refer to the characteristics of a sub-structure of the flow. A subcharacteristic analysis is useful here because the characteristic analysis does not reveal anything about the behavior of the equations in the wall-parallel plane.

The subcharacteristics of the boundary layer equations are obtained by performing the usual characteristic analysis while neglecting the viscous terms. Then, the convective terms play a role. The resulting system is identical to the Euler equations except, of course, for the critical difference in the treatment of density (here an algebraic formula, as opposed to solving the enthalpy equation). The operator matrix for the resulting system is

$$\begin{bmatrix} \frac{\partial \rho}{\partial u}\frac{\partial}{\partial t} + \mathbf{a}_u \cdot \nabla & \rho\frac{\partial}{\partial y} & \frac{\partial \rho}{\partial w}\frac{\partial}{\partial t} + \mathbf{a}_w \cdot \nabla \\ \mathcal{L} & 0 & 0 \\ 0 & 0 & \mathcal{L} \end{bmatrix}$$

where

$$\mathcal{L} = \rho\frac{\partial}{\partial t} + \rho\mathbf{q} \cdot \nabla$$

is the material (or total) derivative operator.

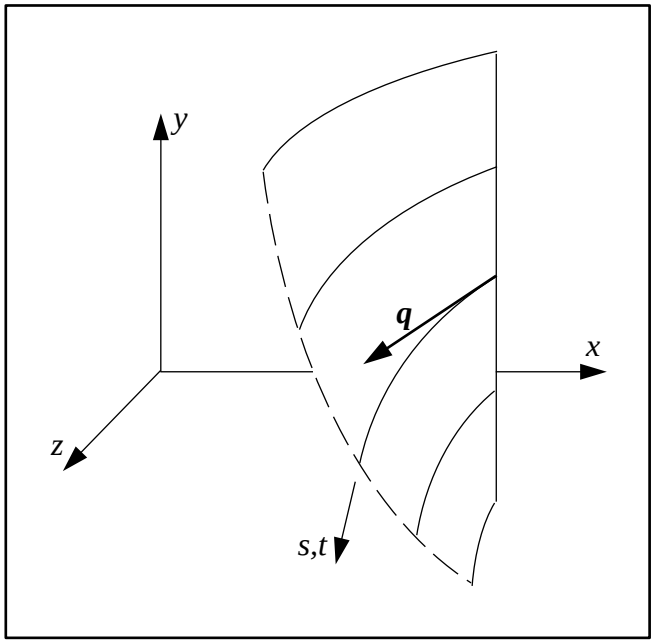

Figure 4-1: A characteristic surface defined by the family of subcharacteristics through a wall-normal line. In steady flow, the subcharacteristics are streamlines; in unsteady flow, they are pathlines.

The corresponding characteristic determinant is

$$Q_s = \begin{vmatrix} \frac{\partial \rho}{\partial u}\frac{\partial \Omega}{\partial t} + \mathbf{a}_u \cdot \nabla\Omega & \rho\frac{\partial \Omega}{\partial y} & \frac{\partial \rho}{\partial w}\frac{\partial \Omega}{\partial t} + \mathbf{a}_w \cdot \nabla\Omega \\ \Delta_{\mathcal{L}} & 0 & 0 \\ 0 & 0 & \Delta_{\mathcal{L}} \end{vmatrix} = 0$$

$$\Rightarrow \quad -\left(\rho\frac{\partial \Omega}{\partial y}\right)(\Delta_{\mathcal{L}})^2 = 0, \quad \Delta_{\mathcal{L}} = \rho\left(\frac{\partial \Omega}{\partial t} + \mathbf{q}\cdot\nabla\Omega\right).$$

The first factor in the characteristic determinant is identical to that in the full characteristic analysis and has the same physical interpretation here as well. The second factor is due to the convective terms in the momentum equations and cannot formally be classified mathematically as either hyperbolic or parabolic in the usual sense because the roots are neither distinct nor equal to zero.

There is a clear geometric interpretation for the second factor, however. Consider first the steady

equations. Here, $\Delta_{\mathcal{L}}$ simplifies to

$$\Delta_{\mathcal{L}} = \mathbf{q} \cdot \nabla\Omega = 0\,,$$

or that the streamlines are everywhere perpendicular to the normal of the characteristic surfaces Ω. Alternatively stated, the streamlines are everywhere tangent to these surfaces as shown in Figure 4-1. The subcharacteristic lines are defined parametrically in terms of s by ordinary differential equations

$$\frac{d\mathbf{x}}{ds} = \mathbf{q}(\mathbf{x}(s)), \quad \mathbf{x}(0) = \mathbf{x}_0\,,$$

where $\mathbf{x} = (x, y, z)^T$. Note that the determinant only implies a condition on the *orientation* of the subcharacteristics but makes no direct statement about the speed of information propagation; the notion of speed is implied by the physical *interpretation* of the direction components as velocity components. This implication acquires significance when contrasted to the infinite speed of information propagation in the wall-normal direction, as deduced earlier.

For the unsteady equations, the second factor is

$$\Delta_{\mathcal{L}} = \frac{\partial\Omega}{\partial t} + \mathbf{q} \cdot \nabla\Omega = 0\,,$$

which leads to the definition of unsteady subcharacteristics, defined parametrically in t by the ordinary differential equations

$$\frac{d\mathbf{x}}{dt} = \mathbf{q}(\mathbf{x}(t), t), \quad \mathbf{x}(0) = \mathbf{x}_0\,.$$

These subcharacteristics are tangent to characteristic surfaces $\Omega(\mathbf{x}(t), t)$. As proof, the rate of change of Ω along a subcharacteristic is

$$\begin{aligned}
\frac{d}{dt}\Omega(\mathbf{x}(t), t) &= \frac{\partial\Omega}{\partial t} + \frac{\partial\Omega}{\partial\mathbf{x}}\frac{d\mathbf{x}}{dt} \\
&= \frac{\partial\Omega}{\partial t} + \mathbf{q} \cdot \nabla\Omega \\
&= 0\,.
\end{aligned}$$

From the definition of the material derivative, the subcharacteristics for the unsteady problem are recognized to be particle trajectories or pathlines. Furthermore, the parameter t is the true time and

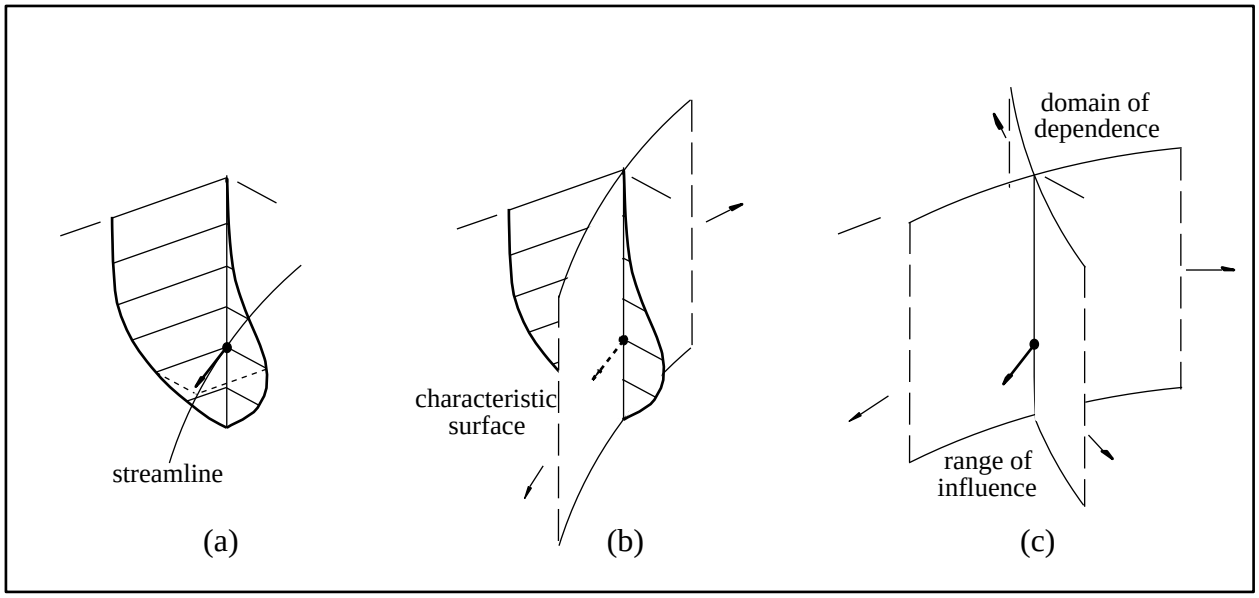

Figure 4-2: Characteristic nature of the steady differential equations, (a) a streamline (subcharacteristic) on the wall-normal, (b) the characteristic surface tangent to the streamline, (c) influence and dependence zones defined by normal surfaces containing the outer-most streamlines on the wall normal.

directly defines the velocity of information propagation as equal to the physical velocity components (unlike the steady problem where it is interpreted). These equal the characteristic surface slopes in the $\mathbf{x} - t$ planes. As is well known, in the steady limit, pathlines and streamlines become identical.

4.3 Influence and dependence zones

The characteristic and subcharacteristic analyses can be used to construct a useful physical picture of information flow implied by the differential boundary-layer equations. Specifically, zones of influence and dependence can be defined.

Consider first the steady equations. A disturbance at a point $\mathbf{x}_0$ in the flow is carried by the subcharacteristic which is the streamline through the point. The disturbance is also immediately communicated, by the diffusion mechanism, to all other subcharacteristics along the wall-normal. The disturbance is felt along all these subcharacteristics as well and, therefore, a range of influence can be defined by two wall-normal surfaces containing the most angularly-oriented subcharacteristics. A domain of dependence is defined as containing all those points whose range of influence touches

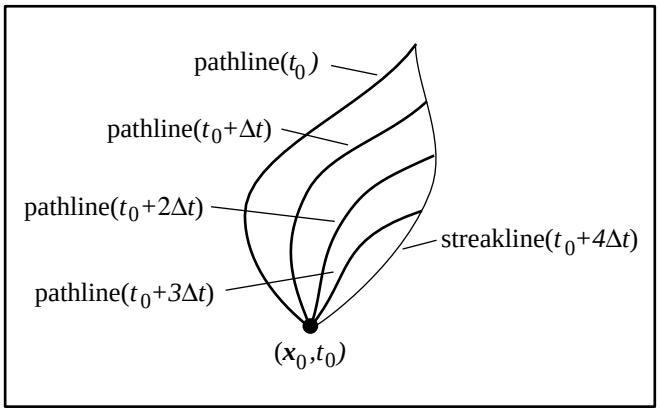

Figure 4-3: The surface swept by the $(\mathbf{x}_0, t_0)$ streakline in the time interval $4\Delta t$.

or contains the wall normal at (x_0, y, z_0). Both zones are semi-infinite in extent and are shown in Figure 4-2.

It is considerably more difficult to define the zones of influence and dependence for unsteady flow. The definitions provided here are limited to a qualitative description of these zones.

It is important to make a distinction between disturbances described by a Dirac delta function at $t = t_0$, and those described by a step function at $t = t_0$. Clearly, the range of influence and domain of dependence of the former will be a subset of those for the latter. The following definitions which assume the latter case will, therefore, also cover the former one.

The introduction of time means that the zones have a finite volume which increases with time as disturbances are convected along the subcharacteristics, which is this case are pathlines. The disturbance at a point $(\mathbf{x}_0, t_0)$, after a time interval Δt is felt by all fluid particles that have passed through it. Alternatively stated, this is the unique surface swept by the streakline originating at the same point through the same interval Δt, as shown in Figure 4-3. Such a surface is stationary in space but increases in downstream extent with time; it is a function of the location of the disturbance point in $\mathbf{x} - t$ and is denoted $S(\mathbf{x}_0, t_0, t)$.

The wall normal diffusivity, as in the steady case, dictates that information be communicated instantly along the wall normal. A cylindrical volume of influence for each wall normal at y_0, fixed in space but increasing in downstream extent with time $V_0(x_0, z_0, t_0, t)$ can then be defined as containing within it, and at most, all surfaces $S(\mathbf{x}_0, t_0, t)$. Clearly this volume, depicted in Figure 4-4, is at least a subset of the range of influence. The range of influence is, however, *potentially* greater

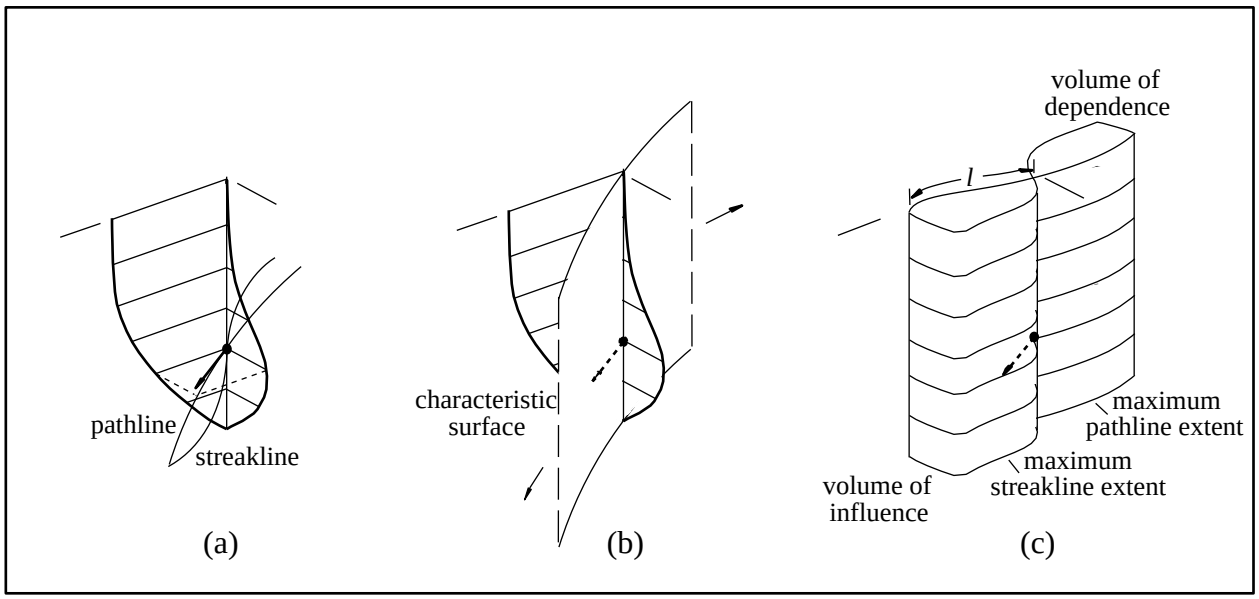

Figure 4-4: Characteristic nature of the unsteady differential equations, (a) a pathline (subcharacteristic) and streakline $(t-t_0)$ on the wall-normal, (b) characteristic surface tangent to the pathline, (c) influence and dependence volumes V_0 defined by normal surfaces containing the outer-most streaklines and pathlines. Here, the length of the pathline is given by $l(t) = \int_{t_0}^{t} q_e(x(t'), z(t'), t')dt'$. These volumes are an estimate of the range of influence and domain of dependence for $(t - t_0)/T_{ref} \ll 1$.

in downstream extent because for time t_1 where $t_0 < t_1 < t$, each wall-normal in the volume $V(x_0, z_0, t_0, t)$ itself has associated with it a volume of influence $V_1(x_0, z_0, t_0, t)$ over the smaller time interval $t - t_1$. This is a direct consequence of velocity gradients existing in the wall-normal direction (so that, by virtue of the infinite wall-normal information speed, the disturbance is communicated from the slower moving fluid near the wall to faster moving fluid near the boundary layer edge that is possibly outside $V_0(x_0, z_0, t_0, t)$). On this basis, another volume of influence can be defined $\tilde{V}_1$ to contain all those corresponding to the wall-normals in V_1. The process is now repeated for $\tilde{V}_n$ so that $n \to \infty$. The range of influence for the disturbance point $(\mathbf{x}_0, t_0)$ can now be defined as containing within it, and at most, V_0 and all cylindrical volumes $\tilde{V}_n(t)$ in the limit $n \to \infty$. The domain of dependence is also a function of time and is the volume containing all those points whose range of influence touches or contains the wall-normal at (x_0, y, z_0, t_0).

An *approximate* estimate of the range of influence is given simply by the volume V_0 as defined above, under the condition that

$$\frac{\Delta t}{T_{ref}} \ll 1\,,$$

where T_{ref} is an appropriate reference time scale in the boundary-layer flow.

The influence and dependence zones for the steady equations can be recovered from those for the unsteady equations in the limit $t \to t_0$. Then, the infinitesimally-short pathlines and streaklines converge to the local streamlines and the range of influence is the semi-infinite volume traced by streamlines through the wall normal at (x_0, z_0, t_0) as defined above for the steady equations.

Mathematically defining these zones precisely is a formidable task and outside the purview of this work. The relevant conclusion needed in the next chapter is simply the physical picture of finite-velocity information convection in the boundary layer.

4.4 Appendix: Determination of characteristic surfaces

Let $\Omega(x, y, z, t) = \omega_0$ define a characteristic surface for the equations, where ω_0 is a constant, and let the vector $\mathbf{p} = (u, v, w)^T$ denote the unknowns in the equations. For systems with just first-order derivative terms, the characteristic analysis can be viewed as seeking wave-like solutions of the form

$$\mathbf{p}(x, y, z, t) = \hat{\mathbf{p}}\, e^{i\Omega(x,y,z,t)}\,,$$

to the homogeneous form of the equations (since the source terms do not affect the characteristic analysis). Here Ω can clearly be interpreted as a phase angle [28]. Some second-order equations can be written as a mini-system of first order equations but this is not always possible. Introducing this test solution into the homogeneous equation system leads to the condition on the characteristic determinant. For convenience, indicial notation $i = x, y, z, t$ is introduced for the four Jacobian matrices and the corresponding gradient-operator components. Then

$$\mathbf{J}_i \cdot \nabla_i \mathbf{p} = (\mathbf{J}_i \cdot \nabla_i \Omega)\mathbf{p} = 0\,.$$

For non-trivial solutions ($\hat{\mathbf{p}} \neq 0$), a condition on the determinant

$$|\mathbf{J}_i \cdot \nabla_i \Omega| = 0$$

exists. Equivalently, the boundary or initial conditions cannot be prescribed on the characteristic surface because the solution on it is determined by the equations.

A more fundamental view of characteristic surfaces Ω as wavefronts is that discontinuities can propagate along them (see, for example, Whitham [69]). For first-order systems, a determinant condition can be derived by allowing discontinuities in $\frac{\partial \mathbf{p}}{\partial \Omega}$ but not necessarily in $\mathbf{p}$ (C^0 continuous in $\mathbf{p}$, for example $p = |\Omega|$). The equation system (retaining source terms) is written in terms of *local* characteristic surface Cartesian coordinates (the coordinate transverse to this surface is Ω)

$$\mathbf{J}_i \cdot \nabla_i \mathbf{p} = (\mathbf{J}_i \cdot \nabla_i \Omega)\frac{\partial \mathbf{p}}{\partial \Omega} = \mathbf{h}$$

The system is evaluated at either side of the surface $\Omega = 0$ and the difference between the two limits is

$$(\mathbf{J}_i \cdot \nabla_i \Omega)\left(\left.\frac{\partial \mathbf{p}}{\partial \Omega}\right|_{\Omega=0^+} - \left.\frac{\partial \mathbf{p}}{\partial \Omega}\right|_{\Omega=0^-} \right) = (\mathbf{J}_i \cdot \nabla_i \Omega)\Delta\frac{\partial \mathbf{p}}{\partial \Omega} = \mathbf{0}$$

Then, for a discontinuity to exist in the parameter-vector first derivative across the characteristic surface $\Delta\frac{\partial \mathbf{p}}{\partial \Omega} \neq \mathbf{0}$, implying that

$$|\mathbf{J}_i \cdot \nabla_i \Omega| = 0\,. \tag{4.1}$$

This is the sought-after determinant condition.

A similar condition can be derived for equations with second-order derivatives. Surfaces are sought normal to which discontinuities in $\frac{\partial^2 \mathbf{p}}{\partial \Omega^2}$ are possible but where $\frac{\partial \mathbf{p}}{\partial \Omega}$ and $\mathbf{p}$ are continuous (C^1 continuous in $\mathbf{p}$, for example $p = |\Omega|\Omega$). Without loss of generality, consider the system in one dimension only

$$\mathbf{J}^{(2)}\frac{\partial^2 \mathbf{p}}{\partial x^2} + \mathbf{J}^{(1)}\frac{\partial \mathbf{p}}{\partial x} = \mathbf{h}\,.$$

Writing the second-order terms in terms of local characteristic surface Cartesian coordinates

$$\frac{\partial^2 \mathbf{p}}{\partial x^2} = \frac{\partial}{\partial x}\left[\frac{\partial \Omega}{\partial x}\frac{\partial \mathbf{p}}{\partial \Omega}\right] = \frac{\partial^2 \Omega}{\partial x^2}\frac{\partial \mathbf{p}}{\partial \Omega} + \left(\frac{\partial \Omega}{\partial x}\right)^2 \frac{\partial^2 \mathbf{p}}{\partial \Omega^2}\,,$$

so that the complete system is

$$\mathbf{J}^{(2)}\left[\frac{\partial^2 \Omega}{\partial x^2}\frac{\partial \mathbf{p}}{\partial \Omega} + \left(\frac{\partial \Omega}{\partial x}\right)^2 \frac{\partial^2 \mathbf{p}}{\partial \Omega^2}\right] + \mathbf{J}^{(1)}\frac{\partial \Omega}{\partial x}\frac{\partial \mathbf{p}}{\partial x} = \mathbf{h}\,.$$

This system is evaluated at either side of the surface $\Omega = 0$ and the difference between the two limits is

$$\mathbf{J}^{(2)}\left[\left(\frac{\partial \Omega}{\partial x}\right)^2 \frac{\partial^2 \mathbf{p}}{\partial \Omega^2}\bigg|_{\Omega=0^+} - \left(\frac{\partial \Omega}{\partial x}\right)^2 \frac{\partial^2 \mathbf{p}}{\partial \Omega^2}\bigg|_{\Omega=0^-}\right] = \mathbf{J}^{(2)}\left(\frac{\partial \Omega}{\partial x}\right)^2 \Delta\frac{\partial^2 \mathbf{p}}{\partial \Omega^2} = \mathbf{0}\,.$$

A necessary condition for the discontinuity in the second derivative $\Delta\frac{\partial^2 \mathbf{p}}{\partial \Omega^2} \neq \mathbf{0}$ is then

$$\left(\frac{\partial \Omega}{\partial x}\right)^2 = 0$$

which is the corresponding characteristic determinant condition. This result is intuitive in that for the simple one-dimensional system considered here, the characteristic surface must be aligned with the x coordinate. The generalization to more dimensions is not needed here but is actually straightforward.

Chapter 5

Nature of Integral Equation Systems

This chapter contains an analysis of the mathematical properties of direct-mode integral boundary-layer equation systems. The flow of information implied by the differential boundary-layer equations is used to justify the requirement for the hyperbolicity of integral systems. The behavior of simple integral systems using traditional closure methods is shown to vary with the closure assumptions. It is shown that traditional closure methods are not sufficient to ensure hyperbolicity; for that, *additional* conditions, their exact form being the subject of the next chapter, have to imposed.

5.1 Justification of integral-system hyperbolicity

The formal analysis of the nature of the differential system, augmented with the physical picture of the flow of information in a boundary layer, provides a qualitative justification for the hyperbolicity of integral systems.

The three differential boundary-layer equations are quasi-linear partial differential equations in time and three space dimensions. The N integral boundary-layer equations derived from these is a system

of quasi-linear partial differential equations in time and two space dimensions:

$$\frac{\partial \mathbf{u}}{\partial t} + \frac{\partial \mathbf{f}}{\partial x} + \frac{\partial \mathbf{g}}{\partial z} = \mathbf{J}_t \frac{\partial \mathbf{p}}{\partial t} + \mathbf{J}_x \frac{\partial \mathbf{p}}{\partial x} + \mathbf{J}_z \frac{\partial \mathbf{p}}{\partial z} = \mathbf{h} \qquad \begin{cases} \mathbf{J}_t = \frac{\partial \mathbf{u}}{\partial \mathbf{p}} \\ \mathbf{J}_x = \frac{\partial \mathbf{f}}{\partial \mathbf{p}} \\ \mathbf{J}_z = \frac{\partial \mathbf{g}}{\partial \mathbf{p}} \end{cases}$$

In going from the differential to the integral form, any direct connection in the nature of the equations is confined to the dependence, through Jacobian matrices, of the flux vectors $\mathbf{u}$, $\mathbf{f}$ and $\mathbf{g}$ on the vector of system parameters $\mathbf{p}$.

The elements of the Jacobian matrices contain integrals of quantities that depend exclusively on the *convective* terms in the differential momentum equations and on the continuity equation. There is no dependence on the viscous diffusion terms. It has already been deduced, on physical grounds, that the infinite propagation speed of information in the wall-normal direction is not connected to the continuity equation, only to the viscous diffusion terms. Therefore, the convective terms which mathematically provide the subcharacteristic transport nature of the differential system should also provide a similar directional-transport nature to the integral equations.

A stronger argument can be made from the physical picture described by the zones of influence and dependence. In the integration, these zones collapse in the wall-normal direction. Clearly, the notions of domain of dependence and range of influence should carry over to the integral system. Thus, the mechanics of information propagation in the wall-normal direction are lost and what should remain is simply the convective transport of information in surfaces parallel to the wall. This directional transport of information can only result if the integral system is hyperbolic.

5.2 The eigenvalues of integral systems

The infinite number of subcharacteristics of the differential system should manifest themselves as a finite number (equal to the order of the system N) of characteristics of the integral system. The full angular range of the zones of influence and dependence in space, and in time for the unsteady equations, do not necessarily have to be captured by the integral equations, but it is clear that the characteristic directions must correspond, in some weighted-average sense, to the subcharacteristic-orientation distribution in the boundary layer. This is illustrated in Figure 5-1 (a) for a third-order

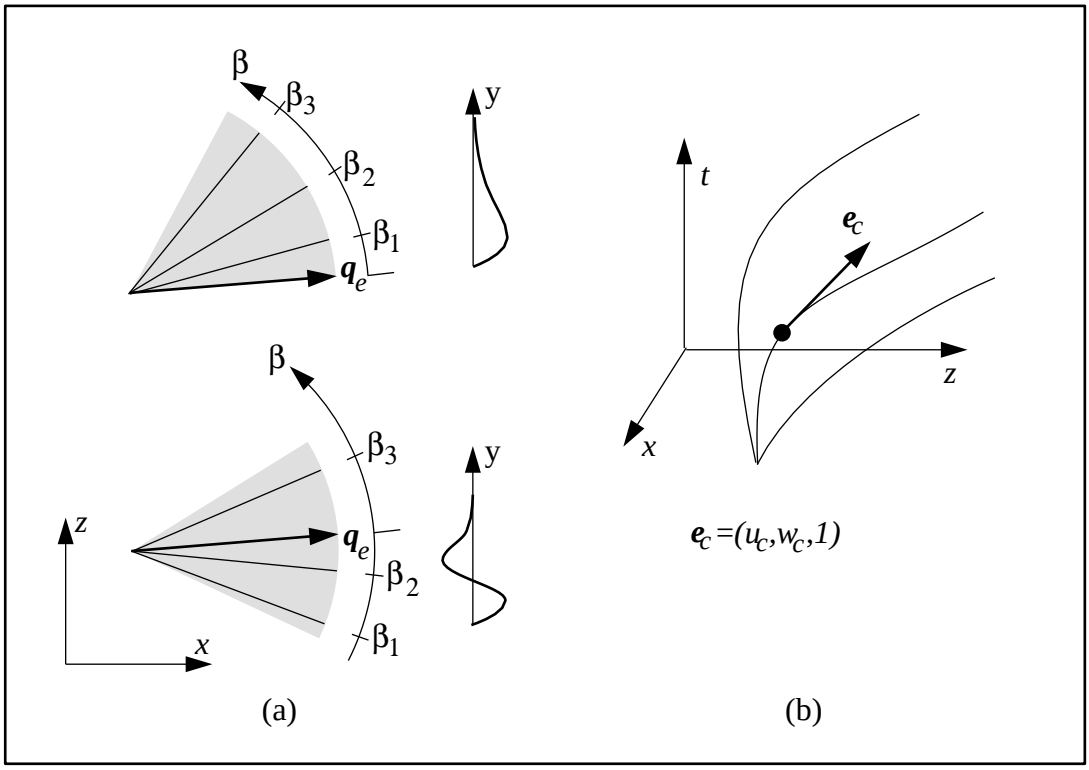

Figure 5-1: (a) Characteristic directions for a steady third order integral system for unidirectional and bidirectional crossflows. (b) Characteristic lines in $(\mathbf{x}, t)$ emanating from a point (x_0, z_0, t_0) and the characteristic velocity implied by their slope.

integral system for both unidirectional and bidirectional crossflows.

The characteristics for the steady equations describe orientations in space. The characteristics for the unsteady equations describe both orientation in space and in time; the slope of the characteristics in the $\mathbf{x} - t$ planes defines a velocity of information propagation as shown in Figure 5-1 (b) for a characteristic. Then each of the characteristic lines in Figure 5-1 (a) could be given a different length to denote the corresponding velocity.

For both steady and unsteady integral systems, characteristic *lines* in the relevant plane are sufficient to describe the flow of information; the notion of characteristic *surfaces* is unnecessary and discarded. Furthermore, instead of describing the orientation of these lines by the two remaining gradient components, it is more convenient to simply use a single angle. In the steady equations for example, if β is the angle (in the $x - z$ plane) that a line subtends to the x direction, then

$$\cos\beta = \frac{\partial\Omega}{\partial z},$$

$$\sin\beta = \quad - \quad \frac{\partial\Omega}{\partial x},.$$

For the steady integral system, the characteristic determinant condition in Equation 4.1 can now simply be written as

$$|\mathbf{J}_x \cos\beta - \mathbf{J}_z \sin\beta| = 0\,.$$

For a hyperbolic system, this characteristic equation must have N real roots. Equivalently, the system is hyperbolic if there exists the eigendecomposition

$$\mathbf{J}_z\mathbf{J}_x^{-1} = \mathbf{X}\mathbf{\Lambda}\mathbf{X}^{-1}, \quad \mathbf{\Lambda}, \mathbf{X} \in \Re\,,$$

with a set of N linearly independent eigenvectors $\mathbf{X}$ defining a set of characteristic variables $\partial\mathbf{v}_s = \mathbf{X}^{-1}\mathbf{J}_x\partial\mathbf{p}$, where the eigenvalues are $\mathbf{\Lambda} = \tan\beta_i$. If the eigenvalues are also distinct, the system is said to be totally hyperbolic [69]. If the eigenvalues are both real and complex, the system is of mixed character and may exhibit hyperbolic, parabolic or elliptic behavior depending on the physical problem [1].

Note that the coordinate axes can be rotated through rotational transform matrices. For example, in space, the space derivatives are related by:

$$\begin{pmatrix} \frac{\partial}{\partial\hat{x}} \\ \\ \frac{\partial}{\partial\hat{z}} \end{pmatrix} = \begin{bmatrix} \cos\theta & \sin\theta \\ \\ -\sin\theta & \cos\theta \end{bmatrix} \begin{pmatrix} \frac{\partial}{\partial x} \\ \\ \frac{\partial}{\partial z} \end{pmatrix}$$

The transform also rotates the eigenvalues, if real, by a corresponding amount

$$\hat{\mathbf{\Lambda}} = \mathbf{\Lambda} - \tan\theta\mathbf{I}\,.$$

There also exists a common non-singular transform matrix that allows the flux vectors $\mathbf{u}$, $\mathbf{f}$ and $\mathbf{g}$ to be expressed in different coordinate systems, which when applied in conjunction with the axes rotation allows the system to be expressed in any direction. Therefore, without loss of generality, the following discussion can be confined to a streamline-aligned coordinate system in space (unless otherwise stated).

In order to cast the full unsteady system into characteristic form, it is convenient to first transform the space derivatives and then use the corresponding eigenvector matrix in the time-derivate transformation. It will be useful to reiterate that the Jacobian matrices are basis dependent. A change of basis from one vector of system parameters $\mathbf{p}$ to another $\mathbf{v}$ is possible through a transformation

$$\frac{\partial}{\partial \mathbf{v}} = \frac{\partial \mathbf{p}}{\partial \mathbf{v}} \frac{\partial}{\partial \mathbf{p}} .$$

Since this is a similarity transformation in the eigendecomposition above, it will not affect the system eigenvalues. The new eigenvector matrix is related to old one through this transform.

The basis of the unsteady system is changed to the space characteristic variables $\partial \mathbf{v}_s = \mathbf{X}_s^{-1} \mathbf{J}_s \partial \mathbf{p}$:

$$\mathbf{X}_s^{-1} \left(\mathbf{J}_t \frac{\partial \mathbf{p}}{\partial t} + \mathbf{J}_s \frac{\partial \mathbf{p}}{\partial s} + \mathbf{J}_n \frac{\partial \mathbf{p}}{\partial n} \right) = \mathbf{X}_s^{-1} \mathbf{h}$$

$$\mathbf{X}_s^{-1} \mathbf{J}_t \frac{\partial \mathbf{p}}{\partial t} + \mathbf{X}_s^{-1} \mathbf{J}_s \frac{\partial \mathbf{p}}{\partial s} + \mathbf{X}_s^{-1} (\mathbf{J}_n \mathbf{J}_s^{-1}) \mathbf{J}_s \frac{\partial \mathbf{p}}{\partial n} = \mathbf{X}_s^{-1} \mathbf{h}$$

$$\mathbf{X}_s^{-1} \mathbf{J}_t \frac{\partial \mathbf{p}}{\partial t} + \mathbf{X}_s^{-1} \mathbf{J}_s \frac{\partial \mathbf{p}}{\partial s} + \mathbf{X}_s^{-1} (\mathbf{X}_s \mathbf{\Lambda}_s \mathbf{X}_s^{-1}) \mathbf{J}_s \frac{\partial \mathbf{p}}{\partial n} = \mathbf{X}_s^{-1} \mathbf{h}$$

$$(\mathbf{X}_s^{-1} \mathbf{J}_t \mathbf{J}_s^{-1} \mathbf{X}_s)(\mathbf{X}_s^{-1} \mathbf{J}_s) \frac{\partial \mathbf{p}}{\partial t} + (\mathbf{X}_s^{-1} \mathbf{J}_s) \frac{\partial \mathbf{p}}{\partial s} + \mathbf{\Lambda}_s (\mathbf{X}_s^{-1} \mathbf{J}_s) \frac{\partial \mathbf{p}}{\partial n} = \mathbf{X}_s^{-1} \mathbf{h}$$

$$(\mathbf{X}_s^{-1} \mathbf{J}_t \mathbf{J}_s^{-1} \mathbf{X}_s) \frac{\partial \mathbf{v}_s}{\partial t} + \frac{\partial \mathbf{v}_s}{\partial s} + \mathbf{\Lambda}_s \frac{\partial \mathbf{v}_s}{\partial n} = \mathbf{X}_s^{-1} \mathbf{h}$$

by employing the eigendecomposition

$$\mathbf{J}_n \mathbf{J}_s^{-1} = \mathbf{X}_s \mathbf{\Lambda}_s \mathbf{X}_s^{-1} .$$

An analogous eigendecomposition with time one coordinate is

$$\mathbf{X}_s^{-1} \mathbf{J}_t \mathbf{J}_s^{-1} \mathbf{X}_s = \mathbf{X}_t \mathbf{\Lambda}_t \mathbf{X}_t^{-1} ,$$

where the eigenvector matrix for the space variables is included for convenience. Therefore, the equations can be said to be hyperbolic in time if

$$\mathbf{\Lambda}_t, \mathbf{X}_t \in \Re ,$$

or if $|\mathbf{J}_s \cos \beta_t - \mathbf{J}_t \sin \beta_t|$ has N real roots, and hyperbolic in space if

$$\mathbf{\Lambda}_s, \mathbf{X}_s \in \Re ,$$

or if $|\mathbf{J}_s \cos\beta_t - \mathbf{J}_t \sin\beta_t|$ has N real roots. Here, β_s is the angle in space of the characteristic line relative to the streamline direction, and β_t is the angle the characteristic makes in space-time to the space streamline direction. The order of magnitude of these angles is related to the ratio of fluxes in the equation. In most cases,

$$\begin{aligned} \mathbf{g}_s &\sim c\,\mathbf{f}_s \quad \Rightarrow \tan\beta_s = \mathcal{O}(c)\,, \\ \mathbf{u} &\sim \frac{1}{q_e}\mathbf{f}_s \quad \Rightarrow \tan\beta_t = \mathcal{O}(\frac{1}{q_e})\,. \end{aligned}$$

It can be shown that the eigenvalues, as expected intuitively, are independent of the boundary layer thickness scale δ (provided that in turbulent flow, Re_δ is held fixed). In some steady computational methods, a lag equation is used in the streamwise direction only (see for example [44, 72]). Clearly, this equation contributes an eigenvalue of $\beta_s = 0$ to the system, and does not influence the eigenvalues of the remaining equations. Finally, note that for infinite-span type calculations, the spanwise derivative terms vanishes in all the equations (in, of course, chordwise-aligned coordinates). Then, the notion of space eigenvalues is not applicable, and attendant restrictions, to be discussed in the next chapter, are removed.

5.2.1 The problem and its possible solution

The eigenvalues of an integral system closed through empirical relationships (such as assumed velocity and density profiles across the boundary layer discussed in Chapter 3) are not necessarily real. Then the integral system behavior is non-hyperbolic, and as discussed in § 5.1, non-physical. The fundamental problem can be formulated in terms of the connection between the two elements that determine the eigenvalues: the equations chosen for the system and physical assumptions necessary to close the system. *The essential, and novel, idea is that these two elements cannot be considered in isolation in formulating the solution to the problem; changes in either, while holding the other fixed, affect the eigenvalues.* While the two elements are not chosen arbitrarily in traditional methods (for example, the facility to capture separation must be reflected in both), the connection between the two needs to be devised more carefully to specifically account for the eigenvalues. This idea is made more concrete in the next chapter.

5.2.2 Literature review

In the large number of different integral systems that have been proposed in the past, many have been claimed to be hyperbolic on the basis of a proto-system analyzed by Myring (1971) [42]. In some cases, this claim is not strictly justifiable because the differences with Myring's equation system are 'too great'. Including Myring's analysis, only a few original studies in the literature were found that were concerned with the characteristic problem and the explicit determination of eigenvalues in investigating it. Hence, the list that follows is fairly complete. All of these employ simple equation systems and closure relations that result in relatively simple Jacobian matrices. This usually permits the eigenvalues in the steady case to be expressed as crossflow-scaled functions of only a single streamwise parameter (for example, the shape factor)

$$\beta_{si} = c\,\mathrm{fn}(H)\,, \quad i = 1, \ldots, N\,,$$

the functional relationship being determined by the streamwise momentum equation and an auxiliary equation.

Myring's study for the commonly-used system for steady incompressible turbulent flow consisted of the two momentum equations and the entrainment equation. For streamwise profiles, the simple one-parameter power law (no Reynolds number dependence, as indicated in Chapter 3) was used

$$u = \left(\frac{y}{\delta}\right)^{1/\zeta}\,,$$

and for crossflow profiles, both Johnston's and Mager's models were used. The eigenvalues for this system were shown to be real for both crossflow models. Furthermore, they were shown to be physically sensible in that they corresponded to the general flow direction.

Cousteix and Houdeville (1981) [10] studied both steady and unsteady equations. For steady incompressible turbulent flow they used Myring's system with a slightly different closure relationship for the streamwise flow (but still neglecting any Reynolds number dependence), so that the entrainment shape factor was given by

$$\frac{\delta - \delta_1^*}{\theta_{11}} = \frac{0.631H^2 + H}{H - 1}\,.$$

The Johnston model was used for the crossflow. The eigenvalues were shown to be real and were actually numerically close to Myring's results. The analytical formula for the largest eigenvalue was

identified to be very similar to that for the limiting streamline for large Clauser numbers. Eigenvalues for unsteady turbulent flow in two dimensions was studied using the momentum and entrainment equations employing the same closure relationship as the steady problem and, not surprisingly, a close analogy between the two was made (the time behavior being qualitatively similar to the neglected space axis).

Van der Wees and Muijden (1990) [64] studied unsteady equations for compressible turbulent flow with a quasi-simultaneous viscous-inviscid method. The unsteady form of Myring's system was used with a very simple interaction law and Cousteix and Houdeville's closure for both streamwise and cross-stream directions. The eigenvalues were computed in the $s-t$ plane for quasi-three-dimensional flow so that the cross-stream derivatives vanish, with (computed numerically) and without (computed analytically) the interaction law. These were generally found to agree with previous results; however, in some cases with the interaction law, they do report that complex eigenvalues were found.

In two related papers, Wigton and Yoshihara (1983) [70] and Wai and Yoshihara (1984) [72] describe a method employing a four-equation system consisting of the entrainment equation, the two momentum equations and Green's lag equation in the streamwise direction only, for steady turbulent flow. In the streamwise closure, the entrainment shape factor correlation is taken from Green's lag-entrainment method [26], and Mager's velocity profile is used for the cross-stream closure. As indicated earlier, the lag equation decouples from the eigenvalue problem for the rest of the system. In both direct mode (where the boundary layer parameters are free variables and external velocity components are imposed) and inverse mode (where the shape factor is imposed and, in this case, the external velocity magnitude is a free variable) calculations, they report that only real system eigenvalues were found. However, for other combinations of the available variables in the parameter vector, complex eigenvalues were found. Consequently, they were forced to limit their solutions to parameter choices where the system was hyperbolic. Furthermore, they also report that none of the inverse-mode characteristics were identifiable with the limiting streamline, namely that their directions did not correspond well to the general flow direction.

Hall (1959) [27] solves the simple system consisting of just the two momentum equations with simple closure relationships for laminar flow that are an extension of Thwaites' method. The system is shown to be hyperbolic for reasonable ranges of the boundary-layer parameters and the characteristics are shown to lie between the external flow streamline and an assumed limiting streamline.

Caille and Schetz (1992) [4] solve a four-equation system, based on full/partial (in boundary-layer wall-normal extent) momentum/shear-stress balances. Two of these are the usual momentum equa-

tions for quantities integrated from the wall to the outer-edge and two are for a region extending from the wall to an arbitrary point in the boundary layer (see literature survey in Chapter 1). The resulting system is, evidently erroneously, claimed to be hyperbolic on the strength of an earlier study by Cousteix and Michel which applied to a different system. All their results are unusually wavy but this waviness probably cannot be ascribed to any non-real eigenvalue behavior, however, because it exists in results for an infinite-span calculation. Nevertheless, the hyperbolicity of the system is not convincingly demonstrated.

5.3 Analysis of some integral systems

Before discussing methods for ensuring hyperbolicity of the equations, a characteristic analysis is performed for two example systems. These analyses will serve to highlight issues already discussed. A simple steady second-order system (Hall's system) will be used to demonstrate that non-hyperbolic behavior can result for plausible closure schemes. A compressible analysis of a steady third-order system with realistic closure relationships is also presented.

5.3.1 A second-order system

The system is simply the two momentum equations. The number of unknowns in the derivative terms is reduced from four to two by assuming that the streamwise profile shape is constant, that the crossflow shape is constant but its the magnitude is allowed to vary. The character of this system can be shown to depend on a single derived parameter.

The primary parameters are chosen to be the streamwise scale of the boundary layer, measured by δ_1^*, and the crosswise scale, measured by δ_2^* so that $\mathbf{p} = (\delta_1^*, \delta_2^*)^T$. Then the four unknowns are:

$$\mathbf{f} \; : \quad \theta_{11} \sim \delta_1^*, \; \theta_{21} \sim \delta_2^*$$

$$\mathbf{g} \; : \quad \theta_{12} \sim \delta_2^*, \; \theta_{22} \sim (\delta_2^*)^2/\delta_1^*$$

With this closure, the system can be written as

$$\begin{bmatrix} \theta_{11} & 0 \\ 0 & \theta_{21} \end{bmatrix} \frac{\partial}{\partial s} \begin{pmatrix} \ln \delta_1^* \\ \ln \delta_2^* \end{pmatrix} + \begin{bmatrix} 0 & \theta_{12} \\ -\theta_{22} & 2\,\theta_{22} \end{bmatrix} \frac{\partial}{\partial n} \begin{pmatrix} \ln \delta_1^* \\ \ln \delta_2^* \end{pmatrix} = \mathbf{h}' \,,$$

where $\mathbf{h}'$ includes the external velocity and density derivatives in the flux vectors as well as the source terms.

The eigenvalues of this system are

$$\tan \beta_{1,2} = \frac{\theta_{22}}{\theta_{21}}(1 \pm \sqrt{(1 - r_m)}), \quad r_m = \frac{\theta_{12}\theta_{21}}{\theta_{11}\theta_{22}} \,.$$

They are real if and only if $r_m \leq 1$. This parameter is a measure of the cross-direction flux of momentum, but so far no physical meaning has been deduced for the hyperbolicity condition. For both constant-defect $u(y)$ and $w(y)$ profiles, as well as Johnston's simple outer-layer crossflow model, $r_m = 1$. Slight deviations in the profiles in both cases can make the system non-hyperbolic.

Of course, the eigenvalues of the system would be different if the closure paradigm were changed or if, for example, the total energy equation were used instead of one of the momentum equations.

5.3.2 A third-order system with Johnston's crossflow model

For general systems of three equations or more, the analytical (so that functional dependencies can be explicitly identified) determination of eigenvalues becomes virtually intractable. In the literature, simplifications in closure relationships were found to be necessary for the analysis to be feasible. Fortunately, for Johnston's crossflow model, the closure leads to simple relationships making it feasible to retain a two-parameter streamwise dependence for steady compressible turbulent flow. Eigenvalues for a system consisting of the two momentum equations and the total kinetic-energy equation can then be determined.

As discussed in Chapter 3, Johnston's model for turbulent flow relates the crossflow velocity linearly to the streamwise velocity with the crossflow parameter c

$$w = c(1 - u)$$

over the outer part of the turbulent boundary layer. The wall-layer contribution to relevant thicknesses is negligible. With the primary parameter vector chosen to be $\mathbf{p} = (\theta_{11}, H, c)^T$, the necessary analytical relationships are:

$$\mathbf{f} = \begin{pmatrix} \rho_e q_e^2 \theta_{11} \\ \rho_e q_e^2 \theta_{21} \\ \rho_e q_e^3 \theta_1^* \end{pmatrix} = \begin{pmatrix} \rho_e q_e^2 \theta_{11} \\ -c\, \rho_e q_e^2 \theta_{11} \\ \rho_e q_e^3 (H^* + c^2 (H^* - 2)) \theta_{11} \end{pmatrix}$$

$$\mathbf{g} = \begin{pmatrix} \rho_e q_e^2 \theta_{12} \\ \rho_e q_e^2 \theta_{22} \\ \rho_e q_e^3 \theta_2^* \end{pmatrix} = \begin{pmatrix} -c \rho_e q_e^2 (\tilde{H} - 1) \theta_{11} \\ -c^2 \rho_e q_e^2 (\tilde{H} - 1) \theta_{11} \\ \rho_e q_e^3 ((c(\tilde{H} + 1 - H^*) - c^3 (H^* - 3 + \tilde{H})) \theta_{11}) \end{pmatrix}$$

The effects of compressibility are introduced through the modified shape factor while the streamwise kinetic-energy shape factor is a function of the modified shape factor and the momentum-thickness Reynolds number

$$\tilde{H} = H - H_\rho(H, M_e), \quad H^* = H^*(\tilde{H}, Re_{\theta_{11}}) .$$

The eigenvalues of the resulting system are

$$\begin{aligned} \tan \beta_1 &= c(\tilde{H} - 1) , \\ \tan \beta_{2,3} &= c(-\xi_1 \pm \sqrt{(\xi_1^2 - 4\xi_2)})/2 , \end{aligned}$$

where

$$\begin{aligned} \xi_1 &= (2 - \tilde{H}) + (H^* - 1 + r) \tfrac{[\tilde{H}]_H}{[H^*]_H} , \\ \xi_2 &= (1 - \tilde{H}) + (H^* - 2 + r) \tfrac{[\tilde{H}]_H}{[H^*]_H} \end{aligned}$$

and $r = Re_{\theta_{11}} [H^*]_{Re_{\theta_{11}}}$ contains the dependence on Reynolds number. Subscripted brackets denote partial derivatives.

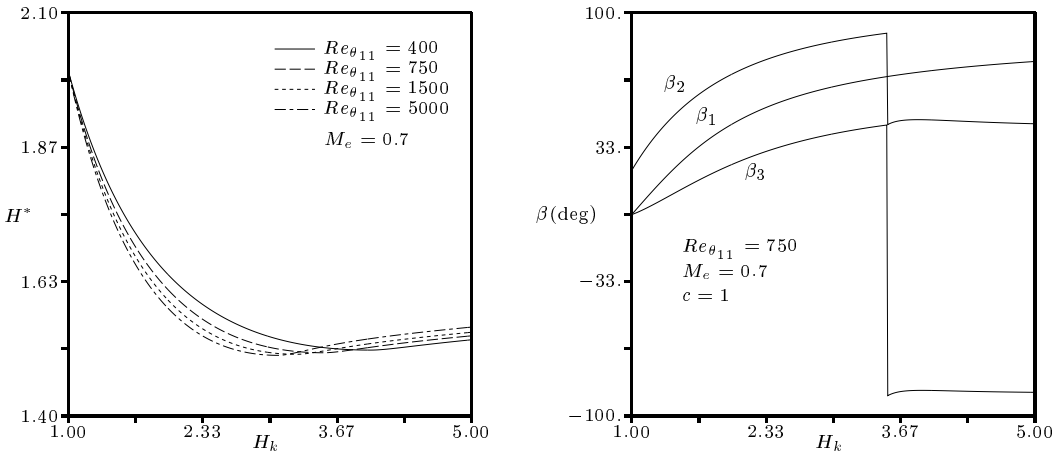

Figure 5-2: The kinetic-energy shape factor (H^*) variation and resulting normalized characteristic directions for Johnston's crossflow model.

The linearity of Johnston's velocity hodograph model manifests itself in the simple cross-flow scaled dependence of $\tan\beta_1$ on only the shape factor, due only to the momentum equations without any kinetic-energy equation dependence. Furthermore, all the eigenvalues are of the form $\tan\beta_i = c\tan\overline{\beta}_i(\tilde{H}, Re_{\theta_{11}})$, or in other words, are related linearly to the crossflow magnitude. This in an unexpected (because the energy thicknesses cannot be expressed in this simple form) but remarkable simplification; the condition on hyperbolicity, as in systems with the entrainment equation, depends solely on the definition of H^*.

The eigenvalues are computed for a realistic kinetic-energy/shape-factor correlation used in the numerical method of Drela [21]. This correlation is plotted in Figure 5-2 for various representative Reynolds numbers at a Mach number of 0.7. The three eigenvalues are real and are plotted in Figure 5-2 for a single value of the Reynolds number. Furthermore, all eigenvalues lie between the outer-edge streamline and an assumed (depending on the cross-stream skin-friction closure) wall-limiting streamline. Note that the outermost characteristic is discontinuous at $H \approx 3.5$ which corresponds to the singular point $[H^*]_H = 0$ (more on this in Chapter 9).

These results are similar to those found by Myring, Cousteix et. al. and van der Wees et. al. who used the entrainment equation instead of the total kinetic-energy equation. This is not surprising because the energy and entrainment shape-factor correlation functions are very similar.

5.4 Summary

Traditional closure methods generally yield systems which are hyperbolic, especially those that are minor variants of the basic three-equation momentum/total kinetic-energy ones. However, there is no formal assurance that these systems (under all realistic closure schemes, or systems that are substantially different) are hyperbolic. *Additional* conditions, coupling the system, in some manner, to the usual closure assumptions have to be applied to ensure hyperbolicity coupled, in some manner, to the usual closure assumptions. This is not a trivial task and is considered in the next chapter.

Chapter 6

Synthesis of Hyperbolic Integral Systems

In Chapter 5, the possibility of complex system eigenvalues leading to non-hyperbolic behavior was raised. It was indicated that additional conditions on the closure scheme for a system have to be imposed in order to ensure hyperbolic behavior. It is a well-known fact that the eigenvalues of a matrix are non-linearly related to its elemental values. For *general, non-symmetric* Jacobian matrices, this fact makes the problem of controlling the eigenvalues of a matrix through imposing conditions on its elements, over some region in parameter space, a formidable one. The inability to physically connect the nature of the differential equations and its derived integral approximations is unfortunate. In particular, the necessity for empiricism in integral closure introduces an arbitrary dimension to the problem, and suggests purely mathematical attempts at solution. These mathematical conditions, however, should be indirectly informed by the physical picture of information flow implied by the differential boundary-layer equations.

The objective of this chapter is to examine ways in which hyperbolicity can be enforced. The greater part of the chapter is devoted to the description of a novel closure scheme that successfully achieves that for general integral systems of arbitrary order. It is restricted by its nature, however, to the linearized form of the system because it operates on the Jacobian matrices. Within the context of most practical solution methods, this is not a major issue because the equations have to linearized in any case.

Before that method is presented, two other ideas for ensuring hyperbolicity, one based on symmetrizing the Jacobian matrices and the other on assembling a system by an induction approach, are outlined for illustrative purposes. Their value is mostly theoretical.

6.1 Symmetric Jacobian-matrices?

The requirement for the hyperbolicity of an integral system is physically connected to the nature of the differential set of equations. This motivates the question: is it possible to pose a closure scheme in such a way such that the system automatically has real eigenvalues, so that additional mathematical constraints do not have to be imposed?

To this end, two immediate possibilities suggest themselves. Consider the steady case only. The first is to choose a parameter basis and a closure scheme so that the combination results in symmetric $\mathbf{J_X}$ and $\mathbf{J_Z}$. Then the eigenvalues will be real if at least one of the two matrices is non-negative definite. The second is to choose a closure scheme so that the coefficient matrix

$$\frac{\partial \mathbf{g}}{\partial \mathbf{f}} = \mathbf{J_Z}\mathbf{J_X}^{-1}$$

is symmetric, and hence automatically has real eigenvalues.

It may be possible in some special situations to exploit a physical symmetry by expressing the equations in one of the two forms above. None have been identified, however, and in general this approach does not seem to be practical.

6.2 System/closure construction by induction

Consider only the steady system. Instead of tackling the problem for all eigenvalues simultaneously, the induction method seeks to build the system one equation at a time. Assuming that a system of order N is hyperbolic, the objective is to find conditions on the closure implied by the addition of an equation to the system so that the eigenvalues of the resulting $N+1$ system coefficient matrix $\mathbf{J_Z}\mathbf{J_X}^{-1}$ are real. Beginning with a scalar equation (eigenvalue is trivially real), it is then possible to construct a hyperbolic system spanning any number of equations.

Consider the roots of the characteristic equation of the $N+1$ order system in the characteristic basis of the lower-order system. For example, for $N = 2$ the resulting characteristic equation is

$$\left| \begin{bmatrix} \lambda_1 & & u_1 \\ & \lambda_2 & u_2 \\ v_1 & v_2 & \sigma \end{bmatrix} - \lambda \mathbf{I} \right| = (\sigma - \lambda)(\lambda_1 - \lambda)(\lambda_2 - \lambda) - u_1 v_1 (\lambda_2 - \lambda) - u_2 v_2 (\lambda_1 - \lambda) = 0 \,,$$

where λ_1, λ_2 are the eigenvalues of the second-order system. This basis is chosen because it yields a conveniently simple characteristic equation. Elements associated with the new equation appear as the addition of a rank-two matrix: the vector $\mathbf{u}$ contains the partial derivatives of the original equations with respect to the new system parameter, the vector $\mathbf{v}$ contains the partial derivatives of the new equation with respect to the characteristic-basis parameters of the smaller system and σ is the partial derivative of the new equation with respect to the new parameter. For a general $N+1$ system, the characteristic equation can be written

$$(\sigma - \lambda) \prod_{i=1}^{N} (\lambda_i - \lambda) - \sum_{j=1}^{N} u_j v_j \prod_{i, i \neq j}^{N} (\lambda_i - \lambda) = 0 \,.$$

Dividing through by $\prod_i^N (\lambda_i - \lambda)$ and rearranging

$$\sigma = \lambda + \sum_{j=1}^{N} u_j v_j \frac{1}{(\lambda_j - \lambda)} \,. \tag{6.1}$$

The equation in this form is simply the sum of translated $1/\lambda$ constituent functions. A sufficient set of conditions to ensure $N+1$ real roots is to require all coefficients to have the same sign, $u_j v_j > 0 \quad \forall j$ or $u_j v_j < 0 \quad \forall j$. In one case, all N eigenvalues of the resulting system will be be greater than the corresponding λ_i and in the other case, all will be less. The remaining eigenvalue will necessarily be real.

The induction process is illustrated for the extension from a two-equation system to a three-equation one in Figure 6-1. The two new eigenvalues are determined, if real, by the intersection of the right-hand side of Equation 6.1, plotted as the thick line, with σ, plotted as the dashed horizontal line. The eigenvalues of the original system are also indicated.

The conditions for real eigenvalues exist on the new elements of the coefficient matrix and effectively place constraints on closure assumptions. While the conditions have a simple form, they are likely

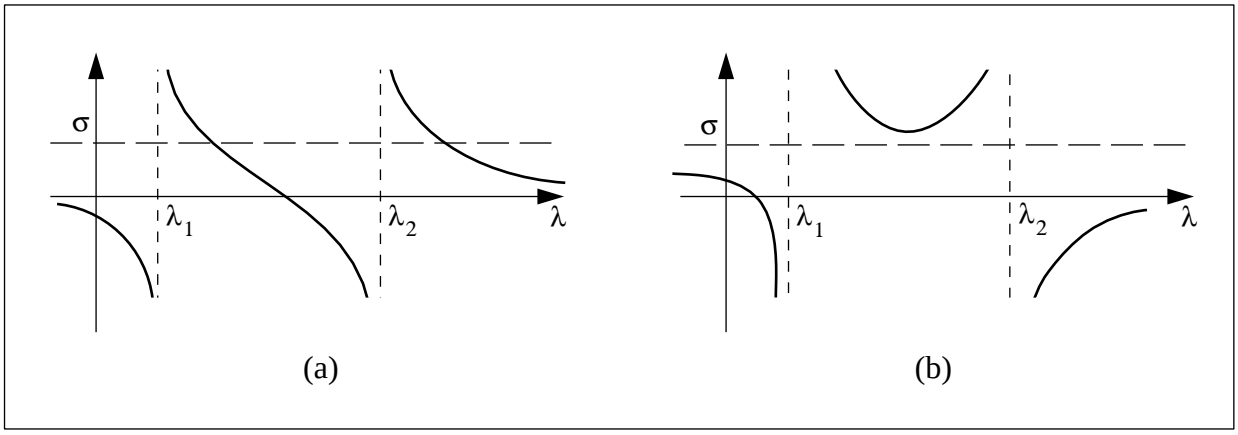

Figure 6-1: Characteristic equations of the original and augmented coefficient matrices for N=2, (a) real eigenvalues with sufficient conditions $u_j v_j > 0 \quad \forall j$, as shown, or $u_j v_j < 0 \quad \forall j$, indicated by the intersection of the thick lines with the constant σ line, (b) complex eigenvalue pair if the hyperbolicity conditions are not met.

to place an unnecessarily excessive constraint. Furthermore, implementing these constraints in any practical closure scheme is a difficult task for a number of reasons, in particular, the need to satisfy them over the entire parameter space, and for all subsequent equations in the system. The fundamental idea also suffers from fact that these are mathematical limitations which require a hierarchical treatment of the equations, with no apparent appeal to the physical basis of the problem.

Nevertheless, it could be of value when used in conjunction with the third-order system of § 5.3.2, which was demonstrated to be hyperbolic, to construct a fourth-order system which could accommodate bidirectional crossflow profiles. This larger system would, of course, be limited by the smaller system's closure. Therefore, this idea is not pursued further and other avenues of more general applicability sought.

6.3 Eigenvalue-based hyperbolic systems

The novel method presented in this section is based on the manipulation of the linearized equation system (which is what determines the eigenvalues) instead of the complete non-linear system. Instead of determining the eigenvalues given a set of closure assumptions, the eigenvalues are prescribed *a priori* and a suitably larger parametric set of closure assumptions used to absorb the conditions imposed by these prescriptions. This method works for arbitrarily large systems, which is a major strength, and is not limited by a hierarchical treatment of the equations.

The steady equations are considered first, for which only one additional mode is required in the conventional set of closure assumptions. This will keep the presentation simple. Then, the method is extended to include the time derivative terms in the equations for which two additional modes in the profile-family closure scheme are required.

6.3.1 Steady equations

The Jacobian matrices resulting from the usual physical-closure assumptions (*laissez-faire*) are written, as before, as $\mathbf{J}$. The objective is to modify these matrices so that the resultant system eigenvalues are real. The modified matrices will be written as $\mathbf{K}$.

The steady system is

$$\frac{\partial \mathbf{f}}{\partial x} + \frac{\partial \mathbf{g}}{\partial z} = \mathbf{J}_x \frac{\partial \mathbf{p}}{\partial x} + \mathbf{J}_z \frac{\partial \mathbf{p}}{\partial z} = \mathbf{h}.$$

The essential idea is to introduce an additional degree of freedom into the closure model through a parameter α and have the resulting system possess imposed eigenvalues. The process will yield conditions of the type

$$\frac{\partial \alpha}{\partial \mathbf{p}} = \mathbf{b}\,,$$

which fixes the first-derivative variation of the additional mode with respect to the original parameter vector. This auxiliary mode is introduced in the velocity and density profile families (with mode shapes ψ, ϕ, ζ):

$$\left.\begin{array}{rcll} u & = & u(\mathbf{p},\alpha;y) & \Leftrightarrow \quad \psi_k,\ \psi_0 \\ w & = & w(\mathbf{p},\alpha;y) & \Leftrightarrow \quad \phi_k,\ \phi_0 \\ \rho & = & \rho(\mathbf{p},\alpha;y) & \Leftrightarrow \quad \zeta_k,\ \zeta_0 \end{array}\right\} \quad k = 1,\ldots,N$$

Here $\mathbf{p}$ is the order N vector of system parameters and α is the parameter associated with the auxiliary modes denoted by the subscript 0. The modes associated with $\mathbf{p}$ correspond to any profile family in the conventional sense. For the present, there is no distinction between the auxiliary mode and the regular profile modes and indeed their role is interchangeable in the following derivation; this, however, will be qualified later for practical application.

The modes are sensitivities of the velocity and density profiles and are computed by taking the profile partial derivatives with respect to the corresponding parameter. These modes provide a convenient way to express the profile sensitivities in another basis vector $\mathbf{v}$ (a similarity transform),

$$\begin{aligned}
\frac{\partial u}{\partial v_j} = \frac{\partial \alpha}{\partial v_j}\frac{\partial u}{\partial \alpha}(y) + \sum_{k=1}^{N}\frac{\partial p_k}{\partial v_j}\frac{\partial u}{\partial p_k}(y) &= \psi_0(y) + \sum_{k=1}^{N} x_{kj}\psi_k(y) \\
\frac{\partial w}{\partial v_j} = \frac{\partial \alpha}{\partial v_j}\frac{\partial w}{\partial \alpha}(y) + \sum_{k=1}^{N}\frac{\partial p_k}{\partial v_j}\frac{\partial w}{\partial p_k}(y) &= \phi_0(y) + \sum_{k=1}^{N} x_{kj}\phi_k(y) \\
\frac{\partial \rho}{\partial v_j} = \frac{\partial \alpha}{\partial v_j}\frac{\partial \rho}{\partial \alpha}(y) + \sum_{k=1}^{N}\frac{\partial p_k}{\partial v_j}\frac{\partial \rho}{\partial p_k}(y) &= \zeta_0(y) + \sum_{k=1}^{N} x_{kj}\zeta_k(y)
\end{aligned}$$

where

$$\frac{\partial \alpha}{\partial v_j} \equiv 1$$

and the partial derivatives are replaced by symbols for expediency.

By substituting these expressions into the flux vectors, the Jacobian matrices with respect to $\mathbf{v}$ are obtained. The columns of the matrices corresponding to each v_j can be expressed as

$$\begin{aligned}
\frac{\partial \mathbf{f}}{\partial v_j} &= \mathbf{r}_s + \mathbf{J}_s\mathbf{x}_j\,, \\
\frac{\partial \mathbf{g}}{\partial v_j} &= \mathbf{r}_n + \mathbf{J}_n\mathbf{x}_j\,,
\end{aligned}$$

where the matrices $\mathbf{J}_s$ and $\mathbf{J}_n$ contain the elements in the summation terms associated with $\mathbf{p}$ and the vectors $\mathbf{r}_s$ and $\mathbf{r}_n$ contain those associated with α, the additional degree of freedom. Exact formulae for the expanded flux derivatives are provided in the appendix to this chapter.

The v_j will be the characteristic variables, with β_j the associated eigenvalues, if the following conditions relating the columns of the Jacobian matrices are satisfied:

$$\sin\beta_j \frac{\partial \mathbf{f}}{\partial v_j} = \cos\beta_j \frac{\partial \mathbf{g}}{\partial v_j}$$

Rearranging to determine the unique expansion coefficients $\mathbf{x}_j$ that yield the prescribed system eigenvalue $\tan\beta_j$,

$$\mathbf{x}_j(\beta_j) = -\left(\mathbf{J}_s\sin\beta_j - \mathbf{J}_n\cos\beta_j\right)^{-1}\left(\mathbf{r}_s\sin\beta_j - \mathbf{r}_n\cos\beta_j\right) \tag{6.2}$$

$$= \quad -\mathbf{J}^{-1}(\beta_j)\ \mathbf{r}(\beta_j), \tag{6.3}$$

provided the matrix inverse exists (more on this later). Assembling for all eigenvalues

$$(\mathbf{J}_s\mathbf{X} + \mathbf{r}_s\mathbf{w}^T)\mathbf{\Lambda} = (\mathbf{J}_n\mathbf{X} + \mathbf{r}_n\mathbf{w}^T), \quad \mathbf{\Lambda} = \tan\beta_j\ ,$$

where the vector $\mathbf{w}$ of length N is $(1,\ \ldots)^T$.

The matrix $\mathbf{X}$ with columns $\mathbf{x}_j$ is also the *new* eigenvector matrix (in the $\mathbf{p}$ basis, $\mathbf{K}_s\mathbf{X}$ in the $\mathbf{f}$ basis) and implicitly defines the new Jacobian matrices

$$\left.\begin{array}{rcl} \mathbf{K}_s\mathbf{X} & = & \mathbf{J}_s\mathbf{X} + \mathbf{r}_s\mathbf{w}^T \\ \mathbf{K}_n\mathbf{X} & = & \mathbf{J}_n\mathbf{X} + \mathbf{r}_n\mathbf{w}^T \end{array}\right\} \mathbf{K}_s^{-1}\mathbf{K}_n = \mathbf{X}\mathbf{\Lambda}\mathbf{X}^{-1}\,.$$

The basis can be reverted back to the primary parameter space from the characteristic one by post-multiplying by $\mathbf{X}^{-1}$

$$\left.\begin{array}{rcl} \mathbf{K}_s & = & \mathbf{J}_s + \mathbf{r}_s\mathbf{b}^T \\ \mathbf{K}_n & = & \mathbf{J}_n + \mathbf{r}_n\mathbf{b}^T \end{array}\right\} \mathbf{b} = \frac{\partial\alpha}{\partial\mathbf{p}} = \mathbf{X}^{-T}\mathbf{w}\,.$$

The vector $\mathbf{b}$ can be used to define a 'total' partial derivative

$$\frac{D}{Dp_j} = \frac{\partial}{\partial p_j} + b_j\frac{\partial}{\partial\alpha}\,,$$

associated with the new sought-after Jacobian matrices. Reiterating:

$$\frac{\partial}{\partial p_j} \quad \Leftrightarrow \quad \mathbf{J}_s,\ \mathbf{J}_n$$

$$\frac{D}{Dp_j} \quad \Leftrightarrow \quad \mathbf{K}_s,\ \mathbf{K}_n$$

This new derivative succinctly shows how much of the new mode needs to be added to the each of the original modes to produce the sought-after eigenvalue behavior. In essence, the eigenvalues acquire the dominant influence on the closure scheme through the equation system as opposed to the primary parameters. This is a more integrated approach.

6.3.2 Some practical issues

Eigenvalue-prescription paradigms

For the eigenvalue-based closure technique described here, the eigenvalues need to be specified as an input. One general paradigm, based on the physical picture of information propagation in the boundary layer as presented in Chapter 4, is to make the eigenvalues realistic functions of the primitive parameters

$$\beta_j = \beta_j(\mathbf{p}, \alpha)\,,$$

and similarly in space-time for the unsteady problem

$$\beta_{s_j} = \beta_{s_j}(\mathbf{p}, \alpha_0, \alpha_{-1})\,, \quad \beta_{t_j} = \beta_{t_j}(\mathbf{p}, \alpha_0, \alpha_{-1})\,,$$

described later. The spatial eigenvalues are specified to approximate the angular range of the velocity vector across the boundary layer while the temporal eigenvalues are specified to be of $\mathcal{O}(q_e)$.

A different paradigm is based on the eigenvalues of the *laissez-faire* system (which, of course, then have to be computed) which if complex, are replaced by eigenvalues approximately equal to their real part. If real, they are not replaced. Therefore, if $\lambda_{j,j+1} = \lambda_R \pm i\lambda_I$, these are replaced by $\lambda_{j,j+1} = \lambda_R \pm \lambda_{sep}$, the new eigenvalue pair suitably separated by a 'small' value λ_{sep} (to ensure diagonalizability). This paradigm, as indicated by Relation 6.4 (given later), yields Jacobian matrices nearest to the *laissez-faire* ones in the complex plane.

Co-incident prescribed eigenvalues

If for some j in the first paradigm, the prescribed β_j coincides with one or more (if repeated) eigenvalues of the $\mathbf{J}_x$ and $\mathbf{J}_z$ system, then $\mathbf{J}$ in Equation 6.3 will be singular to the corresponding degree. In such a situation, the requisite number of eigenvectors can be obtained by replacing appropriate equations with conditions on the eigenvector norms (as is done customarily in eigenvector determination) and inverting the resulting system.

Choice of auxiliary mode in profile families

As was indicated in Chapter 3, one of the primary parameters is chosen to be the scale of the boundary layer δ. A formula for the sensitivity of the velocity and density profiles with respect to δ can be derived from a Taylor expansion in y

$$\begin{aligned}
\psi^{(\delta)} &= \frac{\partial u}{\partial \ln \delta} = -\frac{\partial u}{\partial \ln y} \\
\phi^{(\delta)} &= \frac{\partial w}{\partial \ln \delta} = -\frac{\partial w}{\partial \ln y} \\
\zeta^{(\delta)} &= \frac{\partial \rho}{\partial \ln \delta} = -\frac{\partial \rho}{\partial \ln y}
\end{aligned}$$

Then scale sensitivity is assigned to one mode in the expansion: the corresponding columns in $\mathbf{J}_s, \mathbf{J}_n$ are simply the flux vectors $\mathbf{f}$ and $\mathbf{g}$.

Thus far, the role of the α mode has been indistinguishable from the usual *laissez-faire* $\mathbf{p}$ modes. In practice, it is really only necessary to have an auxiliary mode for one velocity component (the natural choice in a streamline-based empirical framework being w) to provide the necessary space to project the original Jacobian matrices ($\Rightarrow \psi_0 = 0$). However, in the limit of vanishing crossflow, it then becomes necessary to have a non-singular $\mathbf{J}_s$, in addition to requiring that b_j smoothly vanish for all j as $w \to 0$ for consistency. Then, for a typical system of integral equations, a singular $\mathbf{J}_s$ in these conditions is avoided by choosing the scale as a *laissez-faire* parameter ($\in \mathbf{p}$) and associating α with the auxiliary mode ($\mathbf{r}_s$ and $\mathbf{r}_n$).

The use of the additional mode means that profiles of greater variety are possible that in the *laissez-faire* method because the eigenvalue conditions effectively play the role of an additional equation. In particular, bidirectional crossflows are possible with simply a three-equation system.

Increased computational work

The new method entails increased computational work over the *laissez-faire* one. Under the first eigenvalue-prescription paradigm, N matrices of order N have to be inverted in Equation 6.3, one for each eigenvalue. Under the second paradigm, only as many matrices as there are complex eigenvalues of the *laissez-faire* system will have to be inverted; however, the eigenvalues of the original system have to be computed. For most practical situations involving systems consisting of three or four equations this, in fact, not an excessive computational cost.

An estimate of the change in the coefficient matrix

To the extent that it is useful, an estimate of the minimum change in the coefficient matrix $\mathbf{J}_n\mathbf{J}_s^{-1}$ can be obtained from the Bauer-Fike theorem (see, for example, Wilkinson [71]): if $\mu \in \mathcal{C}$ is an eigenvalue of $\mathbf{J}_n\mathbf{J}_s^{-1}$ and $\mathbf{Z}$ is its eigenvector matrix,

$$\| \mathbf{K}_n\mathbf{K}_s^{-1} - \mathbf{J}_n\mathbf{J}_s^{-1} \| \geq \frac{\min|\mu - \tan\beta_j|}{\kappa}, \quad \kappa = \| \mathbf{Z} \| \, \| \mathbf{Z}^{-1} \| \tag{6.4}$$

where the norm can be any of the p-norms and κ is the condition number of $\mathbf{Z}$. The minimum change in the coefficient matrix is directly proportional to the distance in the complex plane of a prescribed eigenvalue and the nearest eigenvalue of the matrix. Furthermore, the minimum change also varies inversely with the departure of the coefficient matrix from normalcy [1].

6.3.3 A note on steady non-linear application

As has already been indicated, the procedure developed here is applied in a linear sense at some point in parameter space. It provides information on the first-derivative sensitivity of the velocity components and density. It does not provide enough information to uniquely determine a profile family over the entire parameter space which also satisfies the hyperbolicity constraints. A non-linear function can be linearized at a point, but in general it is impossible to reconstruct a non-linear variation from an available linearized approximation. In theory, however, a functional relation $F(\mathbf{p}) = \alpha$ can be postulated which satisfies the following gradient conditions:

$$\begin{aligned} \frac{\partial F}{\partial p_j} &= q_j \\ \frac{\partial F}{\partial \alpha} &= 1 \end{aligned}$$

An $N+1$ order, *non-linear* system (the original system augmented with the gradient of F in some direction $\hat{x}$) can be posed

$$\begin{pmatrix} \frac{\partial \mathbf{f}}{\partial x} \\ \\ \frac{\partial F}{\partial \hat{x}} \end{pmatrix} + \begin{pmatrix} \frac{\partial \mathbf{g}}{\partial z} \\ \\ 0 \end{pmatrix} = \begin{pmatrix} \mathbf{h} \\ \\ 0 \end{pmatrix},$$

[1] Normal matrices possess orthogonal eigenvectors (for example, symmetric matrices).

which possesses the prescribed eigenvalues.

In non-conservation form, with $\hat{x}$ angularly inclined to x by the angle γ, the system can be expressed

$$\begin{bmatrix} \mathbf{J}_x & \mathbf{r}_x \\ -\mathbf{q}^T \cos\gamma & \cos\gamma \end{bmatrix} \frac{\partial}{\partial x} \begin{pmatrix} \mathbf{p} \\ \alpha \end{pmatrix} + \begin{bmatrix} \mathbf{J}_z & \mathbf{r}_z \\ -\mathbf{q}^T \sin\gamma & \sin\gamma \end{bmatrix} \frac{\partial}{\partial z} \begin{pmatrix} \mathbf{p} \\ \alpha \end{pmatrix} = \begin{pmatrix} \mathbf{h} \\ 0 \end{pmatrix} .$$

The additional equation allows α to be determined directly. When applied with a uniform boundary condition on α in a well-posed hyperbolic case, this new equation will fix α to the uniform value in the entire domain. In particular, if α is set to zero, the role of the auxiliary mode and equation is restricted to ensuring that the system eigenvalues are equal to the prescribed values; the velocity and density profiles receive no contribution from the assumed mode. This system above can be verified to possess the correct eigenvalues through a simple similarity transform.

6.3.4 Unsteady equations

For the unsteady equations, the objective is to simultaneously ensure that two coefficient matrices, $\mathbf{K}_n\mathbf{K}_s^{-1}$ and $\mathbf{K}_t\mathbf{K}_s^{-1}$, possess real eigenvalues. The system is

$$\frac{\partial \mathbf{u}}{\partial t} + \frac{\partial \mathbf{f}}{\partial x} + \frac{\partial \mathbf{g}}{\partial z} = \mathbf{J}_t \frac{\partial \mathbf{p}}{\partial t} + \mathbf{J}_x \frac{\partial \mathbf{p}}{\partial x} + \mathbf{J}_z \frac{\partial \mathbf{p}}{\partial z} = \mathbf{h}.$$

Here, *two* additional modes are introduced into the velocity and density profiles:

$$\left.\begin{array}{rcll} u & = & u(\mathbf{p}, \alpha_0, \alpha_{-1}; y) & \Leftrightarrow \quad \psi_k,\ \psi_0,\ \psi_{-1} \\ w & = & w(\mathbf{p}, \alpha_0, \alpha_{-1}; y) & \Leftrightarrow \quad \phi_k,\ \phi_0,\ \phi_{-1} \\ \rho & = & \rho(\mathbf{p}, \alpha_0, \alpha_{-1}; y) & \Leftrightarrow \quad \zeta_k,\ \zeta_0,\ \zeta_{-1} \end{array}\right\} \quad k = 1, \ldots, N$$

There are two eigenvector matrices $\mathbf{X}_s$ and $\mathbf{X}_t$ corresponding to each of the two coefficient matrices $\mathbf{K}_n\mathbf{K}_s^{-1}$ and $\mathbf{K}_t\mathbf{K}_s^{-1}$. Carefully following the argument for the steady equations, the hyperbolicity conditions for the eigenvalues λ_s and λ_t can be written as

$$(\mathbf{J}_s\lambda_s - \mathbf{J}_n)\mathbf{x}_{sj} + (\mathbf{r}_s^{(0)}\lambda_s - \mathbf{r}_n^{(0)})\mathbf{b}_0^T\mathbf{x}_{sj} + (\mathbf{r}_s^{(-1)}\lambda_s - \mathbf{r}_n^{(-1)})\mathbf{b}_{-1}^T\mathbf{x}_{sj} = 0\,,$$

$$(\mathbf{J}_s\lambda_t - \mathbf{J}_t)\mathbf{x}_{tj} + (\mathbf{r}_s^{(0)}\lambda_t - \mathbf{r}_t^{(0)})\mathbf{b}_0^T\mathbf{x}_{tj} + (\mathbf{r}_s^{(-1)}\lambda_t - \mathbf{r}_t^{(-1)})\mathbf{b}_{-1}^T\mathbf{x}_{tj} = 0\,.$$

In the steady equations, the length of the eigenvector was set by the condition

$$\frac{\partial\alpha}{\partial v_j} = \mathbf{b}^T\mathbf{x}_j \equiv 1\,,$$

and the vector $\mathbf{b}$ was then computed after the complete eigenvector matrix was determined. In the unsteady case, the length of the eigenvectors in each of the conditions can be set by one of the two modes

$$\frac{\partial\alpha_0}{\partial v_{sj}} = \mathbf{b}_0^T\mathbf{x}_{sj} \equiv 1\,,$$

$$\frac{\partial\alpha_{-1}}{\partial v_{tj}} = \mathbf{b}_{-1}^T\mathbf{x}_{tj} \equiv 1\,.$$

Defining a matrix whose columns each correspond to a prescribed eigenvalue such that

$$\mathbf{T}_{sn}^{(0)}{}_j = (\mathbf{J}_s\lambda_{sj} - \mathbf{J}_n)^{-1}(\mathbf{r}_s^{(0)}\lambda_{sj} - \mathbf{r}_n^{(0)})\,,$$

and *diagonal* matrices with the j^{th} elements

$$\mathbf{B}_{sj} = \mathbf{b}_{-1}^T\mathbf{x}_{sj}\,,$$

$$\mathbf{B}_{tj} = \mathbf{b}_0^T\mathbf{x}_{tj}\,,$$

the hyperbolicity conditions define the new eigenvector matrices implicitly

$$\mathbf{X}_s = -\mathbf{T}_{sn}^{(0)} - \mathbf{T}_{sn}^{(-1)}\mathbf{B}_s\,,$$

$$\mathbf{X}_t = -\mathbf{T}_{st}^{(0)}\mathbf{B}_t - \mathbf{T}_{st}^{(-1)}\,.$$

The eigenvectors together with the length definitions above determine the sought after coefficients $\mathbf{b}_0$ and $\mathbf{b}_{-1}$. Then

$$\frac{D}{Dp_j} = \frac{\partial}{\partial p_j} + (b_{0\,j})\frac{\partial}{\partial\alpha_0} + (b_{-1\,j})\frac{\partial}{\partial\alpha_{-1}}$$

are the new sensitivities associated with the new Jacobian matrices.

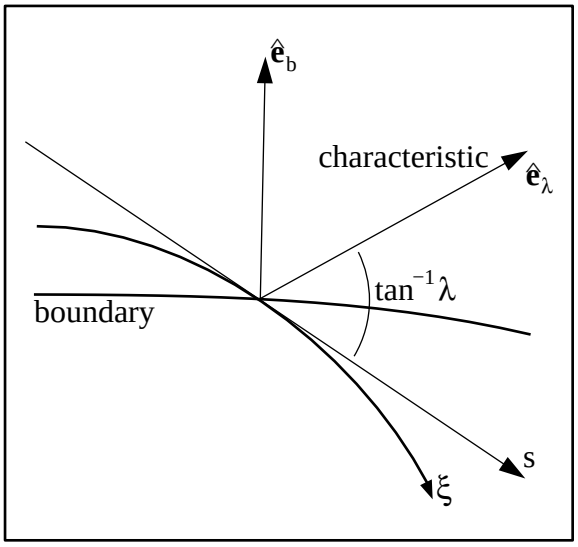

Figure 6-2: Inward-pointed characteristic line indicating the necessity to impose a Dirichlet-type boundary condition.

6.4 Boundary Conditions

For a scalar hyperbolic equation, a boundary condition of the Dirichlet type is necessary along the section of the boundary where the characteristic points into the domain (see for example, Kreiss [34]). No condition is necessary if the characteristic is pointed outward. In streamline-aligned coordinates

$$\frac{\partial f}{\partial s} + \lambda \frac{\partial f}{\partial n} = h\,,$$

a boundary condition is necessary if

$$\hat{e}_b \cdot \hat{e}_\lambda < 1\,,$$

where $\hat{e}_b$ is the inward normal to the boundary as shown in Figure 6-2.

The principle can easily be extended to systems of equations by applying boundary conditions through fixing the characteristic variables in situations where the corresponding characteristic line meets the criterion above. It is considerably more convenient, however, to pose the boundary condition in terms of primary parameters, or recognizable physical quantities, instead of characteristic variables. For a system, this is well-posed if the transform matrix between the imposed characteristic

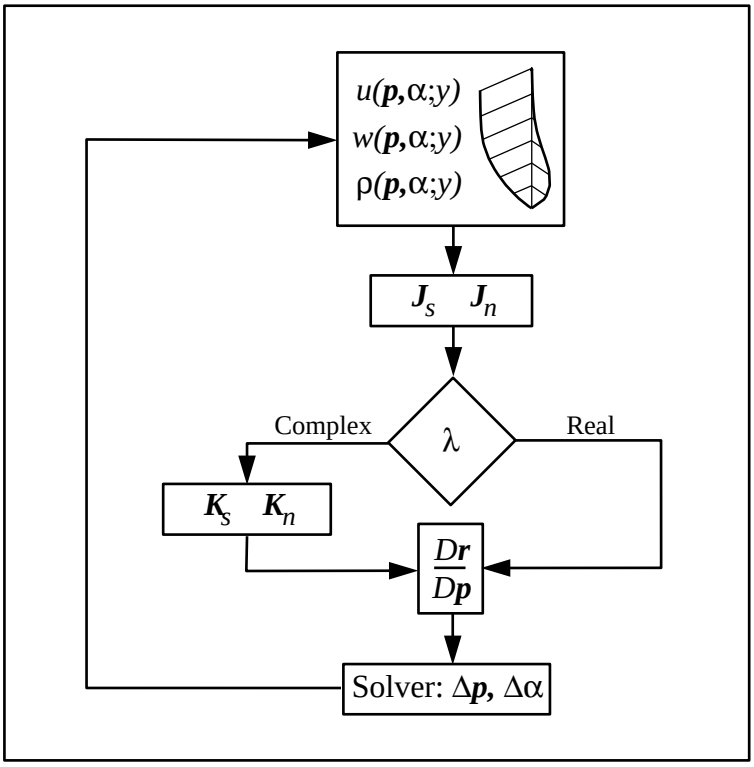

Figure 6-3: A space-marching solution algorithm for the eigenvalue-based method applied to the steady equations under the paradigm where the eigenvalue is replaced only if complex in the *laissez-faire* system.

variables and the imposed boundary layer parameters is non-singular. Then, the number of independent boundary layer parameters imposed must simply equal the number of incoming characteristics, and can be freely chosen depending on the relevant local physical requirements.

6.5 Solution strategies

There are several general strategies that can be employed to solve the equation system. These include steady space marching, unsteady time-stepping and non-linear Newton solution. The Newton method applies only to the non-linear *laissez-faire* ($\mathbf{b} \equiv \mathbf{0}$) system. For the purposes of this section, it is assumed to be hyperbolic.

6.5.1 Steady flow solution by space marching

The steady equations can be solved by a marching procedure in the streamwise direction. This requires that the residual be distributed exclusively to nodes in the marching direction. Furthermore, marching can only be used for flow regions where all characteristic lines are oriented generally in the marching direction (namely only for attached flows). In residual form, with x the marching direction, the system is

$$\mathbf{K}_x \frac{\partial \mathbf{p}}{\partial x} = \mathbf{h} - \frac{\partial \mathbf{g}}{\partial z} = \mathbf{r}(\mathbf{p}, \alpha) \,,$$

where

$$\frac{\partial \alpha}{\partial \mathbf{p}} = \mathbf{b}$$

and where only one additional mode, as explained earlier, is required to ensure hyperbolicity in the eigenvalue-based method. The solution can be advanced in x by any explicit marching scheme (Euler, Runge-Kutta, etc.) with the usual CFL restrictions on the size of Δx. For example, for explicit Euler

$$\text{Explicit Euler:} \qquad \frac{\Delta \mathbf{p}}{\Delta x} = \mathbf{K}_x^{-1}\mathbf{r} + \mathcal{O}(\Delta x)$$
$$\Delta \alpha = \mathbf{b}^T \Delta \mathbf{p} + \mathcal{O}(\Delta x)^2$$

Implicit marching techniques can be used with significantly larger steps (allowing the CFL constraint on stability to be replaced by considerations of accuracy). The residual expanded as a Taylor series in $\mathbf{p}$ is

$$\mathbf{r}(\mathbf{p} + \Delta \mathbf{p}, \alpha) = \mathbf{r}(\mathbf{p}, \alpha) + \left[\frac{\partial \mathbf{r}}{\partial \mathbf{p}} + \frac{\partial \mathbf{r}}{\partial \alpha} \mathbf{b}^T \right] \Delta \mathbf{p} + \mathcal{O}(\Delta \mathbf{p})^2 \,.$$

Then, implicit Euler is

$$\text{Implicit Euler:} \qquad \left(\frac{\mathbf{K}_x}{\Delta x} - \left[\frac{\partial \mathbf{r}}{\partial \mathbf{p}} + \frac{\partial \mathbf{r}}{\partial \alpha} \mathbf{b}^T \right] \right) \Delta \mathbf{p} = \mathbf{r} + \mathcal{O}(\Delta x)$$
$$\Delta \alpha = \mathbf{b}^T \Delta \mathbf{p} + \mathcal{O}(\Delta x)^2$$

The conventional residual Jacobian matrix is modified by the addition of a unit-rank matrix corresponding to the additional mode. More sophisticated schemes for both explicit and implicit marching

can be devised along these lines.

6.5.2 Unsteady flow solution by time stepping

The unsteady equations can be solved by integrating in time. The system written in residual form is

$$\mathbf{K}_t \frac{\partial \mathbf{p}}{\partial t} = \mathbf{h} - \frac{\partial \mathbf{f}}{\partial x} - \frac{\partial \mathbf{g}}{\partial z} = \mathbf{r}(\mathbf{p}, \alpha_0, \alpha_{-1}) \,.$$

Following the space-marching procedure, the solution can be computed at the unknown time level $n+1$ using a variety of explicit schemes. For example, for explicit Euler

$$\text{Explicit Euler:} \qquad \frac{\mathbf{p}^{n+1} - \mathbf{p}^n}{\Delta t} = \mathbf{K}_t^{-1}\mathbf{r} + \mathcal{O}(\Delta t)$$

$$\alpha_0^{n+1} = \alpha_0^n + \mathbf{b}_0^T \Delta \mathbf{p} + \mathcal{O}(\Delta t)^2$$

$$\alpha_{-1}^{n+1} = \alpha_{-1}^n + \mathbf{b}_{-1}^T \Delta \mathbf{p} + \mathcal{O}(\Delta t)^2$$

For an implicit method, again following space marching, the residual is expanded as a Taylor series in $\mathbf{p}$

$$\mathbf{r}(\mathbf{p} + \Delta \mathbf{p}, \alpha_0, \alpha_{-1}) = \mathbf{r}(\mathbf{p}, \alpha_0, \alpha_{-1}) + \left[\frac{\partial \mathbf{r}}{\partial \mathbf{p}} + \frac{\partial \mathbf{r}}{\partial \alpha_0} \mathbf{b}_0^T + \frac{\partial \mathbf{r}}{\partial \alpha_{-1}} \mathbf{b}_{-1}^T \right] \Delta \mathbf{p} + \mathcal{O}(\Delta \mathbf{p})^2 \,.$$

Then, implicit Euler is

$$\text{Implicit Euler:} \qquad \left(\frac{\mathbf{K}_t}{\Delta t} - \left[\frac{\partial \mathbf{r}}{\partial \mathbf{p}} + \frac{\partial \mathbf{r}}{\partial \alpha_0} \mathbf{b}_0^T + \frac{\partial \mathbf{r}}{\partial \alpha_{-1}} \mathbf{b}_{-1}^T \right]^n \right) (\mathbf{p}^{n+1} - \mathbf{p}^n) = \mathbf{r} + \mathcal{O}(\Delta t)$$

$$\alpha_0^{n+1} = \alpha_0^n + \mathbf{b}_0^T \Delta \mathbf{p} + \mathcal{O}(\Delta t)^2$$

$$\alpha_{-1}^{n+1} = \alpha_{-1}^n + \mathbf{b}_{-1}^T \Delta \mathbf{p} + \mathcal{O}(\Delta t)^2$$

More sophisticated schemes for both explicit and implicit marching in time can be devised along these lines.

If the objective is to compute steady flow, then implicit time stepping can be used in a slightly simpler form

$$\text{Lumped implicit Euler:} \qquad \left(\frac{\mathbf{I}}{\Delta t} - \left[\frac{\partial \mathbf{r}}{\partial \mathbf{p}} + \frac{\partial \mathbf{r}}{\partial \alpha_0}\mathbf{b}_0^T + \frac{\partial \mathbf{r}}{\partial \alpha_{-1}}\mathbf{b}_{-1}^T\right]^n\right)(\mathbf{p}^{n+1} - \mathbf{p}^n) = \mathbf{r} + \mathcal{O}(\Delta t)$$

$$\alpha_0^{n+1} = \alpha_0^n + \mathbf{b}_0^T \Delta \mathbf{p} + \mathcal{O}(\Delta t)^2$$

$$\alpha_{-1}^{n+1} = \alpha_{-1}^n + \mathbf{b}_{-1}^T \Delta \mathbf{p} + \mathcal{O}(\Delta t)^2$$

The solution is iterated in time until the residual drops below a specified tolerance value

$$\| \mathbf{r}^n \| \leq r_{tol} \, .$$

6.5.3 Steady flow solution using Newton's method

The Newton method is invaluable in the solution of non-linear systems. As noted before, the eigenvalue-based hyperbolic systems are fundamentally linear in that instead of specifying α as an explicit function of $\mathbf{p}$, it specifies only the sensitivity

$$\frac{\partial \alpha}{\partial \mathbf{p}} = \mathbf{b} \, .$$

Therefore the Newton method is inapplicable to eigenvalue-based hyperbolic systems. However, in their *laissez-faire* form ($\mathbf{b} \equiv \mathbf{0}$), equation systems can be solved using Newton's method either over the whole domain or in a space marching mode.

The Newton method can be derived, in the context of whole-domain solutions, from implicit Euler time stepping by letting $\Delta t \to \infty$. At iteration level n

$$\text{Newton:} \quad \left[\frac{\partial \mathbf{r}}{\partial \mathbf{p}}\right]^n \Delta \mathbf{p} = -\mathbf{r}^n \, ,$$

giving

$$\mathbf{p}^{n+1} = \mathbf{p}^n + \Delta \mathbf{p} \, .$$

The iterations are repeated until the residual drops below a tolerance value

$$\| \mathbf{r}^n \| \leq r_{tol} \, .$$

6.6 Appendix: Formulae for flux derivatives

For the usual boundary layer integral equations (momentum, energy and higher order in velocity), the fluxes can be functionally expressed as

$$\begin{aligned} u_i &= \int \eta_i(\rho,u,w)\,dy \\ f_i &= \int \eta_i(\rho,u,w)u\,dy \\ g_i &= \int \eta_i(\rho,u,w)w\,dy \end{aligned}$$

where $\eta_i(\rho,u,w)$ is a polynomial in u, w and ρ. In the notation of the parent integral equation, Equation 2.13, the integrands are $\eta_i = \rho(\phi_e - \phi)$. Substituting the assumed profile-family derivatives, the resulting Jacobian matrices are

$$\mathbf{K}_t = \frac{\partial u_i}{\partial v_j} = \int (\kappa_{u_t}\psi_0 + \kappa_{w_t}\phi_0 + \kappa_{\rho_t}\zeta_0)\,dy$$

$$+ \sum_k x_{kj} \int (\kappa_{u_t}\psi_k + \kappa_{w_t}\phi_k + \kappa_{\rho_t}\zeta_k)\,dy \qquad \begin{cases} \kappa_{u_t} = \frac{\partial \eta_i}{\partial u} \\ \kappa_{w_t} = \frac{\partial \eta_i}{\partial w} \\ \kappa_{\rho_t} = \frac{\partial \eta_i}{\partial \rho} \end{cases}$$

$$\mathbf{K}_s = \frac{\partial f_i}{\partial v_j} = \int (\kappa_{u_x}\psi_0 + \kappa_{w_x}\phi_0 + \kappa_{\rho_x}\zeta_0)\,dy$$

$$+ \sum_k x_{kj} \int (\kappa_{u_x}\psi_k + \kappa_{w_x}\phi_k + \kappa_{\rho_x}\zeta_k)\,dy \qquad \begin{cases} \kappa_{u_x} = u\frac{\partial \eta_i}{\partial u} + \eta_i \\ \kappa_{w_x} = u\frac{\partial \eta_i}{\partial w} \\ \kappa_{\rho_x} = u\frac{\partial \eta_i}{\partial \rho} \end{cases}$$

$$\mathbf{K}_n = \frac{\partial f_i}{\partial v_j} = \int (\kappa_{u_z}\psi_0 + \kappa_{w_z}\phi_0 + \kappa_{\rho_z}\zeta_0)\,dy$$

$$+ \quad \sum_k x_{kj} \int (\kappa_{u_z} \psi_k + \kappa_{w_z} \phi_k + \kappa_{\rho_z} \zeta_k)\, dy \qquad \begin{cases} \kappa_{u_z} &= w \frac{\partial \eta_i}{\partial u} \\ \kappa_{w_z} &= w \frac{\partial \eta_i}{\partial w} + \eta_i \\ \kappa_{\rho_z} &= w \frac{\partial \eta_i}{\partial \rho} \end{cases}$$

Similar formulae can be derived for entrainment, general moments of momentum and other integral quantities.

Chapter 7

Spatial Numerical Method

The boundary-layer equations are discretized using the finite-element method based on an effective and flexible set of numerical procedures devised by Nishida [44]. The scheme used in this thesis differs from that of Nishida in an important way, however, namely the use of streamline upwinding. This chapter contains a description of the discretization scheme and the application of upwinding.

7.1 Curvilinear and Cartesian coordinate systems

Before describing the numerical discretization of the equations it will be useful to very briefly place the use of Cartesian coordinates in context.

The boundary-layer equations derived in Chapter 2 assume that the boundary-layer thickness

$$\delta \ll r_{min} \,, \tag{7.1}$$

where r_{min} is the minimum principle radius of curvature of the surface. This permits the surface-normal axis to be unstretched consistent with the first-order assumption, and further permits the use of simple Cartesian coordinates.

Traditionally, the equations, driven by finite-difference discretization methods, have been expressed in curvilinear coordinates which include coordinate stretching metrics and curvature terms for the

axes embedded in the surface. The surface-normal axis as noted does not need to be stretched even in curvilinear coordinates for the small curvature assumption. For non-orthogonal surface coordinate axes, the resulting equations are considerably more cumbersome than those using Cartesian coordinates. The use of orthogonal coordinate axes (typically corresponding to the outer-edge streamlines and streamline-normals) makes the equations a little simpler but introduces other restrictions. Most authors also assume that the surfaces are developable for which the Gaussian curvature

$$\frac{1}{r_{min} r_{max}} \equiv 0 \,,$$

which allows at least one of the curvature terms to be identically zero at any point over the extent of the surface. The remaining grid-dependent terms still have to be computed explicitly.

The development of finite-volume and finite-element methods, in conjunction with the recognition that the integral equations can be written in conservation form, allows the use of simple, arbitrarily-oriented Cartesian coordinates [40]. There are no restrictions on the shape of the surface as long as the assumption on the relative magnitude of the curvature 7.1 is observed. The finite-volume and, in particular, the finite-element method provide a convenient way to transform between a local, computational space (natural coordinates) and a global physical one. The result is that the curvature and stretching of the grid is computed systematically, and conveniently, by the finite-volume or finite-element method at the numerical level. This represents a fundamental simplification over the traditional curvilinear-coordinate approach.

7.2 Global and local coordinate systems

The physical domain is subdivided into quadrilateral computational elements. The boundary-layer equations are solved in local Cartesian coordinates for each element (x', z', n), each defined in terms of the global coordinates (x, z, y) as shown in Figure 7-1. The process involved has two stages:

1. The element normal is calculated by taking the cross-product of diagonals $1-3$ and $2-4$ and scaling the resulting vector so that its length is one. The nodes are numbered so that the normal vector points into the flow.

2. The x'-axis is chosen to be fixed in the plane of the element, for example in the direction of diagonal $1-3$, and the z'-axis is then calculated by taking the cross-product of the element

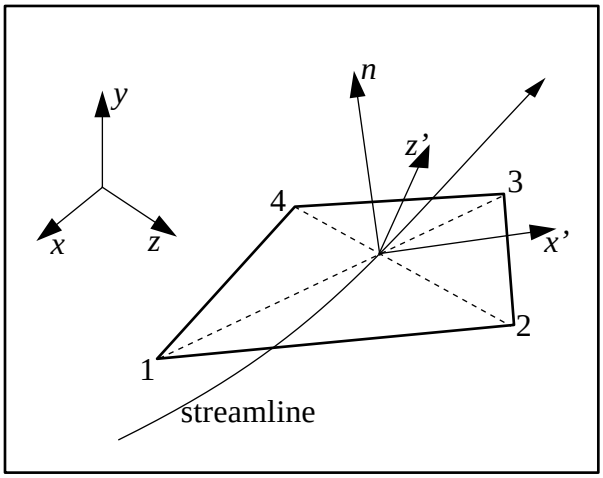

Figure 7-1: The normal vector and coordinate system for an element.

normal and the x'-axis. The nodal positions can then be expressed in the local coordinates. For some applications, the x'-axis is chosen to be the element-averaged outer-edge streamline direction. Note that then, for viscous-inviscid calculations, the element coordinate system is not fixed.

The relevant boundary-layer quantities in an arbitrary direction are related to those in the streamline direction as listed in Appendix I of this chapter. The primitive boundary-layer parameters are used to define quantities in the streamline direction for every *node* as an intermediate step, and these are then expressed in the *element* coordinate direction for inclusion in the numerical differencing scheme.

7.3 Finite-element discretization

Over each element Ω^e, interpolation functions $N_l^{(e)}(x', z')$ are used to determine some quantity $u^{(e)}(x', z')$ in terms of its nodal values u_l

$$u^{(e)}(x', z') = \sum_{l=1}^{4} u_l N_l^{(e)}(x', z') \,.$$

Elemental quantities are denoted by the superscript (e) and l is the local node number as indicated in Figure 7-1. In what follows, the identical symbol is used for the function as well as its nodal value

for convenience, the distinction being implied by the use of a subscript on the latter.

Since the integral equations contain only first-order derivatives, bilinear interpolation functions, defined in natural element coordinates

$$\begin{aligned} N_1 &= (1-\xi)(1-\eta)/4 \\ N_2 &= (1+\xi)(1-\eta)/4 \\ N_3 &= (1+\xi)(1+\eta)/4 \\ N_4 &= (1-\xi)(1+\eta)/4 \end{aligned}$$

will be sufficient to provide the necessary functional continuity. The interpolation functions for an element must satisfy the property $\sum_{l=1}^{4} N_l \equiv 1$ in order to be able to represent a constant function exactly. For isoparametric elements (same interpolation function used for both element geometry and quantity u), the natural coordinates are related to the local physical surface coordinates by

$$\begin{aligned} x'^{(e)}(\xi,\eta) &= \sum_{l=1}^{4} N_l(\xi,\eta) x'_l \\ z'^{(e)}(\xi,\eta) &= \sum_{l=1}^{4} N_l(\xi,\eta) z'_l \end{aligned}$$

The details of the transformations between the two coordinate systems are well known and provided, for example, by Hirsch [28].

The elemental residual $\tilde{r}^{(e)}(x',z')$ for the steady form of the parent integral equation, Equation 2.13, is

$$\begin{aligned} \tilde{r}^{(e)}(x',z') = & \sum_{l=1}^{4} \nabla N_l^{(e)} \cdot (\rho_e q_e^{k+1} \vec{\theta})_l \\ & + \left(\sum_{l=1}^{4} N_l^{(e)} (\phi_e^{(u)})_l \sum_{l=1}^{4} \nabla N_l^{(e)} (u_e)_l + \sum_{l=1}^{4} N_l^{(e)} (\phi_e^{(w)})_l \sum_{l=1}^{4} \nabla N_l^{(e)} (w_e)_l \right) \\ & \qquad \cdot \sum_{l=1}^{4} N_l^{(e)} (\rho_e q_e \vec{\delta}^*)_l \\ & - \left(\sum_{l=1}^{4} N_l^{(e)} (\mathbf{q}_e)_l \cdot \sum_{l=1}^{4} \nabla N_l^{(e)} (u_e)_l \right) \sum_{l=1}^{4} N_l^{(e)} (\rho_e q_e^{k-1} \Phi_x)_l \end{aligned}$$

$$- \left(\sum_{l=1}^{4} N_l^{(e)} (\mathbf{q}_e)_l \cdot \sum_{l=1}^{4} \nabla N_l^{(e)} (w_e)_l \right) \sum_{l=1}^{4} N_l^{(e)} (\rho_e q_e^{k-1} \Phi_z)_l$$

$$- \sum_{l=1}^{4} N_l^{(e)} (\vec{\phi}'|_{y=0})_l \cdot \sum_{l=1}^{4} N_l^{(e)} (\vec{\tau}|_{y=0})_l - \sum_{l=1}^{4} N_l^{(e)} (D_p)_l$$

The individual residuals for the momentum and kinetic-energy equations fall out of this expression as explained in Chapter 2. Explicit expressions for these individual equations are provided by Nishida [44].

7.4 Method of weighted residuals

Following standard finite-element procedure, the elemental residual form of the equations is converted into a weak form by projecting the elemental residuals $\tilde{\mathbf{r}}^{(e)}(x', z')$, which are in the space of the interpolation functions, onto a space of weight functions ($W_i^{(e)}$ for node i) and integrating over the element. This allows the equations to be expressed in terms of nodal quantities. The residual contribution of element Ω^e to one of its nodes, i is

$$\mathbf{r}_i^{(e)} = \iint_{\Omega^e} W_i^{(e)} \tilde{\mathbf{r}}^{(e)} \, dS \, .$$

The integrations are approximated by 2×2 Gauss quadrature for each element, and the contributions to each node assembled globally. The sensitivities necessary for the residual Jacobian matrix are also conveniently assembled by using a routine of a similar format to the one used for the residuals.

7.5 Choice of weight functions

The weight functions can be chosen to yield different discretization schemes. A very lucid description of the various finite difference schemes possible within a finite element framework can be found in Shapiro [52].

The boundary-layer equations contain first derivative terms, the numerical approximation of which needs special treatment to avoid spurious oscillations. A Galerkin (G) approximation, where the weight functions for a node are identical to the interpolation functions, produces a stencil which in

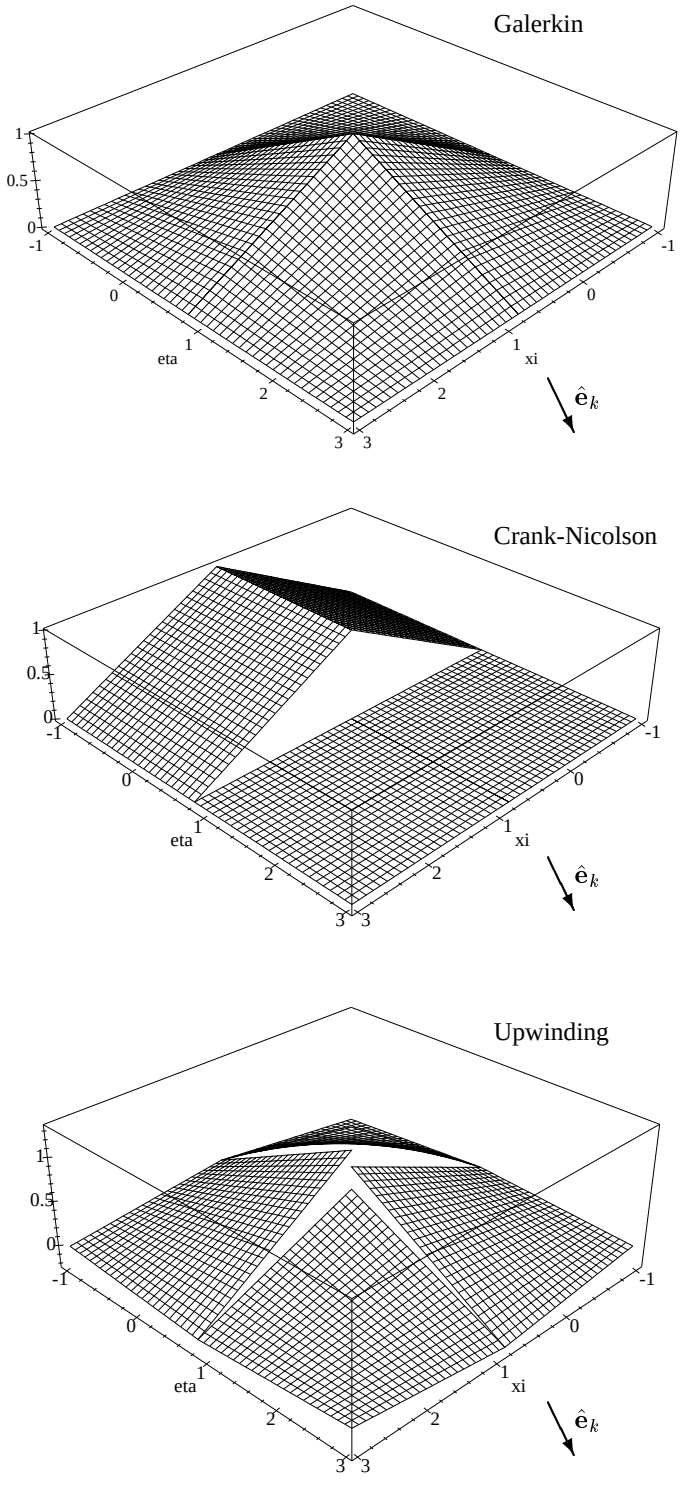

Figure 7-2: Weight functions for the Galerkin, Crank-Nicolson and characteristic upwinding ($\alpha = 0.5$) schemes for a characteristic oriented, as shown, at an angle of 30^0 with respect to the s-axis.

turn is a blend of a finite-volume (FV) stencil (also known as a cell-vertex scheme in finite-element parlance) and a central-difference (CD) one [52]. The resulting residuals satisfy the relation

$$r_{\mathrm{G}}^{(e)} = \frac{2}{3} r_{\mathrm{FV}}^{(e)} + \frac{1}{3} r_{\mathrm{CD}}^{(e)} \,.$$

Spurious sawtooth oscillations are invisible to each of the constituent stencils (for the derivative terms) and hence the Galerkin one as well.

An obvious remedy is to add second order smoothing. This may be useful in certain specific conditions (near separation regions, for example), but is excessive in most cases.

The directional nature of a hyperbolic system of equations suggests the introduction of upwinding based, in some fashion, on the edge-velocity direction. This is considerably better suited to the nature of the problem compared to a generic second-order smoothing term and is also less intrusive. To this end, Nishida used a weight function equivalent to a Crank-Nicolson finite-difference scheme over the two upstream elements. While this is a second-order accurate scheme and works well, it requires the prior designation of what the upstream elements are and, furthermore, is ambiguous for borderline edge velocity orientations. Another consequence is that that the mesh artificially influences the solution. A more general upwinding strategy which is independent of the local grid particulars, and which adapts naturally to coupled systems, is preferred. Such a strategy is developed in the following subsections.

Before proceeding, it may be useful to note that, unlike the general upwinding strategy, the Crank-Nicolson weighting is intrinsically applicable to marching solutions because the residual contribution to a node is exclusively from the upstream elements. The same cannot be said for the Galerkin weighting, or the upwinding strategy that is proposed next. Therefore, the facility to apply Crank-Nicolson weighting is retained for marching calculations.

7.5.1 Upwinding the scalar wave equation

For the scalar non-homogeneous wave equation with constant coefficients

$$\cos\beta \frac{\partial u}{\partial x} + \sin\beta \frac{\partial u}{\partial z} = \hat{\mathbf{e}}_k \cdot \nabla u = h, \qquad \hat{\mathbf{e}}_k = (\cos\beta)\hat{\imath} + (\sin\beta)\hat{k} \,,$$

the elemental residual in local coordinates is

$$\tilde{r}_v^{(e)}(x',z') = \left(\hat{\mathbf{e}}_k^{(e)} \cdot \sum_{l=1}^{4} \nabla N_l^{(e)}(x',z')\right) u_l - \sum_{l=1}^{4} N_l^{(e)}(x',z') h_l \,.$$

The superscript (e) will be dropped from the elemental variables for clarity for the remainder of this chapter and is implied by context. The residual contribution from an element Ω^e to one of its nodes i for a Galerkin approximation is

$$r_i|_G = \iint_{\Omega^e} N_i \tilde{r}_v \, dS \,.$$

Upwinding is introduced by adding a term, proportional to the component of the gradient of the interpolation function $\nabla N_i(x,z)$ in the direction of the characteristic, to the Galerkin weight function

$$r_i|_U = \iint_{\Omega^e} (N_i + k\tilde{W}_i)\tilde{r}_v \, dS \tag{7.2}$$

where

$$\tilde{W}_i(x',z') = \hat{\mathbf{e}}_k \cdot \nabla N_i, \quad k = \alpha\frac{\Delta}{2},$$

Δ is a (somewhat) arbitrary measure of the element size in the direction of $\hat{\mathbf{e}}_k$ as shown in the figure and α is a numerical coefficient [73]. The net effect of the additional term is to redistribute the elemental residual to the nodes taking into account the direction of information flow. Full upwinding corresponds to $\alpha \approx 1$. This addition is equivalent to artificial dissipation, but *only* in the direction of the characteristic; there is no net contribution to the weight function in the direction normal to the characteristic. The elemental residual here is emphasized to be in characteristic form (necessarily for the scalar equation) for future use by use of the subscript v. In the literature, this approach is generally termed "Petrov-Galerkin streamline upwinding (SUPG)". In the context of this section, the streamline is the mathematical characteristic, not necessarily the actual velocity streamline.

The efficacy of this upwinding formulation for the finite element method in suppressing spurious oscillations is demonstrated later. For most situations, small values of α (≈ 0.05) are found to be sufficient. Note also that the presence of the source terms is an important consideration as shown in Appendix II to this chapter.

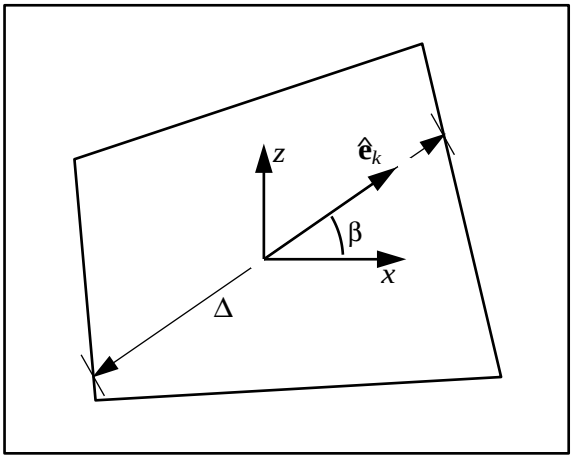

Figure 7-3: Element size in characteristic direction.

Conservative property of streamline upwinding

This modified weighting function maintains the conservative property of the Galerkin scheme. A sufficient condition for conservation is [52]

$$\sum_l W_l = 1$$

for all nodes l on element Ω^e. Then for the upwinding weighting,

$$\sum_l W_l = \sum_l (N_l + k\tilde{W}_l) \tag{7.3}$$

$$= 1 + k \sum_l \nabla N_l \cdot \hat{\mathbf{e}}_k \tag{7.4}$$

$$= 1 + k\nabla \left(\sum_l N_l \right) \cdot \hat{\mathbf{e}}_k = 1\,, \tag{7.5}$$

because $\sum_i N_l \equiv 1$.

7.5.2 Complete upwinding for a coupled system

The vector of finite-element residuals approximating a upwinded system of first-order wave equations (decoupled by default) is expressed in matrix notation

$$\mathbf{r}_{v\,i} = \iint_{\Omega^e} \left(N_i \mathbf{I} + \mathbf{K}\tilde{\mathbf{W}}_i \right) \tilde{\mathbf{r}}_v \, dS \,, \quad \tilde{\mathbf{W}}_i = \nabla N_i \cdot (\mathbf{\Lambda}_c \hat{\imath} + \mathbf{\Lambda}_s \hat{k}) \,,$$

where $\mathbf{K}$ and $\tilde{\mathbf{W}}_i$ are now diagonal matrices. This is a straightforward extension of the scalar case.

Instead of solving the boundary-layer equations in a non-conservative characteristic basis, it is more convenient to solve directly the conservative form. The elemental residual function of the coupled, conservative-form system, denoted by the c subscript, is related to that of the decoupled, non-conservative-form system through the transform

$$\tilde{\mathbf{r}}_c = \mathbf{X}\mathbf{\Lambda}_c^{-1}\tilde{\mathbf{r}}_v$$

where $\mathbf{X}$ is the eigenvector matrix for the flux-basis system and $\mathbf{\Lambda}_c$ is a diagonal matrix of the cosine of the elemental characteristic angles (with respect to the x'-axis).

The upwind-weighted residual system for the conservation-form system is:

$$\begin{aligned}
\mathbf{r}_{c\,i} &= \iint_{\Omega^e} \mathbf{X}\mathbf{\Lambda}_c^{-1}(N_i\mathbf{I} + \mathbf{K}\tilde{\mathbf{W}}_i)\tilde{\mathbf{r}}_v \, dS \\
&= \iint_{\Omega^e} (N_i\mathbf{I} + \mathbf{X}\mathbf{\Lambda}_c^{-1}\mathbf{K}\tilde{\mathbf{W}}_i\mathbf{\Lambda}_c\mathbf{X}^{-1})\tilde{\mathbf{r}}_c \, dS \\
&= \iint_{\Omega^e} (N_i\mathbf{I} + \mathbf{X}\mathbf{K}\tilde{\mathbf{W}}_i\mathbf{X}^{-1})\tilde{\mathbf{r}}_c \, dS \\
&= \iint_{\Omega^e} (N_i\mathbf{I} + \nabla N_i \cdot \mathbf{X}\mathbf{K}(\mathbf{\Lambda}_c\hat{\imath} + \mathbf{\Lambda}_s\hat{k})\mathbf{X}^{-1})\tilde{\mathbf{r}}_c \, dS \\
&= \iint_{\Omega^e} \left(N_i\mathbf{I} + \mathbf{X}\mathbf{K}\left(\frac{\partial N_i}{\partial x'}\mathbf{\Lambda}_c + \frac{\partial N_i}{\partial z'}\mathbf{\Lambda}_s \right) \mathbf{X}^{-1} \right) \tilde{\mathbf{r}}_c \, dS \,, \quad \mathbf{\Lambda}_s\mathbf{\Lambda}_c^{-1} = \mathbf{\Lambda}
\end{aligned}$$

The upwinding weight-function matrix for the conservation equations is no longer necessarily diagonal. Here $\mathbf{\Lambda}_s$ is the diagonal matrix of the sine of the characteristic angles.

It may be more convenient to use flux Jacobian matrices with respect to primary parameters, $\mathbf{J}_{x'}$ and $\mathbf{J}_{z'}$, rather than requiring the evaluation of system eigenvectors for use in the upwinding term.

This can be achieved by restricting $\mathbf{K}$ to the form

$$\mathbf{K} = k\,(\min|\cos\beta_j|)\;\boldsymbol{\Lambda}_c^{-1}$$

so that the upwind-weighted residual contribution for the conservation-form equations is

$$\mathbf{r}_{c\,i} = \iint_{\Omega^e} \left(N_i\mathbf{I} + k\,(\min|\cos\beta_j|) \left(\frac{\partial N_i}{\partial x'} + \mathbf{J}_{z'}\mathbf{J}_{x'}^{-1}\frac{\partial N_i}{\partial z'} \right) \right) \tilde{\mathbf{r}}_c\, dS\,, \quad \mathbf{J}_{z'}\mathbf{J}_{x'}^{-1} = \mathbf{X}\boldsymbol{\Lambda}\mathbf{X}^{-1}\,.$$

Note that $\min|\cos\beta_j| \to 0$ provides the necessary boundedness as $|\mathbf{J}_{x'}| \to 0$.

7.5.3 Simplified upwinding for a coupled system

Implementing the full characteristic upwinding in either characteristic or conservation form is complicated in an implicit/Newton solver, where the residual Jacobian matrix is computed analytically, because the sensitivity of the upwinding weighting term involves partial differentiation of differentiated terms. While this is possible in theory, in this thesis the overall cost-effectiveness was judged to be poor on the basis of successful numerical experiments with a simpler, related formulation; however, this is not to detract from the considerable value and increased robustness of the complete upwinding facility for more general applications.

A simple and effective alternative can be devised based on the essential feature of characteristic upwinding. Each equation in the conservation form system, or some chosen combination of equations, is upwinded individually with the facility to heuristically relate the upwinding direction $\hat{\mathbf{e}}_k$ and the numerical coefficient α to the boundary layer parameters tailored to the particulars of the system

$$\mathbf{r}_{c\,i} = \iint_{\Omega^e} \left(N_i\mathbf{I} + \alpha(\mathbf{p})\frac{\Delta}{2}\nabla N_i \cdot \hat{\mathbf{e}}_k(\mathbf{p})\mathbf{I} \right) \tilde{\mathbf{r}}_c\, dS\,.$$

Typically, just simple upwinding in the outer-edge streamline direction using a constant $\alpha \approx 0.05$ is found to be effective in the majority of cases tested. These are the settings used for the application results presented in subsequent chapters. Regions of large separation ($H > 6$) in interactive mode calculations were, however, found to be troublesome for this heuristic approach; for the cases tested, the actual source of the trouble could partly be attributed to stiffness due to insufficient cross-stream grid resolution.

A comparison of the different weight functions considered here is performed on a rather severe test case. The results are presented in Figure 7-4 for the Galerkin, Crank-Nicolson (upstream nodes chosen are those to the left of a node) and upwind methods. The boundary conditions applied are discontinuous at the upstream bottom corner. The discontinuity persists in the downstream direction because the crossflow is positive (pointed into the discontinuity) below and almost zero above it. This forces the characteristics to effectively merge [1]. As an aside, the discontinuity is more evident in streamwise quantities, which are not plotted here, than in the crossflow displacement thickness which is plotted.

There are two observations that can be made. First, the upwind weighting ($\alpha = 1$) is moderately effective in suppressing the spurious oscillations present in the Galerkin weighting and, to a somewhat lesser extent, in the Crank-Nicolson weighting solutions. In less-severe cases, a far lesser value of α for the upwind weighting, as already noted, or the use of Crank-Nicolson weighting is found to be sufficiently effective. Note here the that the general appearance of the results indicate the presence of stiffness associated with inadequate grid resolution.

A second interesting feature of this test case is the presence of low-wavenumber (about four and a half wave-lengths across the bottom) oscillations associated with the dispersive error of the Galerkin method. Shapiro [52], using a Fourier analysis, demonstrated the existence of these oscillations for the Euler equation solutions near a shock, for Galerkin weighting, among others. Upwind weighting (as one might expect) does not generate these oscillations; Crank-Nicolson, evidently does.

Finally, a comparison is performed with the upwind weighting applied in the outer-edge streamline direction and one applied in a direction oriented slightly toward the crossflow. The results are very similar, although the latter is arguably slightly more effective in suppressing spurious oscillations.

[1] The characteristic mechanics of this situation are similar those that lead to shocks in one-dimensional unsteady Euler-equation solutions (where one characteristic coalesces)

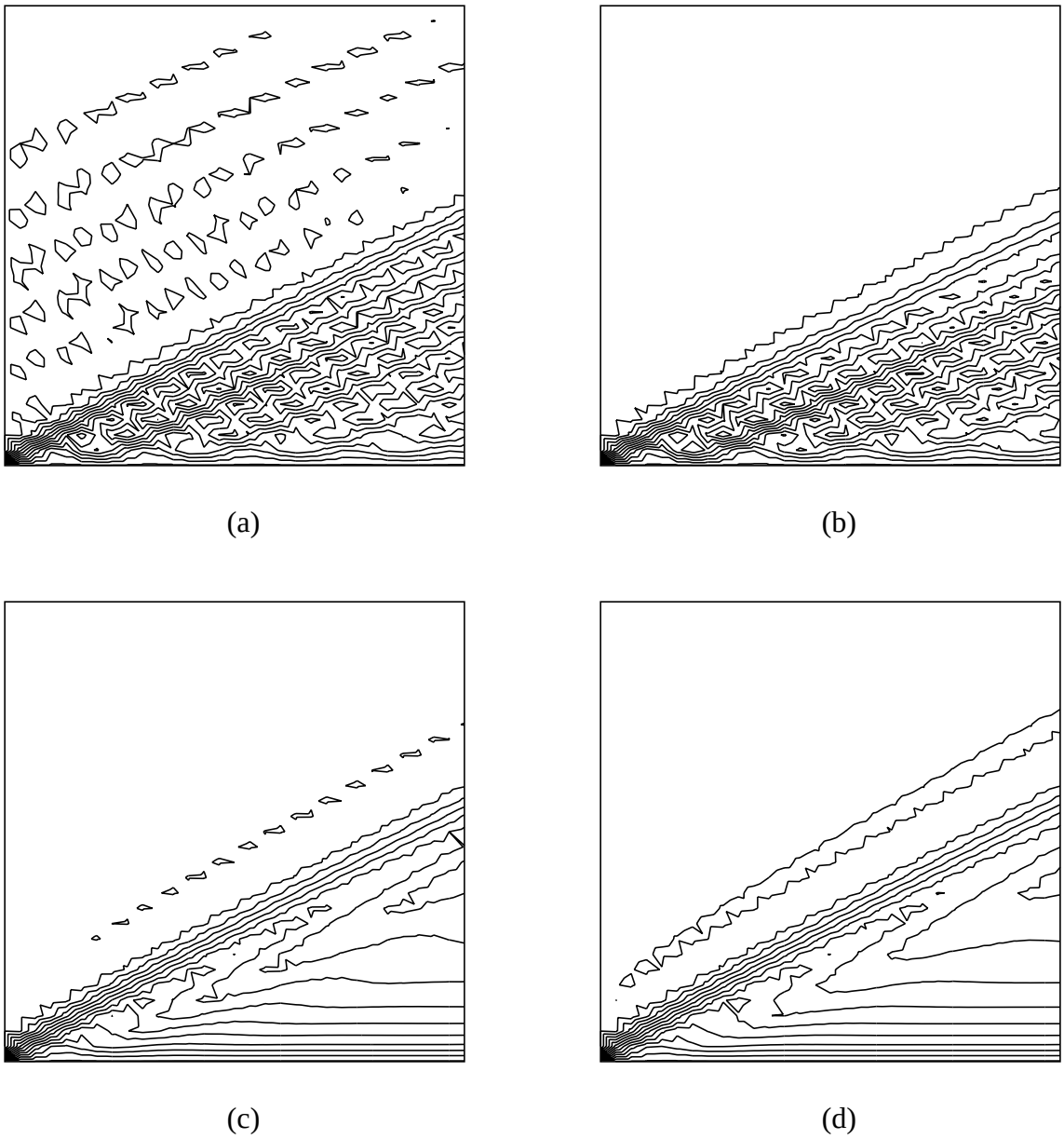

Figure 7-4: The effects of different weight functions: contours of δ_2^* (20 steps from -0.0002 to 0.00001, 30×30 elements) with boundary conditions $\delta = 0.1$, $c = 0.0$ on the left ($x = 0$), $\delta = 0.01$, $c = 0.5$ at the bottom ($z = 0$), and $H = 2.6$ on both edges. The external velocity components are $u_e = 1.0$ and $w_e = 0.5$. (a) Galerkin weighting, (b) Crank-Nicolson weighting in the x direction, (c) upwind weighting with $\alpha = 1$ and $\hat{\mathbf{e}}_k = 0^0$, (d) upwind weighting with $\alpha = 1$ and $\hat{\mathbf{e}}_k = 20^0$.

7.6 Appendix I: Relevant variables in general orientations

Thicknesses and shear stresses in (x, z) coordinates (defined by velocity components (u_e, w_e)) can be directly expressed as functions of their values in streamline (s, n) coordinates (denoted by numeric subscripts).

Kinematic displacement

$$q_e \vartheta_x = u_e \vartheta_1 - w_e \vartheta_2$$

$$q_e \vartheta_z = w_e \vartheta_1 + u_e \vartheta_2$$

Displacement

$$q_e \delta_x^* = u_e \delta_1^* - w_e \delta_2^*$$

$$q_e \delta_z^* = u_e \delta_2^* + w_e \delta_1^*$$

Momentum

$$q_e^2 \theta_{xx} = u_e^2 \theta_{11} + w_e^2 \theta_{22} - u_e w_e (\theta_{12} + \theta_{21})$$

$$q_e^2 \theta_{xz} = u_e^2 \theta_{12} - w_e^2 \theta_{21} + u_e w_e (\theta_{11} - \theta_{22})$$

$$q_e^2 \theta_{zx} = u_e^2 \theta_{21} - w_e^2 \theta_{12} + u_e w_e (\theta_{11} - \theta_{22})$$

$$q_e^2 \theta_{zz} = u_e^2 \theta_{22} + w_e^2 \theta_{11} + u_e w_e (\theta_{12} + \theta_{21})$$

Density

$$q_e \delta_x^{**} = u_e \delta_1^{**} - w_e \delta_2^{**}$$

$$q_e \delta_z^{**} = w_e \delta_1^{**} + u_e \delta_2^{**}$$

Shear stress

$$q_e \tau_x = u_e \tau_1 - w_e \tau_2$$

$$q_e \tau_z = w_e \tau_1 + u_e \tau_2$$

Kinetic energy

$$q_e^3 E_{xx} = u_e^3 E_{11} + u_e^2 w_e(-3E_{12} - 2\delta_2^*) + u_e w_e^2(3E_{21}) - w_e^3 E_{22}$$

$$q_e^3 E_{xz} = u_e^3 E_{12} + u_e^2 w_e(E_{11} - 2E_{21}) + u_e w_e^2(-2E_{12} - 2\delta_2^* + E_{22}) + w_e^3 E_{21}$$

$$q_e^3 E_{zx} = u_e^3 E_{21} + u_e^2 w_e(2E_{12} + 2\delta_2^* - E_{22}) + u_e w_e^2(E_{11} - 2E_{21}) - w_e^3 E_{12}$$

$$q_e^3 E_{zz} = u_e^3 E_{22} + u_e^2 w_e(3E_{21}) + u_e w_e^2(3E_{12} + 2\delta_2^*) + w_e^3 E_{11}$$

$$q_e \theta_x^* = q_e(E_{xx} + E_{zx}) = u_e \theta_1^* - w_e \theta_2^*$$

$$q_e \theta_z^* = q_e(E_{zx} + E_{zz}) = w_e \theta_1^* + u_e \theta_2^*$$

$$q_e^3 E_{mx} = q_e^3 E_{xz} + u_e^2 q_e \delta_z^* - u_e w_e q_e \delta_x^*$$

$$q_e^3 E_{mz} = q_e^3 E_{zx} + w_e^2 q_e \delta_x^* - u_e w_e q_e \delta_z^*$$

Dissipation

$$q_e^2 D_x = u_e^2 D_1 - u_e w_e D_{12} + w_e^2 D_2$$

$$q_e^2 D_z = w_e^2 D_1 + u_e w_e D_{12} + u_e^2 D_2$$

$$D = D_x + D_z = D_1 + D_2$$

$$q_e^2 D_m = (u_e^2 - w_e^2) D_{12} + 2 u_e w_e (D_1 - D_2)$$

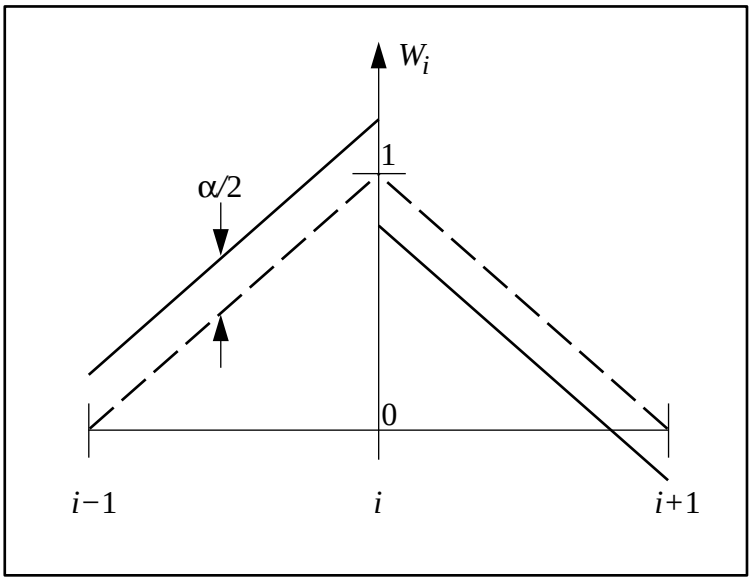

Figure 7-5: Upwinding weight function (solid line) compared to the Galerkin weight function (dashed line) in one dimension. Here the flow is from left to right.

7.7 Appendix II: Streamline upwinding applied to a model problem

A suitable scalar model equation for exploring oscillatory behavior of the integral boundary layer system is

$$\frac{du}{dx} = h(u, x)\,,$$

on the domain $x = [0, 1]$. This domain is discretized into elements Ω^e of equal length Δ. A feature of the weighting scheme is that the source term influences the presence of spurious sawtooth oscillations. For simplicity, the equation is linearized around a solution $u = u_0(x)$,

$$\frac{du}{dx} = \left.\frac{dh}{du}\right|_{u_0} u = A(x)u$$

where the dependent variable can also be viewed as a perturbation around the solution. Upwinding is introduced as in Equation 7.2 through the additional gradient term, here in one dimension,

$$W_i = N_i + k\tilde{W}_i = N_i + \alpha\frac{\Delta}{2}\frac{dN_i}{dx}\,.$$

Figure 7.7 shows the weighing function for an interior node juxtaposed against the Galerkin weighting function (linear interpolation function) for a characteristic oriented to the right.

The weighted residual form for the model equation for a node i in the interior is

$$\int_{\Omega^e} W_i(x) \sum_{l=1}^{2} \left(\frac{dN_l^{(e)}}{dx}(x) u_l - N_l^{(e)}(x) A_l u_l \right) dx \,,$$

integrated over all elements, where A_l and u_l are now the values at the nodes for the element Ω^e. Only the two elements containing the node yield non-zero contributions.

On isoparametric elements, assuming a constant A, the assembled residual equation for an interior node is

$$\left((1-\alpha) - (\frac{1}{3} - \frac{\alpha}{2})p \right) u_{i-1} + \left(2\alpha - 4\frac{p}{3} \right) u_i + \left(-(1+\alpha) - (\frac{1}{3} + \frac{\alpha}{2})p \right) u_{i+1} = 0 \,,$$

where $p = Ah$. The residual has the usual anti-symmetric contribution from the derivative term corresponding to a central finite difference. However, the interpolation functions distribute the source term value to all three nodes. This represents a difference from the conventional finite-difference treatment. The consequence, in upwind weighted residual is that the source terms contributes to the asymmetry in the direction of the the derivative term:

derivative:		$(-1$	0	$1)$
derivative upwind:	α	$(-1$	2	$-1)$
source:		$(-\frac{p}{3}$	$-\frac{4p}{3}$	$-\frac{p}{3})$
source upwind:	α	$(-\frac{p}{2}$	0	$\frac{p}{2})$

Chapter 8

Application I: Bidirectional Crossflow

The basic equation system for calculating unidirectional-crossflow boundary layers contains the two momentum and the total kinetic-energy (or more commonly, in the literature, the entrainment) equation. The calculation of bidirectional crossflows requires an additional mode in the crossflow velocity profile family, and an appropriate auxiliary equation to close the problem, over the basic third-order system. The additional velocity mode, as discussed in Chapter 3, can be included as an extra term

$$w(c, c_1; y) = c\left((w_0(y) + \tilde{c}_1 w_1(y)\right) = c w_0(y) + c_1 w_1(y)\,. \tag{8.1}$$

The choice of the specific additional equation is not straight-forward and is the main subject of this chapter. The system, with the appropriate auxiliary equation, is validated using a quasi-three dimensional finite-difference calculation.

8.1 Choice of additional equation

The natural candidate for the additional equation can be deduced by examining the usual two-equation system for two-dimensional calculations, consisting of the streamwise integral momentum and kinetic-energy equations. There, the unknown parameters are the boundary-layer thickness scale (δ, or equivalently any thickness, for example θ_{11}) and a streamwise profile shape factor (for example, H). The basic idea can be extended to the crossflow direction for three-dimensional flow. With the cross-flow magnitude c as a cross-stream scale, and $\tilde{c}$ the cross-stream profile shape factor, the equation system is extended to include the cross-stream integral momentum and kinetic-energy equations. Equivalently stated, the momentum/kinetic energy combination, which has been shown to accurately simulate variable profile shapes in two dimensional flow, can also used to simulate variable-crossover profile shapes. Stock [56] used these equations in his computational method.

For any general coordinate orientation (including, of course, streamline-aligned), the use of the total kinetic-energy equation in addition to either x or z kinetic-energy component is equivalent to using the two individual components instead (different combinations of the same equations being a similarity transform). Therefore, without loss of generality, and for clarity, the equation system is written with the two individual kinetic energy components:

$$\frac{\partial}{\partial x}(\rho_e q_e^2 \theta_{xx}) + \frac{\partial}{\partial z}(\rho_e q_e^2 \theta_{xz}) + \rho_e q_e \delta_x^* \frac{\partial u_e}{\partial x} + \rho_e q_e \delta_z^* \frac{\partial u_e}{\partial z} = \tau_{x_w}$$

$$\frac{\partial}{\partial x}(\rho_e q_e^2 \theta_{zx}) + \frac{\partial}{\partial z}(\rho_e q_e^2 \theta_{zz}) + \rho_e q_e \delta_x^* \frac{\partial w_e}{\partial x} + \rho_e q_e \delta_z^* \frac{\partial w_e}{\partial z} = \tau_{z_w}$$

$$\frac{\partial}{\partial x}(\rho_e q_e^3 E_{xx}) + \frac{\partial}{\partial z}(\rho_e q_e^3 E_{xz}) + \rho_e q_e \delta_x^* \frac{\partial u_e^2}{\partial x} + \rho_e q_e \delta_z^* \frac{\partial u_e^2}{\partial z}$$

$$- 2\rho_e q_e \vartheta_x \left(u_e \frac{\partial u_e}{\partial x} + w_e \frac{\partial u_e}{\partial z} \right) = 2D_x \tag{8.2}$$

$$\frac{\partial}{\partial x}(\rho_e q_e^3 E_{zx}) + \frac{\partial}{\partial z}(\rho_e q_e^3 E_{zz}) + \rho_e q_e \delta_x^* \frac{\partial w_e^2}{\partial x} + \rho_e q_e \delta_z^* \frac{\partial w_e^2}{\partial z}$$

$$- 2\rho_e q_e \vartheta_z \left(u_e \frac{\partial w_e}{\partial x} + w_e \frac{\partial w_e}{\partial z} \right) = 2D_z \tag{8.3}$$

This proposed system, it turns out, is ill-conditioned in certain conditions in an implicit/Newton solver. Before discussing the reasons, note as an aside, that the derivative-term Jacobian matrices

of this system in streamline-aligned coordinates are

$$\mathbf{J}_s = \begin{bmatrix} \bar{\theta}_{11} & \dot{\bar{\theta}}_{11} & 0 & 0 \\ c\bar{\theta}_{21} & c\dot{\bar{\theta}}_{21} & \bar{\theta}_{21} & c\bar{\theta}'_{21} \\ \bar{E}_{11} & \dot{\bar{E}}_{11} & 0 & 0 \\ c^2\bar{E}_{21} & c^2\dot{\bar{E}}_{21} & 2c\bar{E}_{21} & c^2\bar{E}'_{21} \end{bmatrix}, \tag{8.4}$$

$$\mathbf{J}_n = \begin{bmatrix} c\bar{\theta}_{12} & c\dot{\bar{\theta}}_{12} & \bar{\theta}_{12} & c\bar{\theta}'_{12} \\ c^2\bar{\theta}_{22} & c^2\dot{\bar{\theta}}_{22} & 2c\bar{\theta}_{22} & c^2\bar{\theta}'_{22} \\ c\bar{E}_{12} & c\dot{\bar{E}}_{12} & \bar{E}_{12} & c\bar{E}'_{12} \\ c^3\bar{E}_{22} & c^3\dot{\bar{E}}_{22} & 3c^2\bar{E}_{22} & c^3\bar{E}'_{22} \end{bmatrix}, \tag{8.5}$$

where the columns are partial derivatives with respect to $(\ln\delta, p_1, c, \tilde{c}_1)^T$. The overbar denotes quantities evaluated at $c = 1$ allowing the dependence on c to be clearly shown.

8.1.1 Ill-conditioning property of equation system

In streamline-aligned coordinates, the cross-stream component kinetic-energy equation simplifies to:

$$\begin{array}{ccccccc} \frac{\partial}{\partial s}(\rho_e q_e^3 E_{21}) & + & \frac{\partial}{\partial n}(\rho_e q_e^3 E_{22}) & - & 2u_e\frac{\partial w_e}{\partial s}\rho_e q_e \vartheta_2 & = & 2D_2 \\ \sim c^2 & & \sim c^3 & & \sim c & & \sim c^2 \end{array}$$

The dependence of each term in the equation on the crossflow magnitude parameter is also shown.

The equation is identically satisfied for $c = 0$ and the lowest order term varies as c. A significant problem arises when the pressure gradients in the external flow are zero ($\Rightarrow \frac{\partial w_e}{\partial s} = 0$). Then, the lowest order remaining terms vary as c^2. In any implicit or Newton-like numerical scheme, this results in extreme ill-conditioning for small crossflows because the derivative of the residual tends to zero. In fact, at zero crossflow, the residual Jacobian matrix becomes singular (for the derivative

terms, the singularity is evident in the Jacobian matrices 8.4 and 8.5, where the terms in the last row all vanish for $c = 0$). This makes the overall equation system untenable.

8.1.2 Possible remedies

In theory, the natural fix is to deflate the singularity in the equation by dividing it by a quantity that varies like c. In practice, this would involve identifying the *numerical* direction along which the deflation is to be carried out for each element. The deflation would need to be flanked by transformations between the deflation-direction coordinates and the local element coordinates. This is a difficult and complicated proposition.

Another idea is to introduce an $\mathcal{O}(c)$ dependence (other than in the pressure-gradient term) into the cross-stream kinetic-energy equation by adding some suitable fraction of the entrainment equation. There are at least two problems with this approach. First, the addition involves an arbitrary mix of the two equations, and hence an arbitrary mix of physics. Second, an additional closure relation for the entrainment coefficient will be needed which also introduces more empiricism. Furthermore, systems using the entrainment equation are generally less accurate than those using some form of the kinetic-energy equation.

The desired remedy is to use the mixed-component kinetic energy equation as the auxiliary equation to the original third-order system (one that employs the total kinetic-energy equation). The resulting system replaces Equations 8.2 and 8.3 in the initially proposed system

$$\frac{\partial}{\partial x}(\rho_e q_e^2 \theta_{xx}) + \frac{\partial}{\partial z}(\rho_e q_e^2 \theta_{xz}) + \rho_e q_e \delta_x^* \frac{\partial u_e}{\partial x} + \rho_e q_e \delta_z^* \frac{\partial u_e}{\partial z} = \tau_{x_w} \tag{8.6}$$

$$\frac{\partial}{\partial x}(\rho_e q_e^2 \theta_{zx}) + \frac{\partial}{\partial z}(\rho_e q_e^2 \theta_{zz}) + \rho_e q_e \delta_x^* \frac{\partial w_e}{\partial x} + \rho_e q_e \delta_z^* \frac{\partial w_e}{\partial z} = \tau_{z_w} \tag{8.7}$$

$$\frac{\partial}{\partial x}(\rho_e q_e^3 \theta_x^*) + \frac{\partial}{\partial z}(\rho_e q_e^3 \theta_z^*) + \rho_e q_e \delta_x^* \frac{\partial q_e^2}{\partial x} + \rho_e q_e \delta_z^* \frac{\partial q_e^2}{\partial z} = 2D \tag{8.8}$$

$$\frac{\partial}{\partial x}(\rho_e q_e^3 E_{mx}) + \frac{\partial}{\partial z}(\rho_e q_e^3 E_{mz}) + \frac{1}{2}\left(\rho_e q_e \delta_x^{**} \frac{\partial q_e^2}{\partial z} + \rho_e q_e \delta_z^{**} \frac{\partial q_e^2}{\partial x}\right)$$

$$+ \left(\frac{\partial w_e}{\partial z} - \frac{\partial u_e}{\partial x}\right)(\rho_e u_e q_e \delta_z^* - \rho_e w_e q_e \delta_x^*) = D_m \tag{8.9}$$

For the conditions under which the earlier system was ill-conditioned (zero crossflow, zero pressure gradients), the total kinetic-energy equation becomes identical, of course, to the streamwise kinetic-energy component equation (which is well-conditioned), and the mixed-component kinetic-energy equation in streamline coordinates simplifies to:

$$\begin{array}{ccccccccc} \frac{\partial}{\partial s}(\rho_e q_e^3 E_{12} & + & \rho_e q_e^3 \delta_2^*) & + & \frac{\partial}{\partial n}(\rho_e q_e^3 E_{21}) & = & D_{12} \\ \sim c & & \sim c & & \sim c & & \sim c \end{array}$$

The overall equation system is now clearly well-conditioned because the new equation has a $\mathcal{O}c$ dependence independent of the pressure gradient. Furthermore, use of the mixed-component kinetic-energy equation preserves the fundamental idea of using an energy-type equation to solve for the cross-flow shape factor. However, care must be taken in using this equation because it is orientation-dependent (fundamentally not part of a vector of equations). The obvious direction to use is the streamline-aligned one.

The derivative-term Jacobian matrices for this system are:

$$\mathbf{J}_s = \begin{bmatrix} \bar{\theta}_{11} & \dot{\bar{\theta}}_{11} & 0 & 0 \\ c\bar{\theta}_{21} & c\dot{\bar{\theta}}_{21} & \bar{\theta}_{21} & c\bar{\theta}'_{21} \\ \bar{E}_{11} + c^2\bar{E}_{21} & \dot{\bar{E}}_{11} + c^2\dot{\bar{E}}_{21} & 2c\bar{E}_{21} & c^2\bar{E}'_{21} \\ c^2\bar{E}_{21} & c^2\dot{\bar{E}}_{21} & 2c\bar{E}_{21} & c^2\bar{E}'_{21} \end{bmatrix} \tag{8.10}$$

$$\mathbf{J}_n = \begin{bmatrix} c\bar{\theta}_{12} & c\dot{\bar{\theta}}_{12} & \bar{\theta}_{12} & c\bar{\theta}'_{12} \\ c^2\bar{\theta}_{22} & c^2\dot{\bar{\theta}}_{22} & 2c\bar{\theta}_{22} & c^2\bar{\theta}'_{22} \\ c\bar{E}_{12} + c^3\bar{E}_{22} & c\dot{\bar{E}}_{12} + c^3\dot{\bar{E}}_{22} & \bar{E}_{12} + 3c^2\bar{E}_{22} & c\bar{E}'_{12} + c^3\bar{E}'_{22} \\ c^3\bar{E}_{22} & c^3\dot{\bar{E}}_{22} & 3c^2\bar{E}_{22} & c^3\bar{E}'_{22} \end{bmatrix} \tag{8.11}$$

It is important to use c_1 instead of $\tilde{c}_1$ as the new parameter. To illustrate, consider the last column of the Jacobian matrix (corresponding to the partial derivative with respect to $\tilde{c}_1$) for the source

terms in the residual vector (without the pressure gradient terms)

$$\mathbf{J}_h|_{\tilde{c}_1} = \begin{pmatrix} 0 \\ c\bar{\tau}_{2_w}^{'} \\ 2c^2\bar{D}^{'} \\ c\bar{D}_{12}^{'} \end{pmatrix} .$$

Here, the cross-stream wall-shear stress is assumed derived from the laminar cross-flow profile definition. The last column of the *residual* Jacobian matrix is the sum of some combination of the last columns of $\mathbf{J}_s$ and $\mathbf{J}_n$, as in Matrices 8.10 and 8.11, and of $\mathbf{J}_h|_{\tilde{c}_1}$. As $c \to 0$, all terms in the last column of the residual Jacobian matrix vanish making the system ill-conditioned. This ill-conditioning is avoided simply by defining the cross-flow velocity in Equation 8.1 in terms of c_1 instead of $\tilde{c}_1$. Then, some of the terms are non-zero. The same arguments also apply, in principle, to the system proposed first (which is ill-conditioned of course, but for a different reason).

8.2 Calculation with periodic outer-edge velocity

Equation system 8.6-8.9 is used to solve an infinite-span (quasi-three-dimensional), bidirectional laminar flow with a periodic imposed velocity distribution. This calculation is meant to vividly demonstrate the effect of allowing bidirectionality in the crossflow velocity profile. The assumed family of profiles used for closure are given by Equation 3.7 in the streamwise direction and Equation 8.1 in the cross-stream direction.

Note that the notion of characteristics is not applicable to a quasi-three-dimensional calculation. Hence, the system is solved without recourse to the eigenvalue-based closure method described in Chapter 6, and furthermore, is solved using the Newton method.

The calculation is performed on a domain $x = [0, 1]$ discretized into 100 elements at a reference Reynolds number of $10,000$. The imposed chordwise velocity profile distribution is shown in Figure 8-1 and analytically given by

$$u_e(x) = 1 + \frac{1}{40}\sin^2(3\pi x) .$$

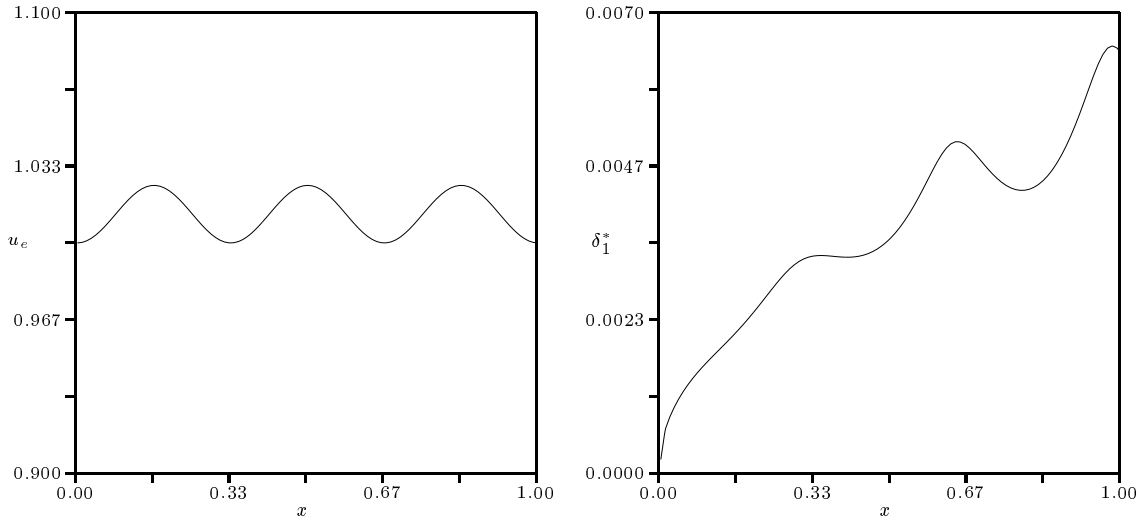

Figure 8-1: Imposed velocity and calculated streamwise displacement thickness

The spanwise velocity is $w_e = 1$. The initial conditions are

$$\begin{aligned} \delta &= 0.00025 \\ \eta_0 &= 0.77 \quad (\text{Blasius} \ : \ H \approx 2.6) \\ c_0 &= 0 \\ c_1 &= 0 \end{aligned}$$

Periodic boundary conditions are imposed at the spanwise edges. Note that the infinite-span outer-edge velocity distribution is always an irrotational flow field; use of the kinetic-energy equations in the system, for which this is a restriction, is therefore valid.

Also shown in Figure 8-1 is the calculated displacement thickness. In Figure 8-2, the calculated streamwise shape factor and crossflow-related parameter distributions are shown. The two crossflow parameters are 'out-of-phase' responding directly to the imposed pressure-gradient. The parameter c_0 is closely related to the cross-stream wall shear-stress through the assumed profile, as shown in Figure 8-3. The calculated physical quantities δ_2^* and c_{f_2} are also out of tandem clearly indicating the presence of a bidirectional crossflow profile.

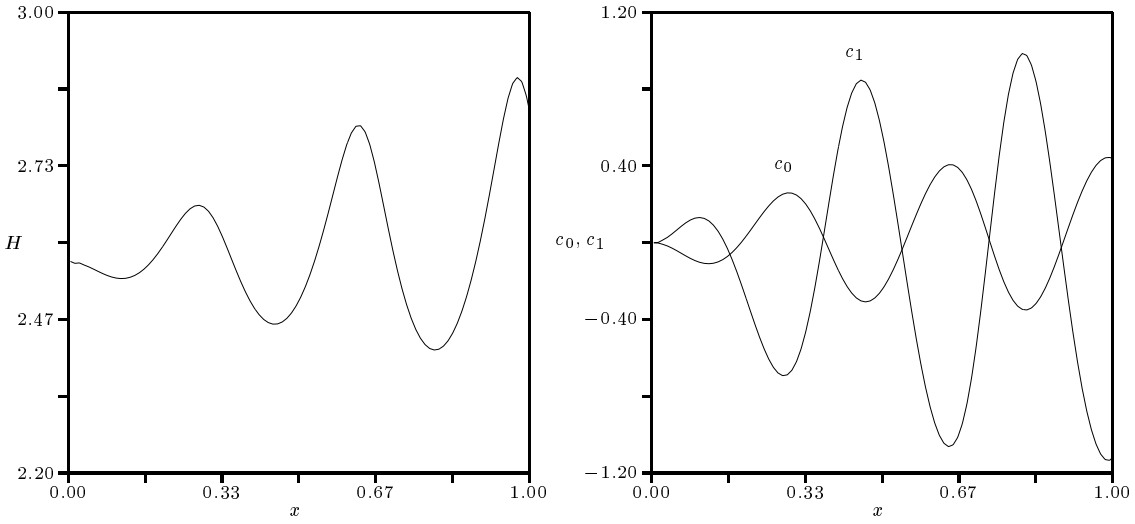

Figure 8-2: Calculated shape factor and the two empirical crossflow parameters

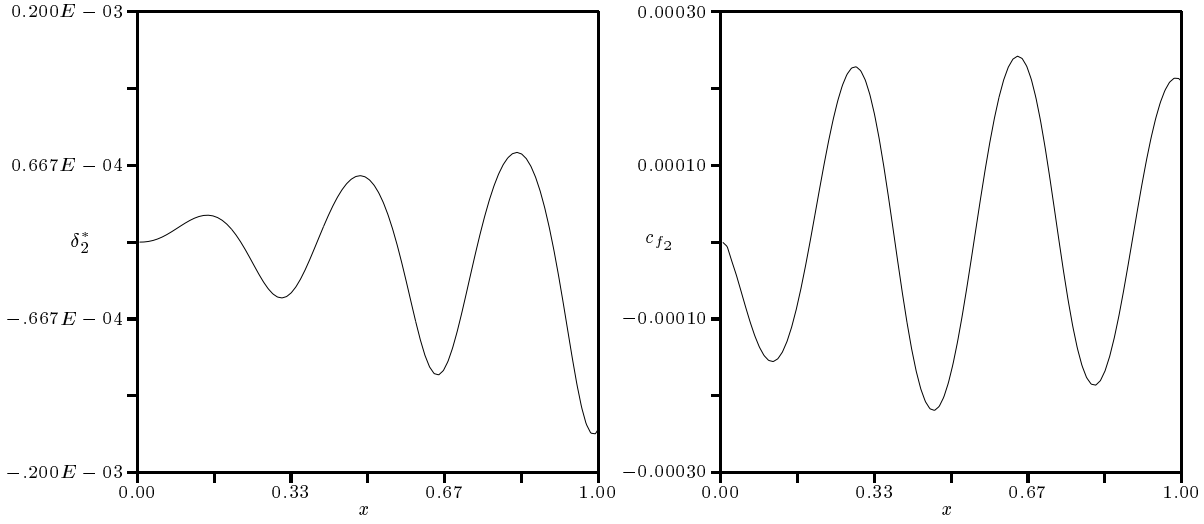

Figure 8-3: Calculated crossflow displacement thickness and skin friction

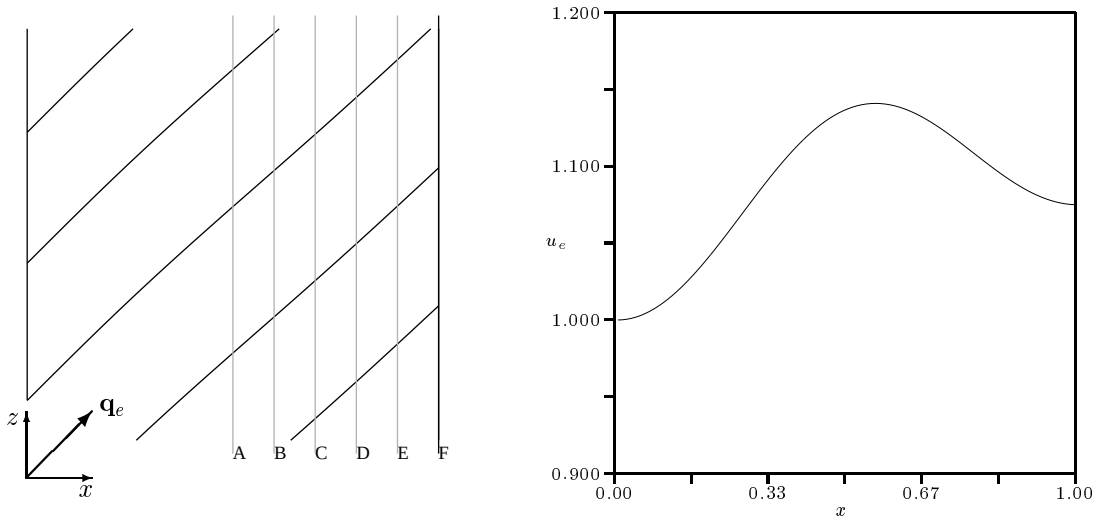

Figure 8-4: (a) Outer-edge streamlines and comparison stations. (b) Imposed chordwise outer-edge velocity distribution.

8.3 Validation of equation system

The Equation system 8.6-8.9 is used to solve for another incompressible infinite-span, attached, laminar flow and the results compared with those from a quasi-three-dimensional finite-difference solver for the *differential* equations provided by Drela [18, 22]. For an infinite-span calculation, the spanwise gradient terms vanish in the differential boundary-layer equations. Letting x be the chordwise direction, the incompressible equations are:

$$\frac{\partial u}{\partial x} + \frac{\partial v}{\partial y} = 0 \tag{8.12}$$

$$u\frac{\partial u}{\partial x} + v\frac{\partial u}{\partial y} = u_e\frac{\partial u_e}{\partial x} + \frac{1}{\nu}\frac{\partial^2 u}{\partial y^2} \tag{8.13}$$

$$u\frac{\partial w}{\partial x} + v\frac{\partial w}{\partial y} = \frac{1}{\nu}\frac{\partial^2 w}{\partial y^2} \tag{8.14}$$

with boundary conditions

$$u = 0,\ v = 0,\ w = 0 \qquad \text{at } y = 0,$$

$$u = u_e(x),\ w = w_e \quad \text{at } y = \infty.$$

Here, it has been assumed that the spanwise component of the outer-edge velocity is constant everywhere. For this system, the chordwise solution, as is well known, decouples from the w velocity. Then, Equations 8.12 and 8.13 can be used to solve for u and v using a finite-difference method [18] and these velocity solutions used in Equation 8.14 to calculate w. This second calculation is a simple quadrature if the well-known Falkner-Skan-Cooke scaling transform is employed.

The finite-difference solution is compared with the integral method. The integral system is, as before, closed by profile families given by Equation 3.7 in the streamwise direction and Equation 8.1 in the cross-stream direction.

The test calculation is performed on a domain $x = [0, 1]$ discretized into 100 elements with the imposed edge-velocity distributions

$$\begin{aligned} u_e &= 1 + \frac{1}{10}\left(\sin^2(\pi x) + \frac{3}{4}\sin^2(\frac{\pi}{2}x)\right), \\ w_e &= 1, \end{aligned}$$

for a reference Reynolds number of $10,000$. For the integral calculation, periodic boundary conditions are imposed on the spanwise edges. For the finite-difference calculation, the upstream boundary condition is provided by similarity solutions; for the integral equations the following conditions are used as an approximate match (it is not important to be exact because of the initial moderate favorable pressure gradient)

$$\begin{aligned} \delta &= 0.001 \\ \eta_0 &= 0.77 \quad (\text{Blasius} : H \approx 2.6) \\ c_0 &= 0 \\ c_1 &= 0 \end{aligned}$$

The chordwise imposed velocity is plotted in Figure 8-4. Also shown are the outer-edge streamlines which barely have a discernible curvature. This is because the chordwise pressure gradient is severely limited for laminar flows which separate easily. Nevertheless, the gradient used here does generate significant crossflows. Also indicated in the Figure are the six stations where the velocity profiles from the finite-difference calculation are compared with the profiles implied by the integral calculation.

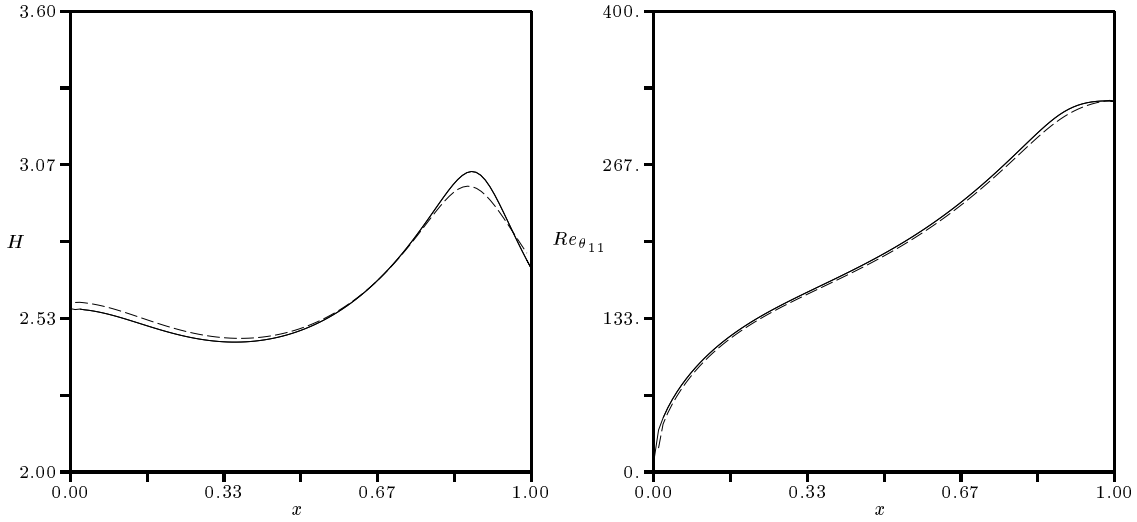

Figure 8-5: Comparison of calculated shape factor and momentum Reynolds-number distributions. The solid line is for the integral system solution.

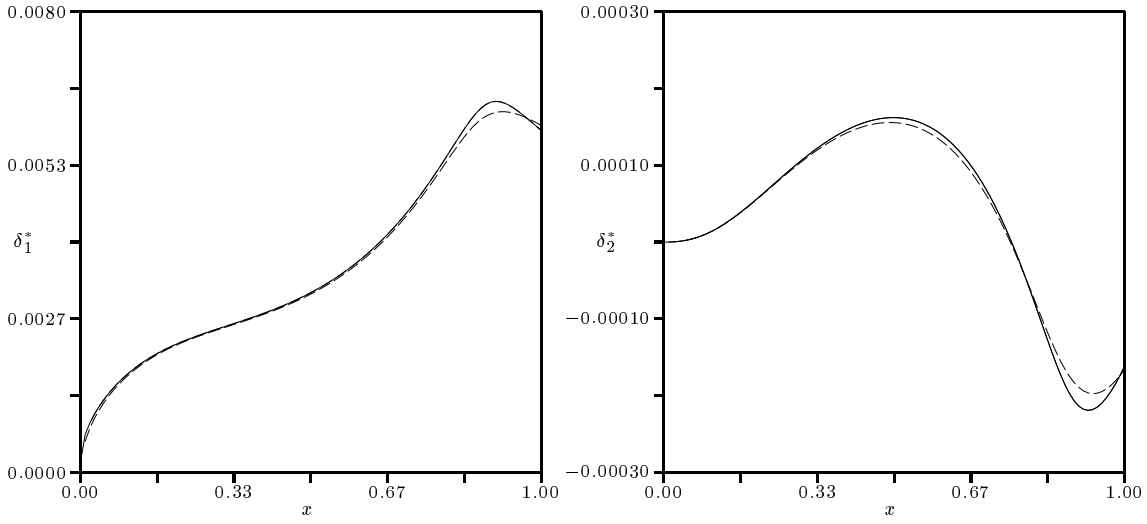

Figure 8-6: Comparison of calculated displacement-thickness components.

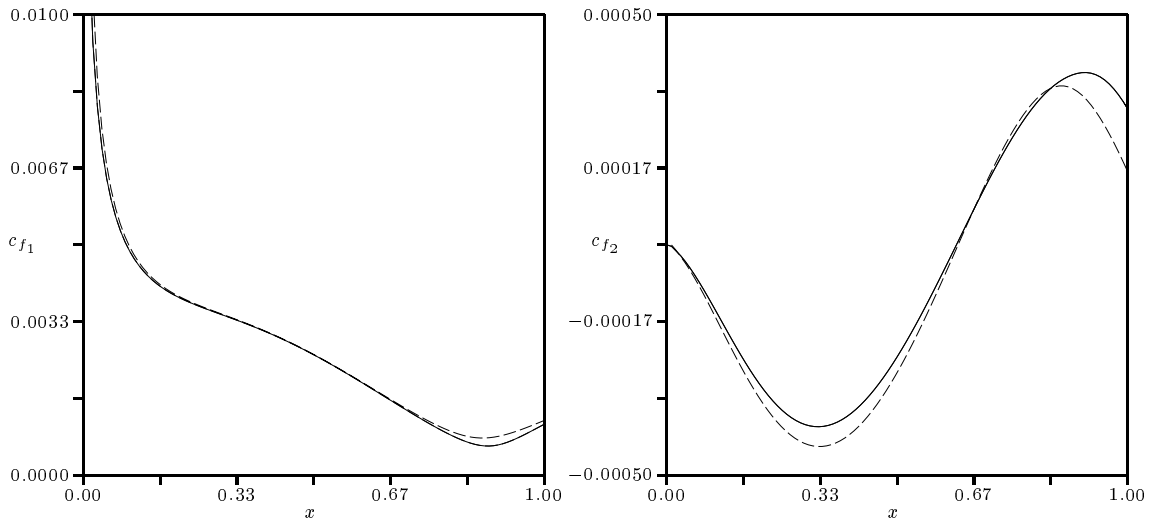

Figure 8-7: Comparison of calculated skin-friction components.

The solid-line results shown in Figures 8-5 to 8-7 are from the integral equation calculation. Note that the results are compared in streamwise coordinates and not chordwise ones. In general, the agreement of the streamwise integral quantities is excellent, while that of the cross-stream quantities is only marginally less so. As expected, the cross-stream displacement thickness and skin friction switch signs in disparate locations indicating the presence of bidirectional crossflow.

The finite-difference calculation velocity profiles are compared with those implied by the velocity profile model used in the integral calculation. In the latter, the profiles are generated for the calculated values shown in Table 8.3 at the comparison stations using the closure models. These profiles

Station	δ	η_0	c_0	c_1
A	0.0178	0.8395	-0.3231	-0.2843
B	0.0195	0.7616	-0.0844	-0.8501
C	0.0218	0.6521	0.2411	-1.4470
D	0.0248	0.5355	0.5561	-1.9230
E	0.0274	0.5000	0.7562	-2.1920
F	0.0293	0.6648	0.6347	-1.9000

Table 8.1: Calculated boundary-layer parameters from the integral system calculation which are used to generate the velocity profiles for comparison with the finite-difference solution.

are shown in Figure 8-8 with those for the integral calculation plotted with bold lines. The agreement is fair given that the profile model was formulated without consideration to this comparison. Clearly, the agreement could be much improved by using a slightly different profile family, but the comparison does seem to indicate that the current model should have wide applicability.

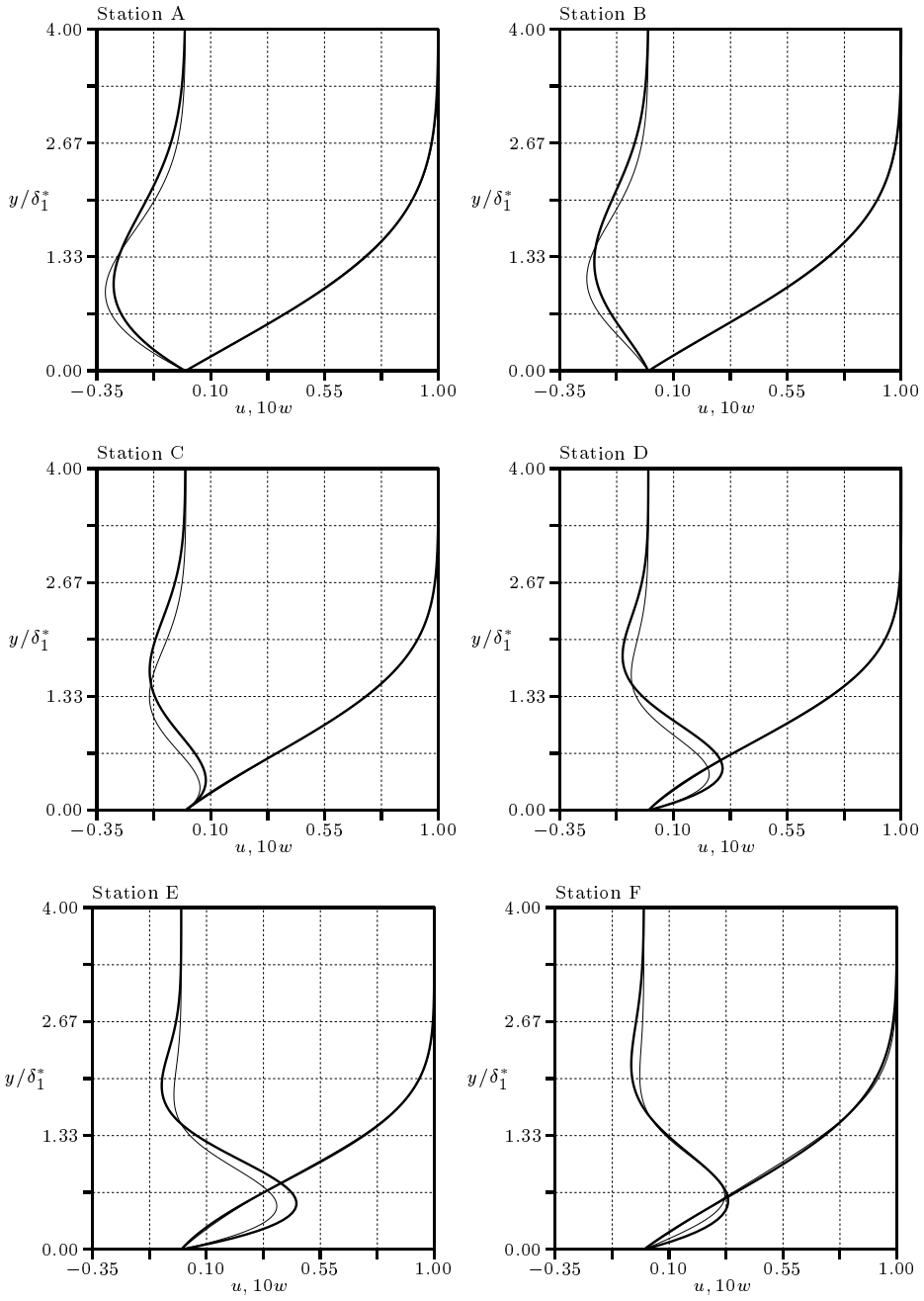

Figure 8-8: Comparison of velocity profiles computed by the finite-difference method (thin lines) with those computed from the integral solution (bold lines). The streamwise profiles are too close to be differentiable here.

Chapter 9

Application II: Separated Flows

The calculation of separated flows using classical boundary-layer solution methods is not possible because of the existence of singularities. In two dimensions, the Goldstein singularity is well-known and documented and has been recognized to be a mathematical artifact of the way the equations are solved. A variety of solution techniques for the equations, spanning the range from inverse to simultaneous, have been devised that do not contain the singularity. More recently, these methods have been successfully extended to the three-dimensional equations.

This chapter contains a brief review of the singularities in the direct-mode ((where the outer-edge velocities, and hence the pressure gradient, are prescribed) solution of both the two-dimensional equations as well as the three-dimensional ones. The singularities in the former are a limiting case of the those in the latter. The practical consequence of these singularities is the difficulty in computing solutions near a separation line. Frequently, the dependent variables become extremely sensitive to small changes in the primary parameters and the calculation breaks down. The discussion here is limited to steady flow.

A fully-simultaneous coupled viscous-inviscid solver based on the Newton method is described. The interaction between the boundary layer and the inviscid flow is based on the wall-transpiration model. This method differs from others in its ability to allow general parametric representations for the closure in the boundary-layer equations. It is used to calculate a separated flow over a smooth three-dimensional bump.

9.1 Separation and singularities in the equations

9.1.1 Two-dimensional flow

The Goldstein singularity in two-dimensional direct-mode calculations using the differential boundary-layer equations also manifests itself in integral equation systems. In particular, this includes systems containing the momentum integral and kinetic-energy/entrainment equations. Paradoxically, the presence of this singularity is an indication that the mathematical properties of the equation system are closely correlated to the actual flow physics.

It will be useful to distinguish between physical and mathematical definitions of separation. Separation, in the *physical* sense occurs at the point where the wall shear stress is zero while the *mathematical* criterion is the singularity of the coefficient matrix (derivative-term Jacobian matrix); the two definitions are close but do not necessarily coincide. The definition relevant to the stability of calculation methods is the mathematical one. For a system containing the momentum and kinetic-energy equations, the determinant of the coefficient matrix (in direct mode, the system parameters are boundary-layer variables) is

$$|\mathbf{J}| = \left| \begin{bmatrix} \theta_{11} & \frac{\partial \theta_{11}}{\partial H} \\ E_{11} & \frac{\partial E_{11}}{\partial H} \end{bmatrix} \right| = \theta_{11}^2 \frac{dH^*}{dH}, \quad H^* = \frac{E_{11}}{\theta_{11}}.$$

In closure schemes for laminar flows where the velocity profile $u(H; y/\delta)$ is obtained by sliding the origin along a given curve, (as discussed in Chapter 3 for Equation 3.7), the correspondence between the physical and mathematical definitions is exact

$$\frac{dH^*}{dH} = 0 \quad \text{if} \quad \left.\frac{\partial u}{\partial y}\right|_w \sim c_{f_1} = 0\,.$$

For most other laminar and turbulent methods employing these equations, the correspondence is very close. Very similar results are obtained, as was noted in Chapter 5, if the entrainment equation is used in place of the kinetic-energy one, because the respective shape-factor functions ($H^*(H)$) both have zero gradients very close to one another.

When the coefficient matrix is singular, the boundary-layer solution is infinitely sensitive to the primary parameters. Inverse or simultaneous methods avoid the Goldstein singularity by capturing

the strong physical coupling that exists between the boundary layer and the external flow in the vicinity of separation. In the inverse mode, where one of the primary parameters is the velocity, the coefficient matrix is well-conditioned near separation.

The inspiration for inverse and fully-simultaneous methods is that the equations at a separation point admit only a unique pressure gradient, which, therefore, cannot be imposed. Consider, again, the two dimensional system containing the momentum and kinetic-energy equations. Near separation the pressure gradient is primarily controlled by the shape parameter equation [21], which is a unique combination of the two equations in the system. In residual form, this equation is

$$r_H = \frac{\theta^2}{\nu}\frac{dq_e}{ds} - \frac{1}{H-1}\left(-Re_\theta\frac{2C_D}{H^*} + Re_\theta\frac{C_f}{2} + Re_\theta\frac{\theta}{H^*}\frac{dH^*}{dH}\frac{dH}{ds}\right) . \tag{9.1}$$

Note that the pressure-gradient parameter is related to Pohlhausen's parameter Λ by

$$\frac{\theta^2}{\nu}\frac{dq_e}{ds} = \frac{\theta^2}{\delta^2}\Lambda$$

and that, for laminar flow, the terms $Re_\theta\frac{2C_D}{H^*}$ and $Re_\theta\frac{C_f}{2}$ are unique functions only of the shape factor H. At separation, $C_f \approx 0$ and $\frac{dH^*}{dH} = 0$ and, therefore,

$$r_{H_{sep}} \approx \frac{\theta^2}{\nu}\frac{dq_e}{ds} - \frac{1}{H_{sep}-1}\left(-Re_\theta\frac{2C_D}{H^*}\bigg|_{H_{sep}}\right) .$$

The residual is only satisfied for a unique pressure gradient which, therefore, cannot be imposed.

9.1.2 Three-dimensional flow

The appearance of separation in three dimensions is considerably more complex than in two because the notion has to be extended from that of a point to that of a line. Separation lines are defined as the envelope of coalescing limiting wall streamlines which demarcate the boundary between fluid with 'different' origins (near the wall). These envelopes are clearly visualizable in experiments from surface oil-flow patterns. In fact, very complicated topologies are possible and have been observed. For the purposes of this thesis, interest will be confined to simple separation bubbles or the separation line in front of a blunt object.

In the direct-mode three-dimensional equations, the notion of characteristic lines is useful in the explanation of singularities. This is particularly true in the case of the outer-most (largest angle

with respect to external streamline) characteristic line. Note that in well-designed closure schemes, it is always possible to closely identify this characteristic with the limiting wall streamline. Cousteix and Houdeville [10] demonstrate this in their study of the nature of a particular system of the integral equations with approximate closure.

The outer-most characteristic lines can also coalesce to form an envelope resembling the separation line. This envelope is called the singularity line. As in the two-dimensional case, the distinction between the physical definition of separation and the mathematical one can be made. The singularity line, and not the separation line, is relevant to the mathematical character of the equations and is responsible for the unstable behavior of direct-mode solution methods. In the depiction in Figure 9-1, the physical appearance of the separation line is contrasted to the mathematical picture of the singularity line for a boundary-layer flow in front of a blunt object. This object generates a pressure field that tends to cause both the outer-edge and limiting wall streamlines to diverge. The separation line is close to the singularity line but the two are not necessarily identical.

Also shown in Figure 9-1 are two features A and B of special interest. The distinction between the two can be made in terms of the properties of the derivative-term Jacobian matrices. In the calculations, it is in general not possible to connect the location of the singularity line, depicted as Region B, to the singular behavior of the matrices. By contrast, the rather special point of symmetry at A is directly related to this behavior.

Singularity saddle points

Consider feature A first. The singularity of a Jacobian matrix associated with one of the coordinate axes indicates that at least one characteristic is aligned with the other coordinate (provided, of course, that the other coefficient matrix is not simultaneously singular). Therefore, if $\mathbf{J}_s$ is singular, at least one characteristic, which is usually the outer-most one, is at right angles to the outer-edge streamline direction (aligned with the n axis). While this singular point resembles the one in two-dimensional flow (especially because the crossflow is zero by symmetry) it is in fact a three-dimensional phenomenon. This is so because some of the cross-stream derivatives (for example, for $\rho_e q_e \theta_{22}$) in the equations are non-zero.

Singular points in three-dimensional flows are, therefore, characterized by $|\mathbf{J}_s| = 0$ and $c = 0$. A variety of systems are used for three-dimensional calculations and, consequently, there are a variety of criteria for singular points as well. Two examples are presented here. Consider first a system

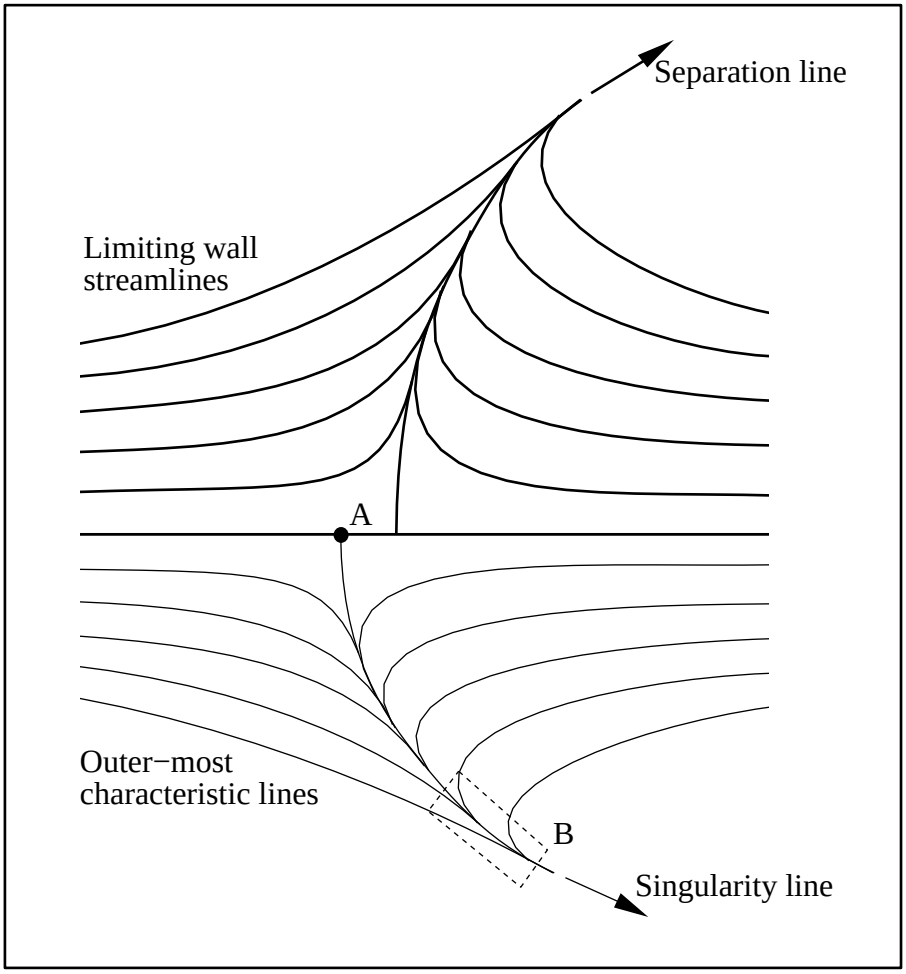

Figure 9-1: The physical separation line (envelope of coalescing limiting wall streamlines shown as thick lines) contrasted with the direct-mode mathematical singularity line (envelope of coalescing outer-most characteristic lines shown as thin lines) in the diverging flow in front of a blunt obstacle. Also marked are two features of special interest.

proposed for the bidirectional crossflow calculations (this system is of course ill-conditioned in certain situations when used in an implicit solver but this fact is not relevant here). The Jacobian matrices are

$$\mathbf{J}_s = \begin{bmatrix} \theta_{11} & \dot{\theta}_{11} & 0 & 0 \\ c\bar{\theta}_{21} & c\dot{\bar{\theta}}_{21} & \bar{\theta}_{21} & c\bar{\theta}'_{21} \\ E_{11} & \dot{E}_{11} & 0 & 0 \\ c^2\bar{E}_{21} & c^2\dot{\bar{E}}_{21} & 2c\bar{E}_{21} & c^2\bar{E}'_{21} \end{bmatrix},$$

$$\mathbf{J}_n = \begin{bmatrix} c\bar{\theta}_{12} & c\dot{\bar{\theta}}_{12} & \bar{\theta}_{12} & c\bar{\theta}'_{12} \\ c^2\bar{\theta}_{22} & c^2\dot{\bar{\theta}}_{22} & 2c\bar{\theta}_{22} & c^2\bar{\theta}'_{22} \\ c\bar{E}_{12} & c\dot{\bar{E}}_{12} & \bar{E}_{12} & c\bar{E}'_{12} \\ c^3\bar{E}_{22} & c^3\dot{\bar{E}}_{22} & 3c^2\bar{E}_{22} & c^3\bar{E}'_{22} \end{bmatrix},$$

where the columns are partial derivatives with respect to $(\ln\delta, p, c, c_1)^T$ and the overbar notation has been retained to clearly show the dependence on c. The determinant of $\mathbf{J}_s$ is

$$|\mathbf{J}_s| = \left[\theta_{11}^2 \frac{\partial}{\partial p_1}\left(\frac{E_{11}}{\theta_{11}}\right)\right]\left[c^2\left(\bar{\theta}_{21}\bar{E}'_{21} - 2\bar{E}_{21}\bar{\theta}'_{21}\right)\right].$$

The first factor is recognized to be identical to the two-dimensional system determinant. The second factor is related to the shape of the crossflow velocity profile and defines a different *mathematical* singularity mechanism. The presence of the c^2 factor may be misleading in that it indicates a singularity of degree two as $c \to 0$. However, note that $|\mathbf{J}_n| \sim c^6$, so that in the limit of zero crossflow, all four characteristics are in fact aligned with the s axis.

The criterion is slightly more complicated if the total kinetic-energy equation is used instead of just the streamwise component in a three-equation system. The Jacobian matrices are

$$\mathbf{J}_s = \begin{bmatrix} \theta_{11} & \dot{\theta}_{11} & 0 \\ c\bar{\theta}_{21} & c\dot{\bar{\theta}}_{21} & \bar{\theta}_{21} \\ E_{11} + c^2\bar{E}_{21} & \dot{E}_{11} + c^2\dot{\bar{E}}_{21} & 2c\bar{E}_{21} \end{bmatrix},$$

$$\mathbf{J}_n = \begin{bmatrix} c\bar{\theta}_{12} & c\dot{\bar{\theta}}_{12} & \bar{\theta}_{12} \\ c^2\bar{\theta}_{22} & c^2\dot{\bar{\theta}}_{22} & 2c\bar{\theta}_{22} \\ c\bar{E}_{12} + c^3\bar{E}_{22} & c\dot{\bar{E}}_{12} + c^3\dot{\bar{E}}_{22} & \bar{E}_{12} + 3c^2\bar{E}_{22} \end{bmatrix},$$

where the columns are partial derivatives with respect to $(\ln\delta, p, c)^T$. The determinant of $\mathbf{J}_s$ is

$$|\mathbf{J}_s| = \theta_{11}^2 \left[-\bar{\theta}_{21} \frac{d}{dp_1}\left(\frac{E_{11} + c^2\bar{E}_{21}}{\theta_{11}}\right) + 2c^2\bar{E}_{21}\frac{d}{dp_1}\left(\frac{\bar{\theta}_{21}}{\theta_{11}}\right)\right].$$

The singularity criterion is identical to the two-dimensional one if $c = 0$ because the lowest-order dependence of $|\mathbf{J}_n|$ is $\sim c$.

Singularity lines

A singularity line (highlighted as feature B), like a separation line, is not necessarily aligned with the cross-stream coordinate everywhere. Computationally, its presence is indicated by unstable behavior. It is usually not possible to predict its location from the singular properties of the Jacobian matrices. There are exceptions in some simple situations, however. An example of this is the separation line for a separating flow on an infinite-span wing [62]. Here, one would look for the singularity of the Jacobian matrix associated with the chordwise-axis to indicate the alignment of the outer-most characteristic line with the spanwise direction.

It is useful to view the problem of well-posedness in the three-dimensional equations in terms of the flow of information implied by the orientation of the characteristic lines. Across a singularity line, discontinuities in the characteristic variable corresponding to the outer-most characteristic are possible. This is a well-known result of the theory of characteristics and is, perhaps, best compared to the formation of a shock in the inviscid Burger's equation. In the boundary-layer equations this implies the possibility of infinite first-derivatives across the singularity line. This is not a realistic situation because it violates the principle of regularity near and across a separation line (despite the existence of large gradients) [10]. Clearly it is an artifact of the direct-mode formulation.

According to an analysis of an integral system that is also found to possess real eigenvalues in the *inverse* mode by Yoshihara and Wai [72], no characteristic line could be identified with the limiting wall streamline. The implication is that a singularity line does not exist here and consequently stability issues (related to well-posedness) do not arise. There is another aspect to the direct-mode

singularity line. In Yoshihara and Wai's direct-mode method where the solution is marched along characteristic lines on an infinite-swept wing in compliance with domain of dependence constraints, the boundary-layer equations are found to violate compatibility conditions along the singularity line. These violations are also traced to the imposition of the pressure-gradient across the singularity line.

9.1.3 Ill-conditioning of residual Jacobian matrix

The coupling scheme presented in this thesis is based on the Newton solution of the equations. It is of interest to examine the singular behavior of the direct-mode residual Jacobian matrix, as opposed to the derivative-term Jacobian matrices. Only the two-dimensional equations in incompressible laminar flow are considered.

The two-equation system can be written in terms of the shape-factor Residual 9.1

$$r_H = \frac{\theta^2}{\nu}\frac{dq_e}{ds} - \frac{1}{H-1}\left(-Re_\theta \frac{2C_D}{H^*} + Re_\theta \frac{C_f}{2} + Re_\theta \frac{\theta}{H^*}\frac{dH^*}{dH}\frac{dH}{ds}\right)$$

and one for the thickness scale of the boundary layer

$$r_\theta = Re_\theta \frac{d\theta}{ds} - Re_\theta \frac{C_f}{2} + (H+2)\frac{\theta^2}{\nu}\frac{dq_e}{ds}\,.$$

Let the system parameters be the boundary-layer variables θ and H for direct-mode calculations. The pressure gradient is prescribed and so the only dependence on H in r_θ is the balance between the skin-friction-term sensitivity and the pressure-gradient parameter. Numerically, these terms tend to cancel out. In the vicinity of separation, the term in parenthesis in r_H is numerically very close to zero [21] indicating that it is also virtually independent of H. Therefore, the residual Jacobian matrix becomes highly ill-conditioned because both terms in the column containing H-derivatives tend to vanish. In fact, numerical experiments show that the global Jacobian matrix determinant of the discrete residual system passes through zero in the vicinity of separation as shown in Figure 9-2, the exact location determined by the imposed pressure gradient. Nishida has also documented this behavior [44].

The ill-conditioning property of the equations can be removed by making the pressure gradient an unknown variable. Historically, a variety of iterative inverse and semi-inverse methods have been proposed. Recently, Nishida developed a robust fully-simultaneous method coupling the Full-Potential equation to the three dimensional boundary layer equations (basic system) in a Newton solver [44].

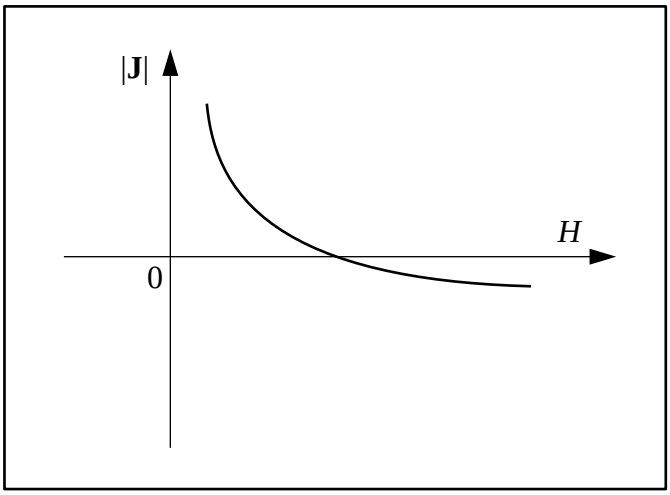

Figure 9-2: The determinant of the residual Jacobian matrix near separation.

Milewski adapted the method, based on the two-dimensional code XFOIL [20], and used lifting Panel techniques for inviscid flow [38]. The general method presented here differs from that of Milewski in that instead of using generic second-order artificial dissipation to control spurious oscillations, the considerably less intrusive, and better-suited, directional upwinding is used. Furthermore, Milewski requires the use of mass-defect components as two of the boundary-layer parameters. The method presented below is not restricted in this manner.

9.2 A fully-simultaneous coupling scheme

The objective here is to develop an ability to couple general boundary-layer systems that use empirical velocity and density profile parameters instead of the mass-defect components. Such an approach is more flexible in the use of different assumed profile families. It also allows systems of arbitrary order to be easily coupled to the inviscid flow.

Since the objectives are limited, the goal will be to calculate separated flow over a smooth three-dimensional bump using a viscous-inviscid interaction procedure. Simple Panel methods are convenient and expeditious for this purpose. Moreover, since the surface body will not generate lift, the need for a Kutta condition is obviated and the perturbative influence of the body on the ambient velocity field can be modeled by a sheet of sources only (doublets will not be needed, but may be

added easily if desired).

The interaction between the inviscid flow and the boundary layer is also naturally formulated in terms of the source-sheet strength. This coupling scheme can serve as a useful test bed for investigating more sophisticated viscous as well as inviscid solvers (such as Full-Potential, lifting Panel, Euler, etc.).

9.2.1 Inviscid flow

A general inviscid flow over a non-lifting surface is constructed by superimposing a free-stream potential and the perturbation potential of a source sheet

$$\begin{aligned}\Phi(x,y,z) &= \Phi_\infty + \phi \\ &= (u_\infty x + v_\infty y + w_\infty z) - \frac{1}{4\pi}\int_S \frac{\sigma(x_0,y_0,z_0)}{\sqrt{(x-x_0)^2+(y-y_0)^2+(z-z_0)^2}}\,dS\,.\end{aligned}$$

The velocity components generated at an arbitrary point (x,y,z) are computed by taking the derivatives of Φ

$$\mathbf{q} = (u,v,w) = (\frac{\partial\Phi}{\partial x}, \frac{\partial\Phi}{\partial y}, \frac{\partial\Phi}{\partial z})\,.$$

Following standard procedure, the surface is discretized into K flat panels $S_k(x_0,y_0,z_0)$ of constant-strength σ_k, with a perturbation potential at (x,y,z) given by the integral over the surface of the panel

$$\phi_k = -\frac{1}{4\pi}\int_{S_k} \frac{\sigma(x_0,y_0,z_0)}{\sqrt{(x-x_0)^2+(y-y_0)^2+(z-z_0)^2}}\,dx_0\,dy_0\,dz_0\,, \tag{9.2}$$

and for each an outwardly-directed normal vector $\hat{\mathbf{e}}_{n_k}$ is defined. The velocity induced by all panels at the centroid of the kth panel (x,y,z) is determined by summing their contributions

$$v_{n_k} = \left(\sum_j \nabla\phi_j(x,y,z)\right)\cdot\hat{\mathbf{e}}_{n_k} = P_{kj}\sigma_j, \quad j,k = 1,\ldots,K\,,$$

where the gradient function involves an integral over the surface of a contributing panel. The kth panel contribution to the normal velocity is simply $\sigma_k/2$. The result is conveniently expressed in matrix format so that $\mathbf{P}$ is the resultant $K\times K$ influence matrix.

The inviscid velocity field is now expressed in terms of K panel source strengths. This field is determined by the K collocation conditions requiring wall-parallel flow. Therefore, setting the total induced normal velocity equal to negative the component corresponding to the freestream

$$\sigma_j = P_{jk}^{-1} v_{n_k} = -P_{jk}^{-1} \mathbf{q}_\infty \cdot \hat{\mathbf{e}}_{n_k}$$

fixes the source strengths and also the inviscid velocity field.

It is convenient to directly express the inviscid velocity components at the N number of panel nodes in terms of the normal velocities induced by the panel sources at their centroids. The source strengths can be eliminated by again summing the gradient of the potential function to generate three matrices $\mathbf{E}^{(u)}, \mathbf{E}^{(v)}, \mathbf{E}^{(w)}$, each of order $N \times K$, one for each velocity component. The components of inviscid velocity at node $i (i = 1, \ldots, N)$ is then given by :

$$u_{I_i} = -E_{ij}^{(u)} P_{jk}^{-1} \mathbf{q}_\infty \cdot \hat{\mathbf{e}}_{n_k} = -D_{ik}^{(u)} \mathbf{q}_\infty \cdot \hat{\mathbf{e}}_{n_k}$$

$$v_{I_i} = -E_{ij}^{(v)} P_{jk}^{-1} \mathbf{q}_\infty \cdot \hat{\mathbf{e}}_{n_k} = -D_{ik}^{(v)} \mathbf{q}_\infty \cdot \hat{\mathbf{e}}_{n_k}$$

$$w_{I_i} = -E_{ij}^{(w)} P_{jk}^{-1} \mathbf{q}_\infty \cdot \hat{\mathbf{e}}_{n_k} = -D_{ik}^{(w)} \mathbf{q}_\infty \cdot \hat{\mathbf{e}}_{n_k}$$

Each of the three matrices $\mathbf{D}$ is only a function of the surface geometry. Hence, each is computed once and stored for later use.

For the exploratory purposes of this thesis, the integrals in Equation 9.2 are approximately evaluated using 2 by 2 Gauss quadrature instead of the usual cumbersome analytical expressions (though these can be substituted if desired). The velocity contribution of a panel to its nodes are approximately calculated assuming an equivalent point source at the panel centroid. Finally, edge effects are mitigated at the boundary nodes by assuming an equal effect from a reflected virtual panel containing the node of the same geometry and source strength reflected outside the domain.

9.2.2 Incorporation of displacement effects

The entrainment equation, Equation 2.6, was derived in Chapter 2 and, for the purposes here, is written in terms of the outer-edge component of normal mass flux

$$\rho_e v_e = \nabla \cdot (\rho_e q_e \vec{\delta^*}) - \delta \nabla \cdot \rho_e \mathbf{q}_e \, .$$

This expression is for real viscous flow (RVF). The value of this normal mass flux is compared to one derived using an equivalent inviscid flow (EIF) model. There, it is assumed that ρu and ρw are constant in y across the extent of the boundary layer $y = [0, \delta]$ and equal to their respective values at the outer-edge in RVF. Hence, in EIF

$$\frac{\partial^2 \rho v}{\partial y^2} = 0 \quad \text{(EIF)}$$

by taking the y partial derivative of the continuity equation. The two scenarios are compared in Figure 9-3. The displacement effect of the boundary layer in EIF is now borne by a wall-transpiration mass flux. The mass flux ρv at the edge is:

$$\rho_e v_e = \rho_w v_w + \int_0^\delta \frac{\partial \rho v}{\partial y} \, dy$$

$$\rho_e v_e = \rho_w v_w - \int_0^\delta \nabla \cdot \rho \mathbf{q} \, dy$$

$$\rho_e v_e = \rho_w v_w - \delta \, (\nabla \cdot \rho_e \mathbf{q}_e) \tag{9.3}$$

Comparing Equations 2.6 and 9.3, the wall transpiration flux that is equivalent to the displacement effect of the boundary layer is

$$\rho_w v_w = \nabla \cdot (\rho_e q_e \vec{\delta^*}) \, . \tag{9.4}$$

The transpiration model is naturally suited for a panel-method-based interaction scheme. The displacement effect is incorporated through the panel source strengths so that the outer-edge velocities at the nodes are linearly superimposed on the undisturbed inviscid flow field ($k = 1, \ldots, K$, $i = 1, \ldots, N$):

$$u_{e_i} = u_{I_i} + \sum_k D_{ik}^{(u)} [\nabla \cdot (\rho_e q_e \vec{\delta^*})]_k \tag{9.5}$$

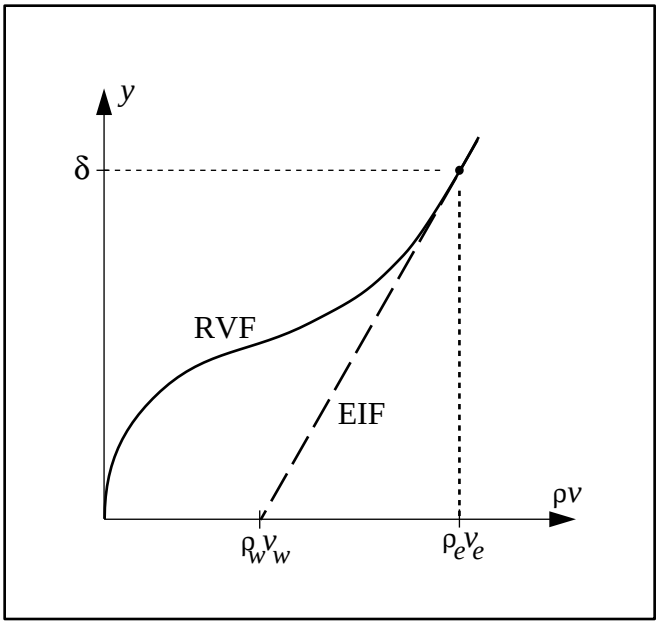

Figure 9-3: The variation of the wall-normal component of mass flux in real viscous flow (RVF) and equivalent inviscid flow (EIF).

$$v_{e_i} = v_{I_i} + \sum_k D_{ik}^{(v)} [\nabla \cdot (\rho_e q_e \vec{\delta}^*)]_k \tag{9.6}$$

$$w_{e_i} = w_{I_i} + \sum_k D_{ik}^{(w)} [\nabla \cdot (\rho_e q_e \vec{\delta}^*)]_k \tag{9.7}$$

The mass-defect vector divergence is computed over the kth panel/element. At this point, these expressions could be further simplified for a particular discretization scheme by computing the divergences for all elements, and storing the coefficients of the resulting relationships between the nodal values of the outer-edge velocity components and the mass-defect components. However, this would represent a restriction in the use of assumed profile families, which would then have to be defined in terms of these mass-defect components as opposed to natural empirical parameters. Therefore, the outer-edge velocity expressions are left in the form shown above.

9.2.3 Equivalent boundary-layer parameters

It has already been noted that the transpiration mass flux in Equation 9.4 is a function of the two boundary-layer mass-defect components, which are natural candidates for primary parameters in a

solution scheme. If used as such, the resulting Newton matrix is not as full which can be exploited (as in XFOIL for two dimensions [20]) for more computational efficiency and speed. However, as has been pointed out, the use of the mass-defect components as primary parameters restricts the ability to use profile families. The ability to retain the use of empirical profile parameters is sought.

By employing empirical profile parameters as primary parameters, the outer-edge velocity definitions become tautologies (circularly defined) because of the appearance of the local velocity magnitude on the right hand side of Equations 9.5- 9.7. To overcome this complication, the simple functional relationship of the two mass-defect components to the two universal boundary-layer parameters δ and c (the case of two mode crossflow profiles is a simple extension) is used. Changes in the mass-defect components due to changes in the velocity magnitude are borne by these boundary-layer parameters while, at the same time, keeping the velocity magnitude fixed at the non-perturbed value. These modified parameters values, which together with the non-perturbed inviscid velocity field, yield the correct mass-defect divergence are termed equivalent boundary-layer parameters (EBLP) as opposed to real boundary-layer parameters (RBLP).

The EBLP values, denoted by the subscript ep, are derived by equating the value of the mass-defect components expressed in terms of RBLPs using q_e to that expressed in terms of EBLPs using q_I. Denote the displacement thicknesses evaluated at $\delta = 1$ and $c = 1$ by the overbar notation. Consider first the streamwise mass defect

$$m_1^* : \quad \rho_e q_e \; \delta \; \overline{\delta}_1^*(q_e) = \rho_e q_I \; \delta_{ep} \; \overline{\delta}_1^*(q_I) \, .$$

This leads to the relation

$$\delta = \frac{q_I}{q_e} \frac{\overline{\delta}_1^*(q_I)}{\overline{\delta}_1^*(q_e)} \; \delta_{ep} \, . \tag{9.8}$$

Similarly, consider the cross-stream mass defect

$$m_2^* : \quad \rho_e q_e \; \delta \; c \; \overline{\delta}_2^*(q_e) = \rho_e q_I \; \delta_{ep} \; c_{ep} \; \overline{\delta}_2^*(q_I) \, .$$

This leads to another relation

$$c = \frac{\overline{\delta}_1^*(q_e)}{\overline{\delta}_1^*(q_I)} \frac{\overline{\delta}_2^*(q_I)}{\overline{\delta}_2^*(q_e)} \; c_{ep} \, . \tag{9.9}$$

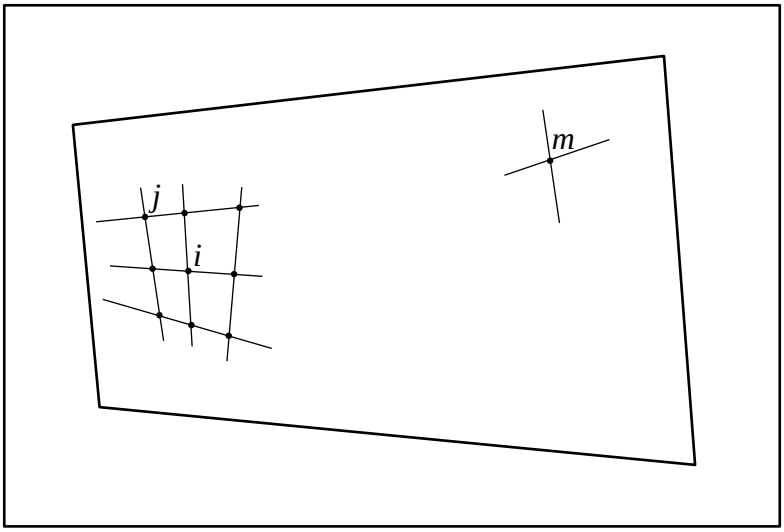

Figure 9-4: Nodal neighbors of i.

In the equations above, the dependence of the displacement thicknesses on velocity is necessary because of the profile-shape dependence on Reynolds number Re_δ in turbulent flow. For laminar flow, where there is no such dependence, a single, simpler equivalence suffices based only on the streamwise mass-defect definition

$$\delta = \frac{q_I}{q_e}\,\delta_{ep}\,.$$

In the interests of generality, the full dependencies are assumed in what follows.

9.2.4 Direct and interactive algorithms/data structures

Before outlining the algorithms and data structures for the two calculation modes, it will be convenient to define some notation.

1. For an unstructured grid, it is useful to define a function $j = \Delta_{map}(i, l)$ to denote the immediate nodal neighbors of a node i. The function maps the local node number $l = 1, \ldots, 9$ for eight neighboring nodes to the global node number j. The ninth node is i itself, $i = \Delta_{map}(i, 9)$. Appropriate allowances for the boundaries are made.

2. It is useful to define two primary parameter vectors. The first containing the RBLPs is denoted $\tilde{\mathbf{p}} = (\delta, c, \ldots)^T$, where the ellipses refer to profile shape factors. The second vector, where the

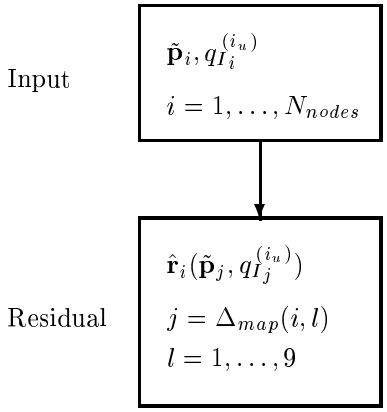

Figure 9-5: Main features of the direct-mode algorithm.

two RBLP's are replaced by EBLPs, is denoted $\mathbf{p} = (\delta_{ep}, c_{ep}, \ldots)^T$. Both vectors, of course, are of order N which is also the order of the integral-equation system.

3. For brevity, the three velocity components (u, v, w) are denoted by $q^{(i_u)}$, where $i_u = 1, \ldots, 3$.

The direct-mode algorithm is summarized in Figure 9-5. Nodal values of the primary parameter vector $\tilde{\mathbf{p}}$ and the unperturbed inviscid velocities are the inputs to the spatial discretization scheme. After visiting each element, the assembled vector of residuals (of order N) at each node is a function only of the parameter values at its neighboring nodes.

The interactive-mode algorithm is summarized, as a contrast to the direct-mode one, in Figure 9-6. Here, the system parameters are chosen to be $\mathbf{p}$ instead of $\tilde{\mathbf{p}}$ as in the direct mode. These are used together with the unperturbed velocity field to generate the transpiration fluxes for all elements, and then the perturbed velocity field. The nodal RBLP's are computed next and, together with the nodal values of the perturbed velocity components, are used to generate the residual vector at the nodes using the same scheme as in the direct mode. Because the perturbed velocities are a *global* function of the primary parameters through Equations 9.5-9.7, the residual vector at node i is also a global function of the parameters.

The implicit/Newton-solver Jacobian matrix in the direct mode is sparse. The global/elliptic character of the interactive mode fills the matrices. Moreover, the analytical determination of this matrix is considerably more cumbersome. The elements are the sensitivities of the residual vector at node

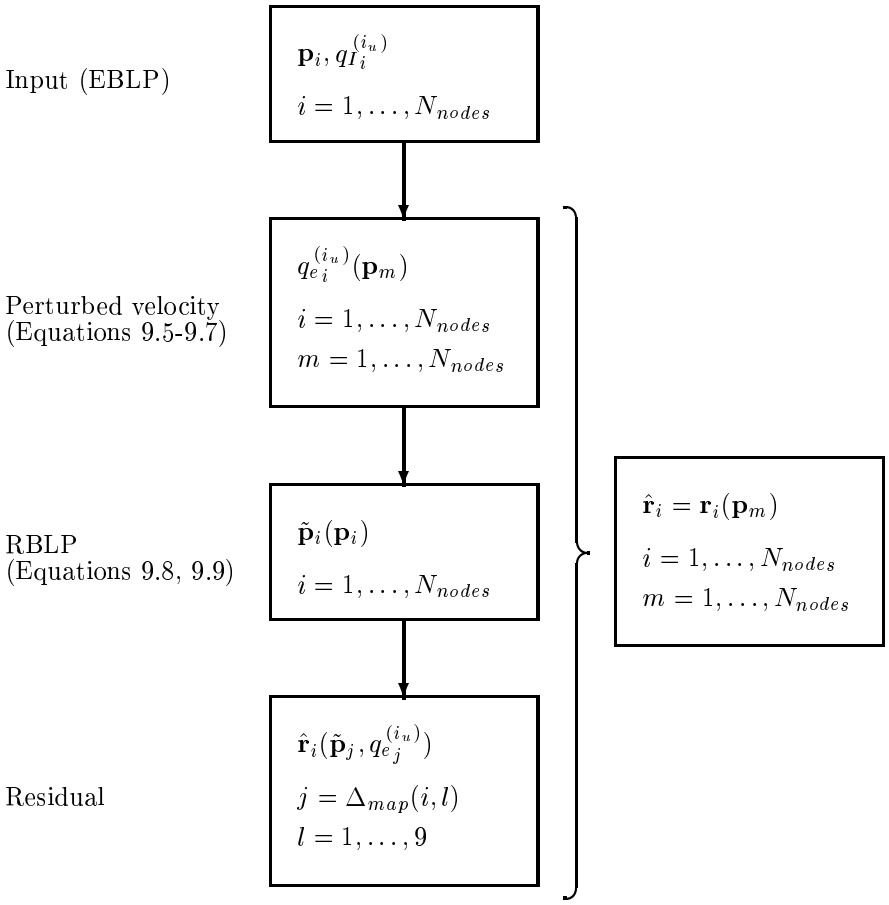

Figure 9-6: Main features of the interactive-mode algorithm.

i with respect to the parameter vector at node m (the nodes defined as shown in Figure 9-4):

$$\begin{aligned}
\frac{\partial \mathbf{r}_i}{\partial \mathbf{p}_m} &= \sum_{l=1}^{9} \frac{\partial \hat{\mathbf{r}}_i}{\partial \delta_j} \left(\sum_{i_u=1}^{3} \frac{\partial \delta_j}{\partial q_j^{e^{(i_u)}}} \frac{\partial q_j^{e^{(i_u)}}}{\partial \mathbf{p}_m} + \frac{\partial \delta_j}{\partial \mathbf{p}_m} \right) \\
&+ \sum_{l=1}^{9} \frac{\partial \hat{\mathbf{r}}_i}{\partial c_j} \left(\sum_{i_u=1}^{3} \frac{\partial c_j}{\partial q_j^{e^{(i_u)}}} \frac{\partial q_j^{e^{(i_u)}}}{\partial \mathbf{p}_m} + \frac{\partial c_j}{\partial \mathbf{p}_m} \right) \\
&+ \sum_{l=1}^{9} \sum_{i_u=1}^{3} \frac{\partial \hat{\mathbf{r}}_i}{\partial q_j^{e^{(i_u)}}} \frac{\partial q_j^{e^{(i_u)}}}{\partial \mathbf{p}_m} + \mu_{sw} \sum_{l=1}^{9} \frac{\partial \hat{\mathbf{r}}_i}{\partial \tilde{\mathbf{p}}_j} \frac{\partial \tilde{\mathbf{p}}_j}{\partial \mathbf{p}_m}, \quad \mu_{sw} = \begin{cases} 0 & \text{if } \tilde{\mathbf{p}} \text{ is } \delta \text{ or } c \\ 1 & \text{otherwise} \end{cases}
\end{aligned}$$

Here, the hatted residual vectors are emphasized to be in terms of local nodal quantities. The global dependence clearly enters through the perturbed velocity values. Also, $j = \Delta_{map}(i, l)$ in the expression above.

9.2.5 A word on the mathematical nature of the coupled system

The global dependence of the outer-edge velocities through Equations 9.5-9.7 makes the coupled system formally elliptic. In the neighborhood of the singularity line, the coupling will be strong. However, it is expected that the underlying mathematical nature of the direct and inverse-mode formulations will still apply to the boundary-layer equations especially away from separation. This is because in the limit of infinite Reynolds number, the coupled system degenerates into direct and inverse mode formulations in the attached and separated regions respectively. Therefore, the orientation of direct and inverse mode characteristic lines can be used to impose boundary conditions and, if needed, used in upwinding the equations.

9.3 Calculation of a separated flow

The fully-simultaneous coupling scheme is demonstrated by calculating the laminar, incompressible flow over a smooth sine-squared hill. The boundary layer separates downstream of the hill where a separation bubble forms.

The standard third-order system is used containing the streamwise and cross-stream momentum equations and the total kinetic-energy equation. Since the inviscid flow is irrotational, the simpler

irrotational version of the kinetic-energy equation is used. The calculation is performed on a domain $x = [0,1], z = [0,1]$ discretized into 30 elements to a side as shown in Figure 9-7. Also shown is the diagonal cut away of the hill, which has a maximum height of 0.02. The coarseness of the grid is driven by the provisional nature of the matrix-inversion routine (a direct solver) used in the code which entails a large memory requirement. There is, of course, considerable room for improvement here.

The assumed family of profiles used for closure are given by Equation 3.7 in the streamwise direction and Equation 8.1 with $c_1 = 0$ in the cross-stream direction. This closure system closely resembles the turbulent closure system with Johnston's crossflow model investigated in § 5.3.2 which was shown to be hyperbolic. On these grounds, this system is assumed to be hyperbolic.

The freestream velocity components are $u_I = 1$ and $w_I = 1$ and the reference Reynolds number $Re_{ref} = 10,000$. Because of the orientation of the freestream velocity vector, the application of boundary conditions is unambiguous. These are imposed along two sides of the domain indicated by the heavy lines in Figure 9-8(a):

$$\delta = 0.01$$

$$c = 0$$

$$\eta_0 = 0.77$$

The objective here is to capture the separation bubble, not to compute an accurate flow for comparison. The value chosen for δ is strictly not in compliance with the small-curvature rule for first-order boundary-layer theory, but is tolerable, nevertheless, in view of the limited objectives.

The computed outer-edge velocity streamlines are shown in Figure 9-8(a) and the velocity magnitude is shown in Figure 9-8(b). An approximate check of the Falkner-Skan pressure-gradient parameter β_u computed at the upstream separation line gives the figure of 0.08 which compares favorably with the similarity value of 0.0904.

Computed limiting wall streamlines (skin-friction lines) are shown in Figures 9-9(a) with a more detailed plot shown in Figures 9-9(b). While the separation bubble is large enough to be apparent, details are clearly not adequately resolved (about five elements across bubble). The resolution, as indicated earlier, is limited by the inefficient solver used. Note that the orientation of the limiting

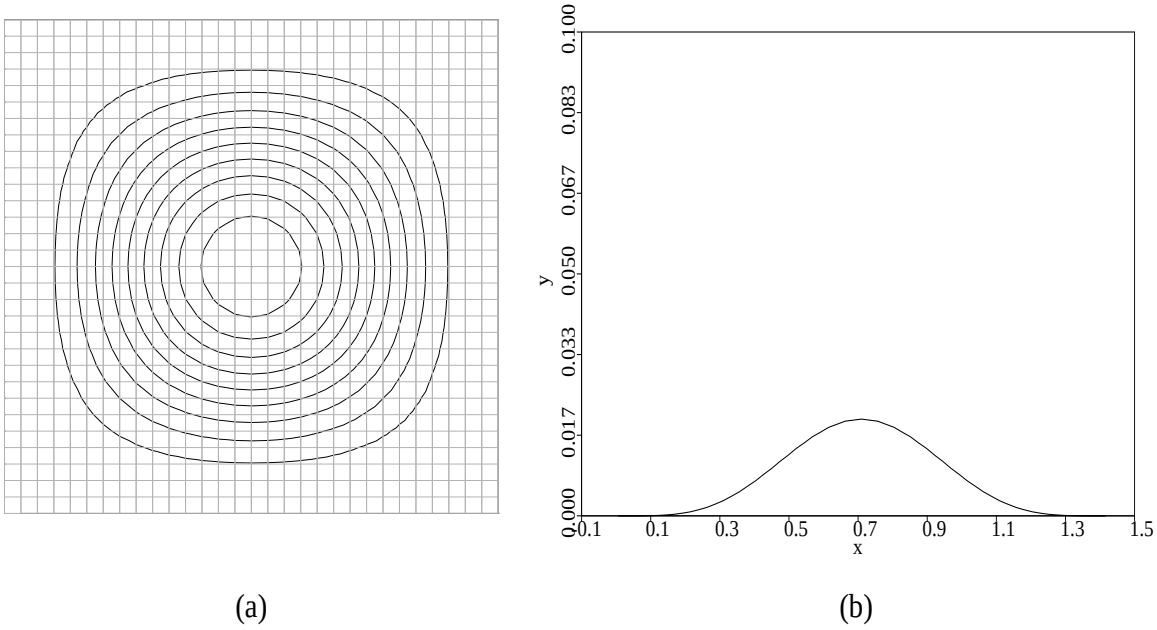

Figure 9-7: (a) Surface-relief contours and computational grid. (b) Profile (not-to-scale) of surface along diagonal.

wall streamlines is opposite to that depicted in Figure 9-1 which is for the flow in front of a blunt obstacle. This is because the pressure gradient here, indicated by the curvature of the outer-edge streamlines, is in the opposite direction due to the presence of the hill.

The susceptibility of laminar boundary layers to separation limits the severity of the allowable pressure gradients (effectively the height of the hill). Consequently, the crossflows generated are small as indicated in Figures 9-12 and 9-14.

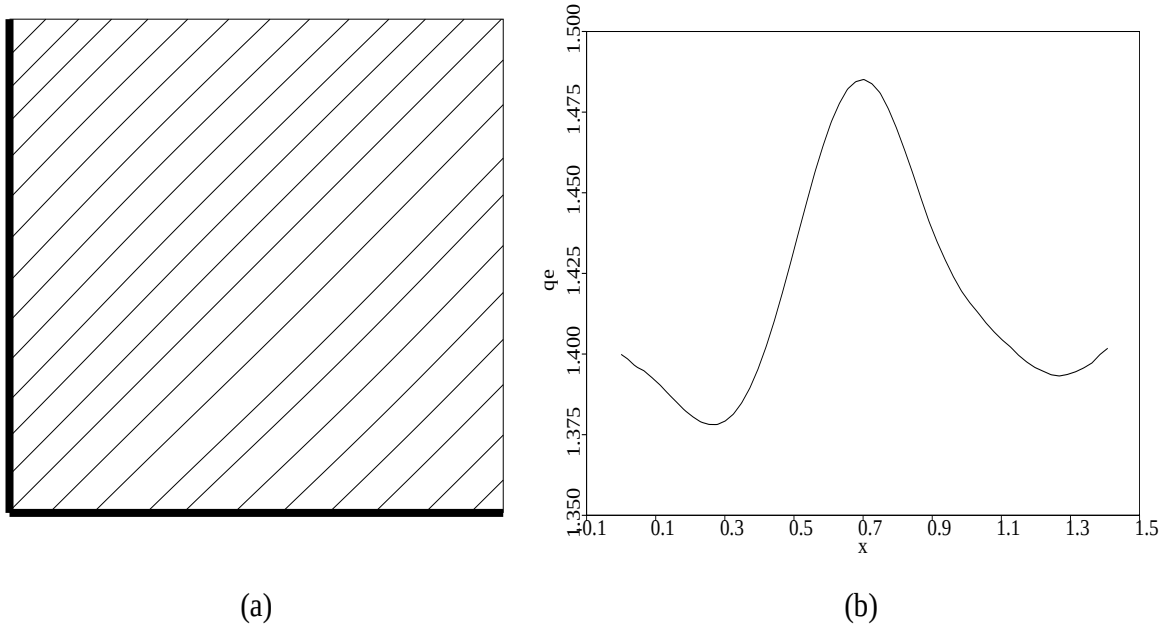

Figure 9-8: (a) Selected outer-edge velocity streamlines, and boundaries where the input conditions are applied. (b) Outer-edge velocity magnitude along streamwise diagonal.

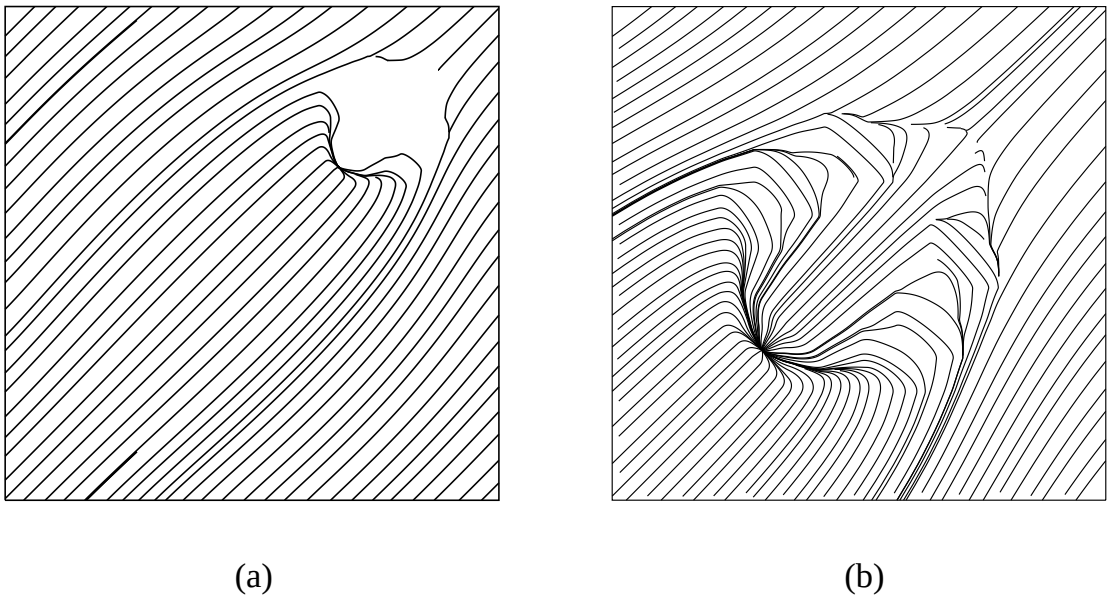

Figure 9-9: (a) Selected limiting wall streamlines. (b) Close-up detail of separated region.

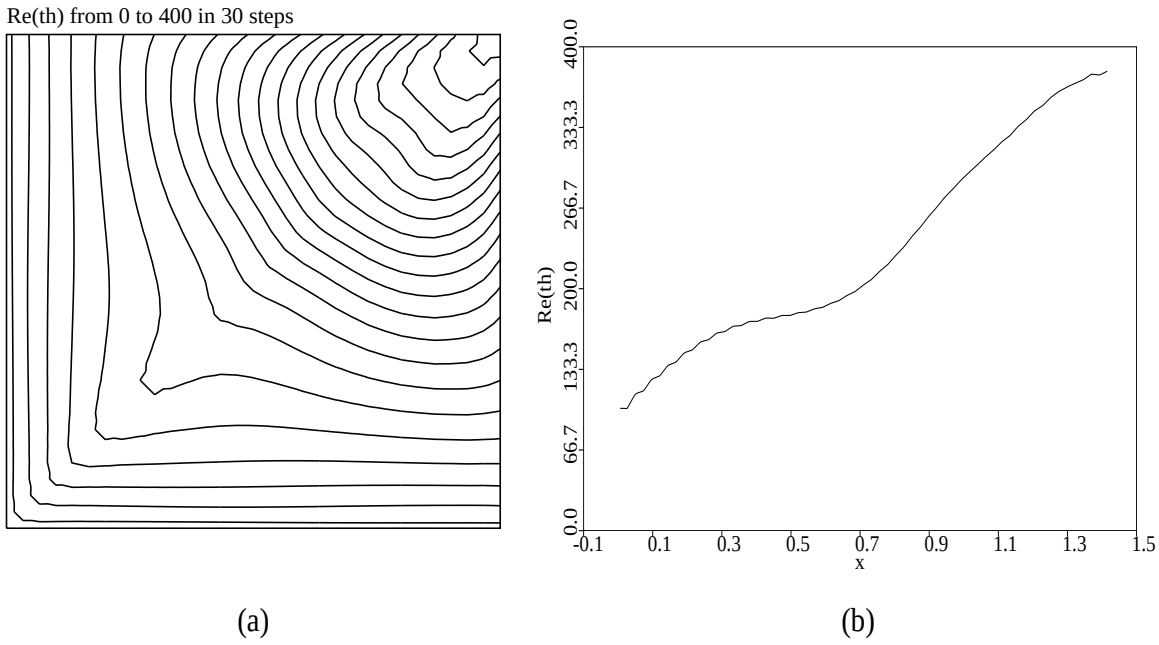

Figure 9-10: (a) Momentum Reynolds-number contours. (b) Variation along streamwise diagonal.

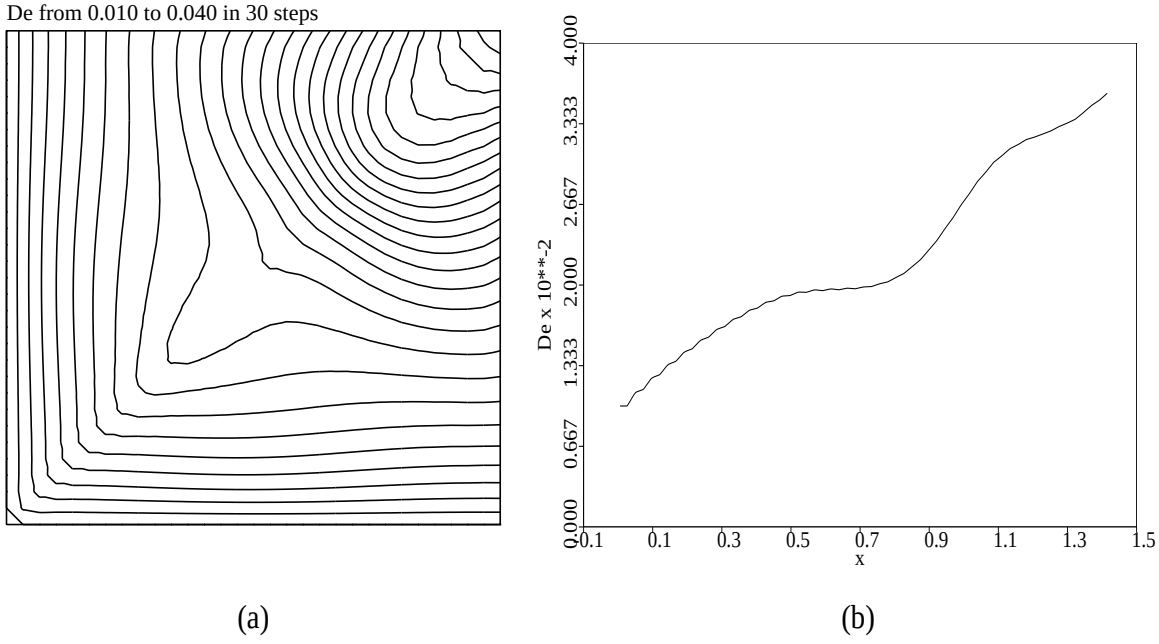

Figure 9-11: (a) Boundary layer thickness parameter contours. (b) Variation along streamwise diagonal.

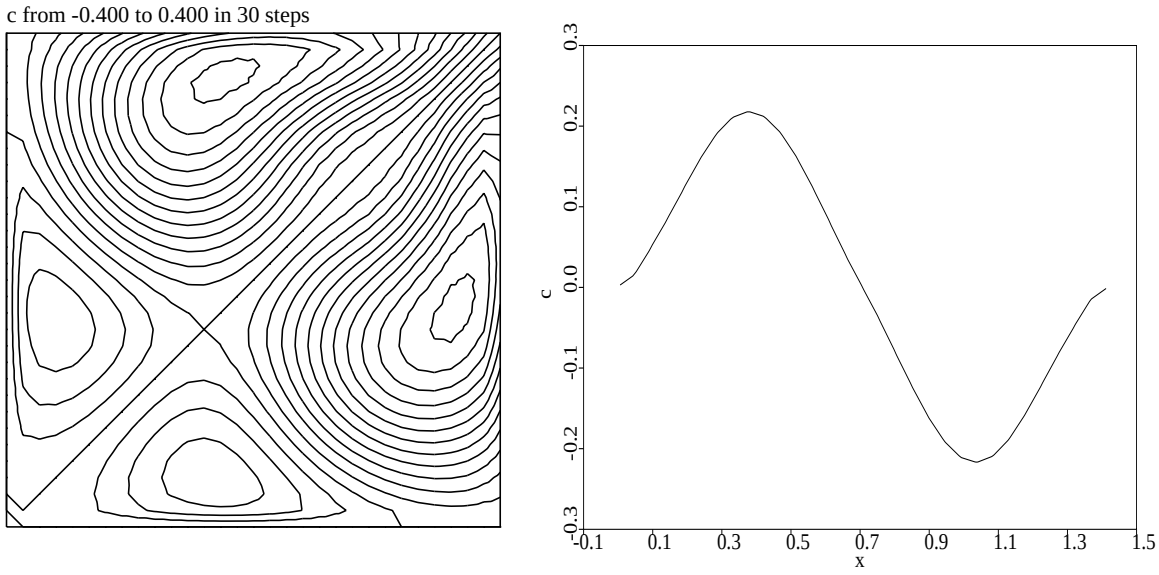

(a) (b)

Figure 9-12: (a) Crossflow magnitude parameter contours. (b) Variation along cross-stream diagonal.

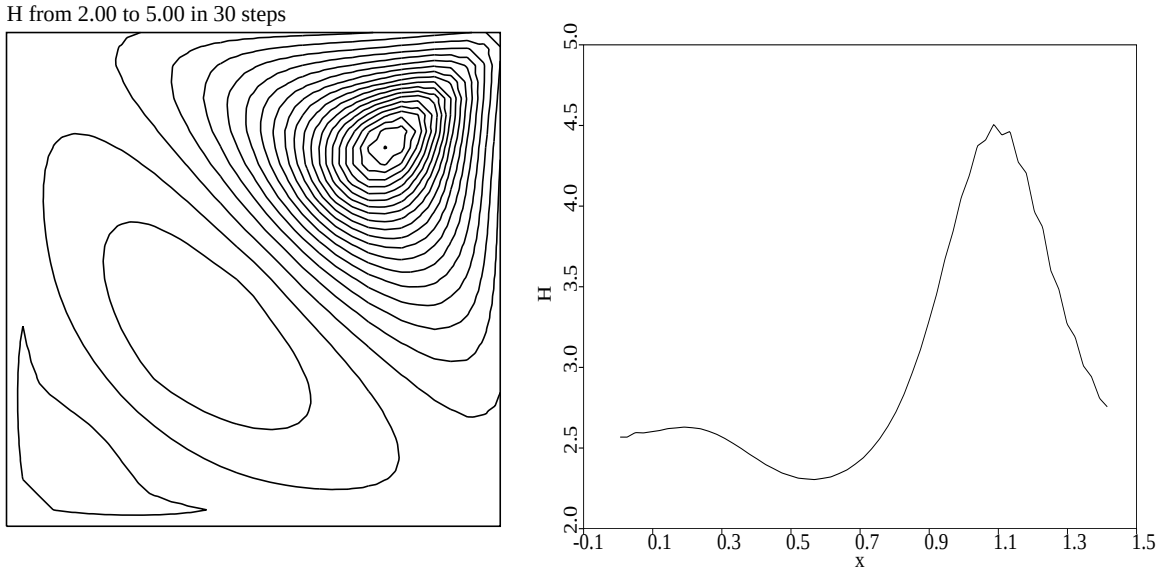

(a) (b)

Figure 9-13: (a) Shape-factor contours. (b) Variation along streamwise diagonal.

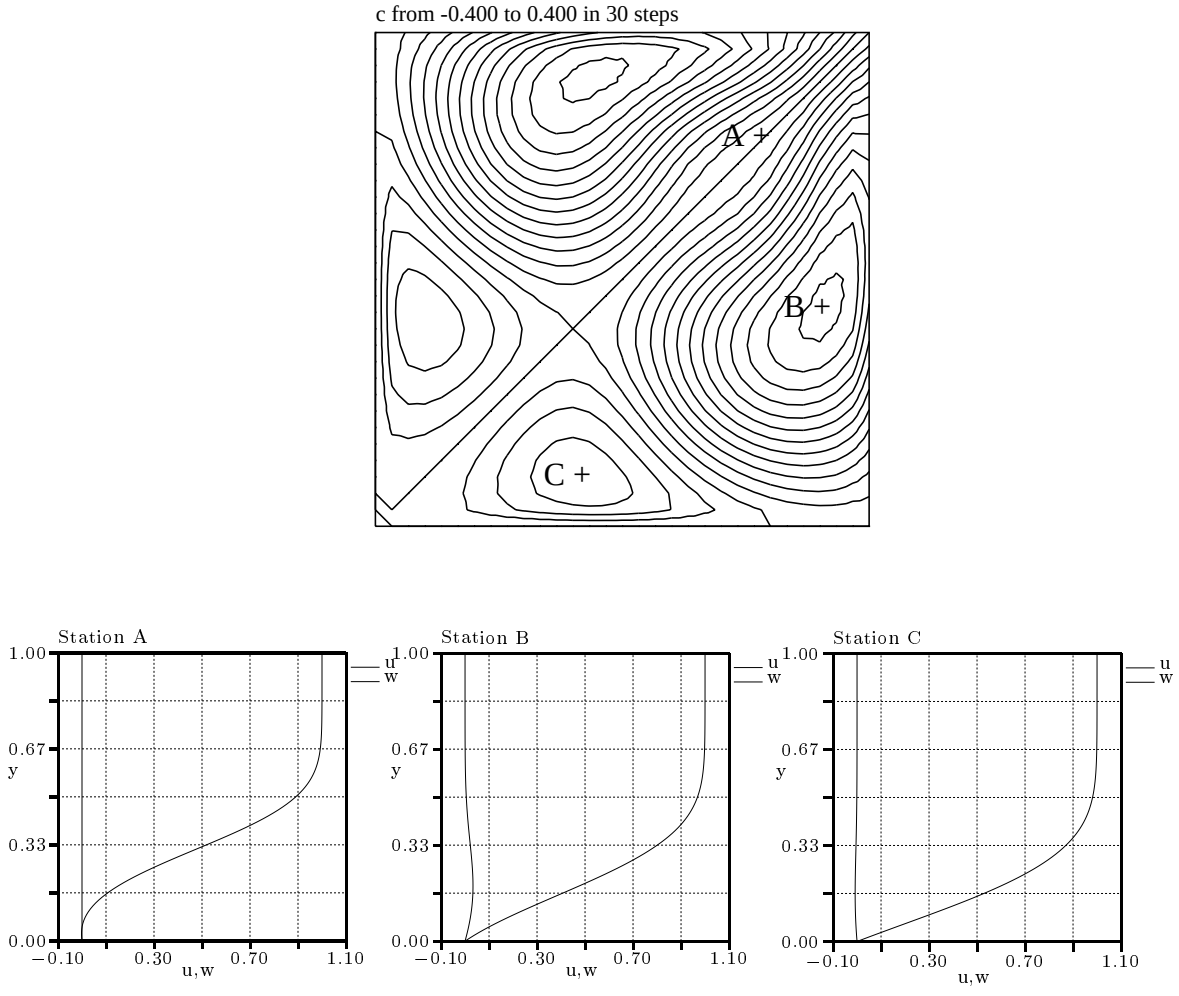

Figure 9-14: Velocity profiles at stations A,B and C.

Chapter 10

Concluding Remarks

In this thesis, several issues concerned with the integral solution of three-dimensional boundary layers have been addressed in a novel manner. Some of these issues involve mathematical properties of integral systems while others arise in their practical solution. The contributions of this work are listed below.

10.1 Hyperbolic integral-equation systems

A major contribution of this thesis is the eigenvalue-based method for the closure of an integral system in direct-mode formulation. The resulting system is always hyperbolic. In the traditional method, the system and its closure are not directly related; the character of the resulting system has an element of arbitrariness and can be non-hyperbolic. The new method is based on the recognition that the closure, here formulated in terms of assumed profile families for velocity, is not independent of the equation system. The two must be considered in an integrated manner.

A key feature of the eigenvalue-based method is the provision to prescribe the characteristic directions in a manner consistent with the physical flow of information in the boundary layer. This physical picture is carefully constructed from the nature of the differential boundary-layer equations. The hyperbolicity of integral systems is also justified on these grounds.

One inherent limitation of the method is its linearized treatment of the problem. This prevents its use in conjunction with the very useful Newton solution method. However, no restriction exists for use in the usual array of implicit and explicit solution methods for which it is well suited. There, both space-marching strategies for the steady equations and time stepping ones for the unsteady equations can be employed.

10.2 Application of streamline upwinding

Petrov-Galerkin streamline upwinding is applied to the boundary-layer equations, in the context of the finite-element discretization. This includes the extension of the idea from a scalar equation to a coupled system. In practice, however, the use of the full extension is probably not warranted nor feasible (in an implicit/Newton solver with analytically-computed sensitivities); in its place, a simple heuristic version is shown to be effective. The upwinding represents a significant improvement over the traditional use of generic second-order artificial smoothing.

10.3 Well-conditioned system for bidirectional flows

There is only one method in the literature, to the author's knowledge, where bidirectional crossflow profiles have been computed using a true integral system [56]. This method uses a space marching strategy in the solution of the equations. In this thesis, it is shown that the auxiliary equation employed for the purpose produces ill-conditioned residual Jacobian matrices in an implicit or Newton solver, under most equilibrium conditions. An alternative equation is proposed and shown to be well-conditioned. Moreover, the use of this equation is validated using a finite-difference solution of the differential boundary layer equations on an infinite-span wing.

10.4 Fully-simultaneous Panel coupling for general systems

A fully-simultaneous coupling of the integral boundary-layer equations to a simple Panel method for the inviscid flow has been developed to calculate separated flows. The novelty of this method is the built-in ability to incorporate into this coupling scheme any general assumed profile family.

10.5 Other contributions

There are a few minor contributions in this thesis in addition to the ones listed above. These include:

1. The parent integral equation derived in Chapter 2 is a convenient means to derive any moment-of-momentum equation, including the well-established lower-moment ones: momentum and kinetic energy.

2. The tools to investigate the nature of the steady differential equations are applied to the unsteady equations. It is shown that information is convected along pathlines. A qualitative description of the unsteady domain of dependence and range of influence is then possible.

3. An analysis of the standard third-order equation system with Johnston's turbulent crossflow model while retaining Reynolds number and Mach number dependence in the assumed streamwise closure relations is performed. The system is shown to be hyperbolic. Previous analyses were limited to approximate one-parameter, incompressible closures.

10.6 Recommendations for future work

In this thesis, many issues were touched upon that hold the potential for interesting and fruitful further study. Some issues related to theory include:

1. The derivation of the parent integral equation vividly illustrates the existence of an infinite series consisting of integral equation approximations to the differential system. The natural question then is is whether a convergent subset of this series can be shown to be an 'exact' approximation to the differential system, and if so what would be an 'optimal' finite system for practical solution.

2. The proposed eigenvalue-based method for ensuring hyperbolicity should be implemented and with practical experience further refined. One feature of the method is the ability to compute bidirectional crossflows with the standard third-order integral system. The eigenvalue prescription conditions essentially substitute for the additional equation needed in traditional closure. The exact role of the eigenvalues in the equation system/closure scheme needs further investigation.

More practically-oriented issues include:

1. Many accurate closure models for laminar attachment-line flow, for the criterion for turbulent flow along the attachment-line, for laminar-turbulent transition including that triggered by crossflow instabilities exist in the literature. Wake flows are simply calculated by setting wall shear-stress terms to zero in the conventional turbulent flow models and in the integral-momentum equations. All these models can be used to calculate complete flows over aerodynamic bodies within the current framework.

2. The closure in this thesis is achieved through profile families which are used to compute necessary boundary-layer integral quantities on the fly with numerical quadrature. In the code, these thicknesses are all defined and stored independently. Since the discretization method also involves rotating these thicknesses, the code is fairly complicated. Actually, these thicknesses need not be computed and stored independently. The data structure can be dramatically simplified by integrating the differential boundary-layer equations themselves numerically on the fly. This is equivalent to performing the derivation of Chapter 2 numerically instead of *a priori* as in current practice. The rotations of thicknesses would be replaced by simply rotating the velocity components. This simpler approach has great potential in terms of ease of coding as well as reducing storage needs.

3. The matrix inversion solver used in the current code is a simple direct Gaussian-elimination-based routine. While the fully-coupled scheme produces a full residual Jacobian matrix many of the elements are negligible in most calculations. The memory-storage requirements as well as run-times can be greatly improved by using an iterative sparse solver in conjunction with drop tolerances.

Bibliography

[1] D.A. Anderson, Tannehill J.C., and Pletcher R.H. *Computational Fluid Mechanics and Heat Transfer*. Hemisphere Publishing Corporation, New York, 1984.

[2] R. Bradley. Approximate solutions for compressible turbulent boundary layers in three-dimensional flow. *AIAA Journal*, 6(5), May 1968.

[3] P. Bradshaw and N. Pontikos. Measurements in the turbulent boundary layer on an 'infinite' swept wing. *Journal of Fluid Mechanics*, 159:105–130, 1985.

[4] J. Caille and J. Schetz. Three-dimensional strip-integral method for incompressible turbulent boundary layers. *AIAA Journal*, 30(5):1207–1213, May 1992.

[5] D. E. Coles. The law of the wake in the turbulent boundary layer. *Journal of Fluid Mechanics*, 1:193–226, 1956.

[6] J. C. Cooke. Approximate calculation of three-dimensional laminar boundary layers. R & M Report 3201, Aeronautical Research Council, HMSO, London, 1961.

[7] J. Cousteix. Integral method and turbulence models applied to three-dimensional boundary layers. In H. Fernholz and E. Krause, editors, *Three-Dimensional Turbulent Boundary Layers*. Springer-Verlag, 1982.

[8] J. Cousteix. Three-dimensional and unsteady boundary-layer computations. In et. al. Van Dyke, editor, *Annual Review of Fluid Mechanics*, volume 18. Annual Reviews, Inc., 1986.

[9] J. Cousteix. Three-dimensional boundary layers. introduction to calculation methods. In *Computation of Three-Dimensional Boundary Layers Including Separation*, Apr 1986. AGARD-R-741.

[10] J. Cousteix and R. Houdeville. Singularities in three-dimensional turbulent boundary layer calcuations and separation phenomena. *AIAA Journal*, 19(8), Aug 1981.

[11] A.G.T. Cross. Calculation of compressible three-dimensional turbulent boundary layers with particular reference to wings and bodies. *BAe (Brough) Report YAD 3379*, 1979.

[12] N. A. Cumpsty and M. R. Head. The calculation of three-dimensional turbulent boundary layers. part i: Flow over the rear of an infinite swept wing. *The Aeronautical Quarterly*, XVIII:55–84, Feb 1967.

[13] N. A. Cumpsty and M. R. Head. The calculation of three-dimensional turbulent boundary layers. part ii: Attachment-line flow on an infinite swept wing. *The Aeronautical Quarterly*, XVIII:150–164, May 1967.

[14] A. T. Degani and J. D. A. Walker. Computation of three-dimensional turbulent boundary layers using the embedded-function method. AIAA-92-0440, 1992.

[15] A. T. Degani and J. D. A. Walker. Computation of attached three-dimensional turbulent boundary layers. *Journal of Computational Physics*, 109(2):202–214, Dec 1993.

[16] Smith F. T. Degani, A. T. and J. D. A. Walker. The three-dimensional turbulent boundary layer near a plane of symmetry. *Journal of Fluid Mechanics*, 234:329–360, Jan 1992.

[17] Smith F. T. Degani, A. T. and J. D. A. Walker. The structure of a three-dimensional turbulent boundary layer. *Journal of Fluid Mechanics*, 250:43–68, May 1993.

[18] M. Drela. A new transformation and integration scheme for the compressible boundary layer equations, and solution behavior at separation. Report 172, MIT Gas Turbine & Plasma Dynamics Laboratory, May 1983.

[19] M. Drela. *Two-Dimensional Transonic Aerodynamic Design and Analysis Using the Euler Equations*. PhD thesis, MIT, Dec 1985. Also, MIT Gas Turbine & Plasma Dynamics Laboratory Report No. 187, Feb 1986.

[20] M. Drela. XFOIL: An analysis and design system for low Reynolds number airfoils. In T.J. Mueller, editor, *Low Reynolds Number Aerodynamics*. Springer-Verlag, Jun 1989. Lecture Notes in Engineering, No. 54.

[21] M. Drela. Improvements in low Reynolds number airfoil flow predictions with ISES and XFOIL. CFDL techinical report, MIT, Jun 1990.

[22] M. Drela. Personal communication, Aug 1997.

[23] Eichelbrenner and J. Peube. The role of s-shaped crossflow profiles in three-dimensional boundary layer theory. Technical report, Laboratoire de Mechanique des Fluides, Poitiers, 1966.

[24] Michel et. al. Methode pratique de prevision des couches limites turbulentes bi- et tridimensionelles. *La Recheche Aerospatiale*, 1, 1972.

[25] D. Geropp. Bemerkung zum system der unendlich vielen integralbedingungen der grenzschichttheorie. *Zeitschrift für Angewandte Mathematik und Mechanik*, 48(7):492–493, Oct 1968.

[26] J. E. Green, D. J. Weeks, and J. W. Brooman. Prediction of turbulent boundary layers and wakes in compressible flow by a lag entrainment method. R & M Report 3791, Aeronautical Research Council, HMSO, London, 1973.

[27] M. G. Hall. On the momentum integral equations for three-dimensional laminar boundary layers in incompressible flow. Technical Report ACA-62, Australian Aeronautical Research Committee, Sydney, 1959.

[28] C. Hirsch. *Numerical Computation of Internal and External Flows.* Wiley, New York, 1988.

[29] M. Holt. *Numerical Methods in Fluid Dynamics.* Springer-Verlag, Berlin, 1984.

[30] J. P. Johnston. *The three-dinemsional turbulent boundary layer.* PhD thesis, MIT, May 1957. Also, MIT Gas Turbine Laboratory Report No. 39, 1957.

[31] M. T. Karimipanah and E. Olsson. Calculation of three-dimensional boundary layers on rotor blades using integral methods. In *International Gas Turbine and Aeroengine Congress and Exposition.* ASME, Jun 1992. 92-G1-210.

[32] T. Karman and C. Millikan. On the theory of laminar boundary layers involving separation. Technical Report 504, N.A.C.A., 1934.

[33] E. Krause. Numerical treatment of boundary-layer problems. In *Advances in Numerical Fluid Mechanics*, Mar 1973. AGARD-LS-64.

[34] H. Kreiss. Boundary conditions for difference approximation of hyperbolic equations. In *Advances in Numerical Fluid Mechanics*, Mar 1973. AGARD-LS-64.

[35] J.C. LeBalleur. Strong matching method for computing transonic viscous flows including wakes and separations. lifting airfoils. *La Recherche Aerospatiale*, pages 21–45, 1981-3. English Edition.

[36] R.C. Lock. Prediction of the drag of wings at subsonic speeds by viscous/inviscid interaction techniques. 1985. AGARD-R-723.

[37] A. Mager. Generalization of boundary-layer momentum integral equations to three-dimensional flows, including those of rotating systems. Technical Report 1067, N.A.C.A., 1952.

[38] W. M. Milewski. *Three-Dimensional Viscous Flow Computations Using the Integral Boundary Layer Equations Simultaneously Coupled with a Low Order Panel Method.* PhD thesis, MIT, May 1997.

[39] H. L. Moses. A strip-Integral method for predicting the behavior of turbulent boundary layers. In *Proceedings Computation of Turbulent Boundary Layers - 1968*, Stanford, CA, 1969. AFOSR-IFP-STANFORD Conference, Vol 1, Stanford University.

[40] B. H. Mughal. A calculation method for the three-dimensional boundary-layer equations in integral form. Master's thesis, MIT, Sep 1992.

[41] B. H. Mughal and M. Drela. A calculation method for the three-dimensional boundary layer equations in integral form. AIAA-93-0786, 1993.

[42] D. F. Myring. An integral prediction method for three-dimensional turbulent boundary layers in incompressible flow. Technical Report 70147, Royal Aircraft Establishment, 1970.

[43] J. F. Nash and V. C. Patel. *Three-Dimensional Turbulent Boundary Layers.* SBC Technical Books, Atlanta, 1972.

[44] B. Nishida. *Fully Simultaneous Coupling of the Full Potential Equation and the Integral Boundary Layer Equations in Three Dimensions.* PhD thesis, MIT, Feb 1996.

[45] H. Pfeil and T. Amberg. Differing development of the velocity profiles of three-dimensional turbulent boundary layers. *AIAA Journal*, 27(10):1456–1459, 1989.

[46] G.S. Raetz. A method of calculating three-dimensional laminar boundary-layers of steady compressible flows. Technical Report NAI-58-73, Northrop Aircraft Inc., 1957.

[47] L. Rosenhead. *Laminar Boundary Layers.* Dover, New York, 1966.

[48] J. A Schetz. *Boundary Layer Analysis.* Prentice Hall, New Jersey, 1993.

[49] H. Schlichting. *Boundary-layer theory.* McGraw-Hill, New York, 1979. Translation of Grenzschicht-Theorie, 7th Edition.

[50] J. Shanebrook and W. Sumner. A small cross flow theory for three-dimensional, compressible turbulent boundary layers on adiabatic walls. *AIAA Journal*, 11(7), Jul 1973.

[51] J. R. Shanebrook and W. J. Sumner. Crossflow profiles for compressible, turbulent boundary layers. *Journal of Aircraft*, 8(3):188–190, Mar 1971.

[52] R. A. Shapiro. *Adaptive Finite Element Solution Algorithm for the Euler Equations.* PhD thesis, MIT, 1988. Also in Notes on Numerical Fluid Mechanics, Vol. 32, Vieweg, 1991.

[53] P. D. Smith. Calculation methods for three-dimensional turbulent boundary layers. R & M Report 3523, Aeronautical Research Council, HMSO, London, 1968.

[54] P. D. Smith. An integral prediction method for three-dimensional compressible turbulent boundary layers. R & M Report 3739, Aeronautical Research Council, HMSO, London, 1972.

[55] T. M. Sorensen. *Aeroelastic Analysis and Sensitivity Calculations Using the Newton Method.* PhD thesis, MIT, Sep 1995.

[56] H. W. Stock. Integral method for the calculation of three-dimensional, laminar and turbulent boundary layers. NASA Technical Memorandum 75320, Dornier GMBH, 1978. Translation of Integralverfahren Zur Berechnung Dreidimensionaler, Laminarer Und Turbulenter Grenzschichten, October 1977.

[57] B. Stratford. Flow in the laminar boundary layer near separation. R & M Report 3002, Aeronautical Research Council, HMSO, London, 1954.

[58] T. W. Swafford. Analytical approximation of two-dimensional separated turbulent boundary-layer velocity profiles. *AIAA Journal*, 21(6):923–926, 1983.

[59] T.W. Swafford and D.L. Whitfield. Time-dependent solution of three-dimensional compressible turbulent integral boundary-layer equations. *AIAA Journal*, 23(7):1005–1013, Jul 1985.

[60] T. Tai. An integral method for three-dimensional turbulent boundary layer with large crossflow. AIAA-87-1254, 1987.

[61] T. C. Tai. Application of two-dimensional velocity profile to three-dimensional boundary-layer flow. *AIAA Journal*, 24(3):370–376, 1986.

[62] B. van den Berg and A. Elsenaar. Measurements in a three-dimensional incompressible turbulent boundary layer in an adverse pressure gradient under infinite swept wing conditions. Technical Report NLR TR 72092U, Nationaal Lucht-En Ruimtevaartlaboratorium, Amsterdam, 1972.

[63] B. van den Berg, D.A. Humphreys, E. Krause, and J.P.F. Lindhout. Three-dimensional turbulent boundary layers – calculations and experiments. Notes on numerical fluid mechanics, Germany, 1988.

[64] A. J. van der Wees and J. van Muijden. A robust quasi-simultaneous interaction method for a full potential flow with a boundary layer with application to wing/body configurations. Technical Report N93-27465, National Aerospace Laboratory NLR, The Netherlands, 1990.

[65] M. VanDyke. *Perturbation Methods in Fluid Mechanics.* The Parabolic Press, Stanford, 1975.

[66] A. Walz. *Boundary Layers of Flow and Temperature.* The M.I.T. Press, Cambridge, 1969.

[67] K. C. Wang. On the determination of the zones of influence and dependence for three-dimensional boundary-layer equations. *Journal of Fluid Mechanics*, 48:397–404, 1971.

[68] F. M. White. *Viscous Fluid Flow.* McGraw-Hill, New York, 1974.

[69] G. Whitham. *Linear and Nonlinear Waves.* Wiley, New York, 1973.

[70] L. Wigton and H. Yoshihara. Viscous-inviscid interactions with a three-dimensional inverse boundary-layer code. In *Second Symposium on Numerical and Physical Aspects of Aerodynamic Flows*, Long Beach, California, Jan 1983. California State University.

[71] J. H. Wilkinson. *The Algebraic Eigenvalue Problem.* Oxford University Press, Oxford, 1988.

[72] H. Yoshihara and J. Wai. Transonic turbulent separation on swept wings - a return to the direct formulation. AIAA-84-0265, 1984.

[73] O. C. Zienkiewicz and R. L. Taylor. *The Finite Element Method.* McGraw-Hill, London, Fourth Edition.